Article

Lithocholic acid binds TULP3 to activate sirtuins and AMPK to slow down ageing

https://doi.org/10.1038/s41586-024-08348-2

Received: 6 November 2023

Accepted: 5 November 2024

Published online: 18 December 2024

Open access

Check for updates

Qi Qu[1,7], Yan Chen[1,7], Yu Wang[1,7], Weiche Wang[1,7], Shating Long[1], Heng-Ye Yang[1], Jianfeng Wu[2], Mengqi Li[1], Xiao Tian[1], Xiaoyan Wei[1], Yan-Hui Liu[1], Shengrong Xu[1], Jinye Xiong[1], Chunyan Yang[1], Zhenhua Wu[1], Xi Huang[1], Changchuan Xie[1], Yaying Wu[1], Zheni Xu[1], Cixiong Zhang[1], Baoding Zhang[1], Jin-Wei Feng[1], Junjie Chen[3], Yuanji Feng[4], Huapan Fang[4], Liyun Lin[1], ZK Xie[1], Beibei Sun[1], Huayu Tian[4], Yong Yu[1], Hai-Long Piao[5], Xiao-Song Xie[6], Xianming Deng[1], Chen-Song Zhang[1]✉ & Sheng-Cai Lin[1]✉

Lithocholic acid (LCA) is accumulated in mammals during calorie restriction and it can activate AMP-activated protein kinase (AMPK) to slow down ageing[1]. However, the molecular details of how LCA activates AMPK and induces these biological effects are unclear. Here we show that LCA enhances the activity of sirtuins to deacetylate and subsequently inhibit vacuolar H^+-ATPase (v-ATPase), which leads to AMPK activation through the lysosomal glucose-sensing pathway. Proteomics analyses of proteins that co-immunoprecipitated with sirtuin 1 (SIRT1) identified TUB-like protein 3 (TULP3), a sirtuin-interacting protein[2], as a LCA receptor. In detail, LCA-bound TULP3 allosterically activates sirtuins, which then deacetylate the V1E1 subunit of v-ATPase on residues K52, K99 and K191. Muscle-specific expression of a V1E1 mutant (3KR), which mimics the deacetylated state, strongly activates AMPK and rejuvenates muscles in aged mice. In nematodes and flies, LCA depends on the TULP3 homologues *tub-1* and *ktub*, respectively, to activate AMPK and extend lifespan and healthspan. Our study demonstrates that activation of the TULP3–sirtuin–v-ATPase–AMPK pathway by LCA reproduces the benefits of calorie restriction.

The dietary intervention of calorie restriction (CR) can extend lifespan and healthspan in diverse species, including worms, fruit flies and primates[3]. CR induces a range of molecular, cellular and physiological changes to maintain mitochondrial quality and quantity, reduce oxidative damage and suppress inflammation, all of which are commonly dysregulated in aged animals[3]. CR can thereby help slow down age-associated metabolic disorders and diseases, including central obesity, insulin resistance, muscle degeneration and cancer[4]. AMPK, a master regulator of metabolic homeostasis, has an essential role in mediating these benefits of CR[5]. We recently identified that the metabolite LCA, which is increased after CR, can alone activate AMPK in mice, nematodes and flies[1]. AMPK is also required for LCA to effect rejuvenation of muscle in aged mice, and extension of lifespan and healthspan in nematodes, flies and mice[1]. However, how AMPK is activated by LCA to produce these benefits is unknown.

AMPK can be activated in multiple ways depending on the severity of cellular nutrient stress[6], energy stress[7] or Ca^{2+} levels[8]. The ancestral role of AMPK is thought to include sensing glucose levels[9]. Under falling levels of glucose and consequently reduced levels of the glycolytic intermediate fructose-1,6-bisphosphate (FBP)[10], AMPK is activated at the lysosome through the glucose-sensing pathway independently of increases in AMP levels[11]. As reported in our companion paper[1], LCA activates AMPK without increasing AMP-to-ATP or ADP-to-ATP ratios or global Ca^{2+} levels. This finding indicates that LCA activates AMPK independently of increases in AMP, ADP or Ca^{2+}. This leaves the lysosomal glucose-sensing pathway as a possible route for LCA to activate AMPK. In this pathway, lack of FBP is directly sensed by aldolase together with the lysosomal proton pump v-ATPase. This complex blocks the transient receptor potential vanilloid (TRPV) family of calcium channel receptors, which are localized on endoplasmic reticulum. TRPV receptors convert the low cellular glucose and FBP levels to low local Ca^{2+} signals at the endoplasmic reticulum–lysosome contact site[10,12]. TRPV receptors then interact with v-ATPase to induce reconfiguration and inhibition of the aldolase–v-ATPase complex[12]. Next, AXIN utilizes v-ATPase and its associated Ragulator multiprotein complex as docking sites to tether liver kinase B1 (LKB1), an AMPK upstream kinase, and LKB1 activates AMPK by phosphorylating the Thr172 residue of AMPKα[11]. Notably, metformin at clinically relevant doses binds PEN2, which in turn binds and inhibits v-ATPase to activate AMPK through the lysosomal pathway and consequently produce lifespan extension benefits[13–15].

In this study, we tested whether LCA activates AMPK through the lysosomal pathway. Concentrations as low as 1 μM LCA, similar to that detected in the serum of CR-treated mice, induced AXIN–LKB1 to translocate to the lysosome in mouse embryonic fibroblasts (MEFs), as evidenced by immunofluorescence co-staining with the lysosomal marker LAMP2 (Extended Data Fig. 1a,b). As a result, the formation of a

[1]State Key Laboratory for Cellular Stress Biology, School of Life Sciences, Xiamen University, Xiamen, China. [2]Laboratory Animal Research Centre, Xiamen University, Xiamen, China. [3]Analysis and Measurement Centre, School of Pharmaceutical Sciences, Xiamen University, Xiamen, China. [4]State Key Laboratory of Physical Chemistry of Solid Surfaces, College of Chemistry and Chemical Engineering, Xiamen University, Xiamen, China. [5]CAS Key Laboratory of Separation Science for Analytical Chemistry, Dalian Institute of Chemical Physics, Chinese Academy of Sciences, Dalian, China. [6]McDermott Center of Human Growth and Development, University of Texas Southwestern Medical Center, Dallas, TX, USA. [7]These authors contributed equally: Qi Qu, Yan Chen, Yu Wang, Weiche Wang. ✉e-mail: cszhang@xmu.edu.cn; linsc@xmu.edu.cn

complex between AXIN–LKB1 and v-ATPase–Ragulator was increased by LCA (Extended Data Fig. 1c). LCA also inhibited v-ATPase in MEFs, as evidenced by reduced signals from the dye LysoSensor Green DND-189, which is weakened with increases in lysosomal pH (Extended Data Fig. 1d). The proton transport rates of v-ATPase in purified lysosomes was also reduced (Extended Data Fig. 1e). Knock down of the gene encoding the V0C subunit of v-ATPase (ATP6V0C), which rendered v-ATPase devoid of the docking site for AXIN–LKB1 (ref. 11), blocked AMPK activation by LCA. This in turn caused reduced phosphorylation of AMPKα (pAMPKα) and ACC (pACC; also known as pACC1/2) (Extended Data Fig. 1f). Knockout of *Axin1* (the only homologue expressed in MEFs[16]) or *Lamtor1* (which encodes a subunit of Ragulator) in MEFs also blocked LCA-mediated AMPK activation (Extended Data Fig. 1g–j). We also tested other components of the lysosomal AMPK pathway by treating mice with LCA (coated with (2-hydroxypropyl)-β-cyclodextrin) at 1 g l^{-1} in drinking water, which led to the accumulation of approximately 1.1 μM LCA in the serum (figure 2f of ref. 1). Knockout of *Lamtor1* or *Axin* (in liver, knockout of *Axin1*, as only this homologue is expressed in the liver; in muscles, knockout of both *Axin1* and *Axin2* due to redundancy[16–18]) abolished LCA-mediated AMPK activation in mouse tissue (Extended Data Fig. 1k–n). These results indicate that LCA inhibits v-ATPase to activate AMPK through the lysosomal pathway.

We next explored how LCA inhibits v-ATPase. As AMPK activation displays a linear regression relationship with glucose and therefore FBP levels[10], and both LCA and CR can reduce blood glucose to some extent (Extended Data Fig. 2a and extended data figure 2f of ref. 1), we determined whether the reduction in glucose and FBP levels observed during CR and LCA treatment can cause v-ATPase inhibition. Blood glucose levels of ad libitum-fed mice were reduced from approximately 9 mM (postprandial) to 5.5 mM (after 4 h of fasting), which further decreased to 4.5 mM after 8 h (Extended Data Fig. 2a). For AMPK activation, we observed a slight increase in muscular pAMPKα and pACC levels at 4 h of fasting, which increased and plateaued after 8 h in these mice (Extended Data Fig. 2a). By comparison, in mice subjected to 4 months of CR, blood glucose levels did not decrease to below 5.5 mM throughout the day. Moreover, AMPK activation in these mice was constant and at a level comparable to that to ad libitum-fed mice at 8 h of fasting (Extended Data Fig. 2a,b). Similarly, FBP levels were substantially reduced during the fasting state of ad libitum-fed mice, whereas the change was small in CR-treated mice (Extended Data Fig. 2a). These data suggest that the reduction in glucose and FBP levels alone is not the primary factor responsible for triggering AMPK activation in CR-treated mice. In addition, LCA could still activate AMPK in MEFs expressing the D34S mutant of aldolase A (ALDOA), which is constitutively bound to FBP and hence blocks AMPK activation even in low glucose conditions[10,19] (Extended Data Fig. 2c–e). This result indicates that LCA activates AMPK through a different entry point, downstream of aldolase, of the lysosomal AMPK activation pathway. Similarly, knockout of genes encoding the receptors TRPV1–TRPV4 in MEFs (MEFs have low expression of other TRPV receptors[12]) did not affect LCA-mediated AMPK activation (Extended Data Fig. 2f–h). Notably, the PEN2–ATP6AP1 shunt used by metformin does not have a role in the activation of AMPK by LCA (Supplementary Fig. 2a–f).

The above data indicated that LCA acts downstream of aldolase and TRPV receptors to enter the lysosomal AMPK pathway. We then wondered whether post-translational modifications of v-ATPase might be the initiating point in LCA-mediated AMPK activation. To this end, we immunoprecipitated all 21 subunits of v-ATPase (tagged with haemagglutinin (HA)) from HEK293T cells and performed mass spectrometry (MS) analyses. Among the post-translational modifications analysed, acetylation was the most common, with a total of 263 residues identified (Supplementary Table 1). Addition of nicotinamide and trichostatin A, which inhibit deacetylases, prevented LCA-mediated AMPK activation (Extended Data Fig. 3a), which implicated deacetylation as a possible mechanism of action of LCA. We then determined acetylation and deacetylation of which residues are involved in modulating AMPK activation. We mutated all 263 acetylated lysine residues across the 21 subunits of v-ATPase to arginine (mimicking the deacetylated state) in different combinations. As shown in Extended Data Fig. 3b, single mutations to arginine of K52, K99 and K191 of the V1E1 subunit (ATP6V1E1), and K60 and K118 of the V1E2 subunit (ATP6V1E2) of v-ATPase led to constitutive activation of AMPK. As V1E2 is specifically expressed in spermatocytes, spermatids and mature sperm of the testis[20], we focused on the role of V1E1 deacetylation in AMPK activation hereafter. Double mutations of any two of the three sites also induced activation of AMPK (Fig. 1a; for validation data for the expression levels of these mutants, see Extended Data Fig. 3c). Triple mutation of K52, K99 and K191 to arginine (V1E1(3KR)) led to increased activation of AMPK, similar to the extent induced by LCA treatment (Fig. 1a–c and Extended Data Fig. 3d; for validation data, see Extended Data Fig. 3c,e). Notably, LCA did not further activate AMPK in V1E1(3KR)-expressing cells (Fig. 1d). By contrast, the V1E1(3KQ) mutant, which mimics constitutively acetylated V1E1, inhibited AMPK activation by LCA (Fig. 1d and Extended Data Fig. 3f). Moreover, AMPK activation by V1E1(3KR) in MEFs was abrogated by knockout of *Lamtor1* or *Axin* (Extended Data Fig. 3g–j), thereby confirming the connection of this subunit to the lysosomal AMPK pathway. Additionally, V1E1 acetylation did not affect its ubiquitination[21] or stability (Extended Data Fig. 3k). We next attempted to generate site-sensitive antibodies against each of the three acetylated residues of V1E1 and successfully obtained an antibody against acetylated K99 (V1E1(K99)ac; Extended Data Fig. 3l). Using this antibody, we observed that K99 is deacetylated in MEFs, mouse muscle and liver after LCA administration (Fig. 1e–g). V1E1(K99)ac was inversely correlated with an increase in AMPK activation under LCA treatment, whereby levels of V1E1(K99)ac started to decrease after 1 h of LCA treatment, along with gradual activation of AMPK (Fig. 1h). AMPK activation reached a plateau at around 4 h of LCA treatment, after which the acetylated V1E1 concentration fell to basal levels (Fig. 1h). Similarly, deacetylation of K99 was observed in muscle and liver tissues from CR-treated mice (Fig. 1i,j) and in MEFs treated with serum obtained from these mice (Fig. 1k). Together, these data demonstrate that it is the deacetylation of V1E1 by LCA that activates AMPK through the lysosomal pathway.

We next explored how LCA leads to V1E1 deacetylation. Ectopic expression of any member of the sirtuin deacetylase family (SIRT1–SIRT7), but not their dominant-negative mutants, sufficiently led to deacetylation of V1E1 as determined by anti-V1E1(K99)ac antibody treatment in HEK293T cells (Fig. 2a). By comparison, none of the histone deacetylases (HDAC1–HDAC11) deacetylated K99 (Extended Data Fig. 4a). These results indicated that sirtuins and not HDACs participate in the deacetylation of V1E1. Ectopic expression of individual sirtuins led to v-ATPase inhibition and AMPK activation (Fig. 2a and Extended Data Fig. 4b). Single knockout of sirtuin members did not block LCA-mediated AMPK activation or V1E1 deacetylation; although *Sirt1* knockout had a mild effect (Extended Data Fig. 4c–k; for validation data, see Supplementary Table 2). This result suggested that sirtuins redundantly regulate AMPK by LCA. Knockout of genes encoding SIRT1–SIRT7 (*Sirt1–7*$^{-/-}$; validated in Supplementary Table 2 and Extended Data Fig. 4l) in MEFs blocked LCA-induced V1E1 deacetylation, v-ATPase inhibition and AMPK activation (Fig. 2b–d and Extended Data Fig. 4m). As *Sirt1–7*$^{-/-}$ MEFs grew much slower than wild-type MEFs (Extended Data Fig. 4n and ref. 22), we generated MEFs in which *Sirt2–Sirt7* were knocked out (*Sirt2–7*$^{-/-}$; validated in Supplementary Table 2 and Extended Data Fig. 5a) that grew at a similar rate to that of wild-type MEFs (Extended Data Fig. 5b). When the SIRT1 inhibitor EX-527 was added to *Sirt2–7*$^{-/-}$ MEFs, LCA did not activate AMPK in these cells (Extended Data Fig. 5c–e). Re-introduction of individual sirtuins into *Sirt1–7*$^{-/-}$ MEFs partially restored AMPK activation by LCA, and SIRT1 produced the strongest effect (Fig. 2e). As SIRT1 is predominantly located in the nucleus, with a small portion in the cytosol[23], these results suggested that the non-nuclear fraction of SIRT1 is responsible for

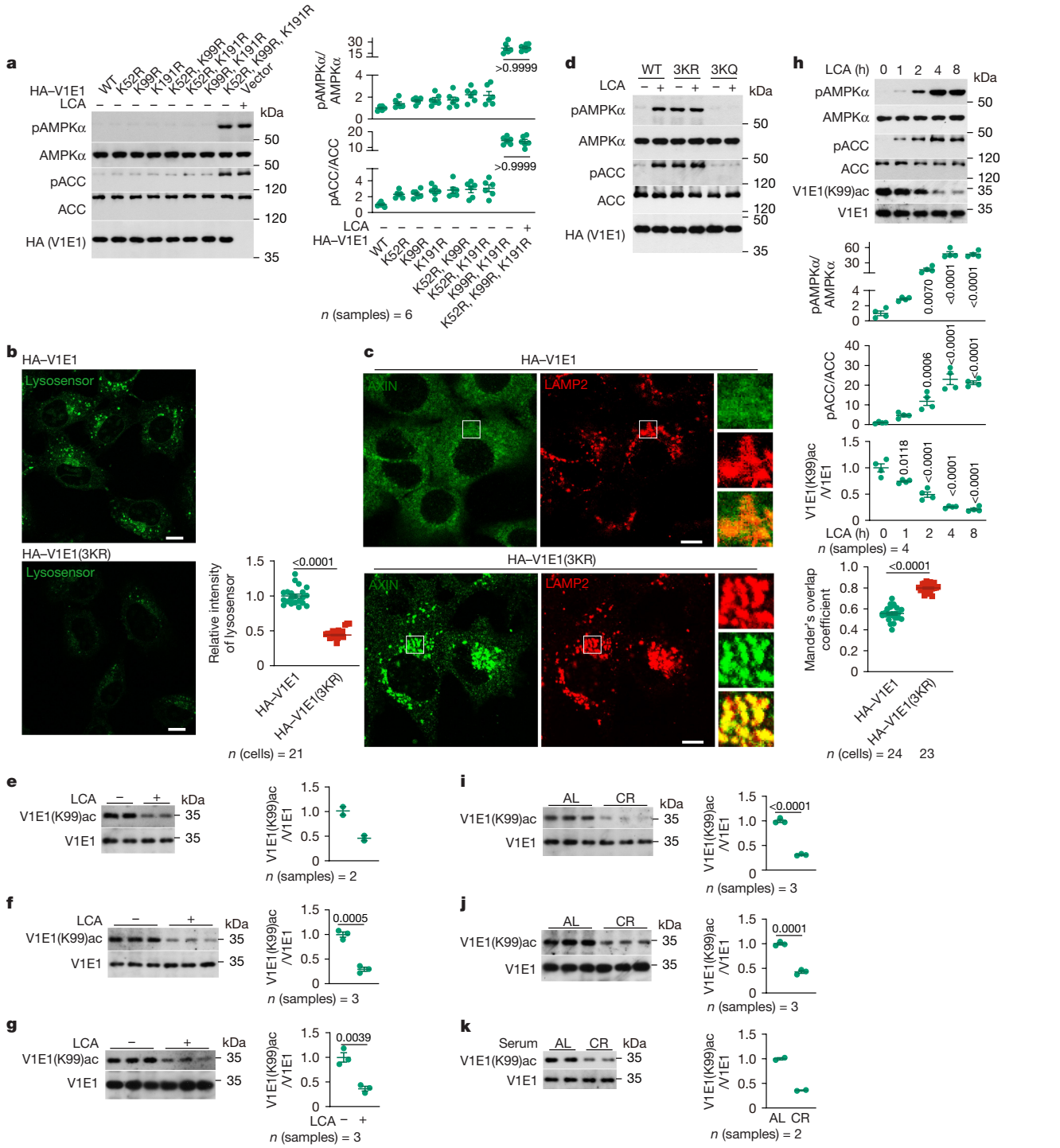

Fig. 1 | LCA causes v-ATPase deacetylation to activate AMPK. **a**–**c**, Deacetylation of the V1E1 subunit on K52, K99 and K191 leads to AMPK activation. MEFs were infected with lentivirus carrying HA-tagged V1E1 or various V1E1 mutants, including V1E1(3KR) (mimicking the deacetylated state of V1E1). **a**, Image (left) and quantification (right) of AMPK activation by different V1E1 mutants determined by immunoblotting (IB; blots hereafter are from IB). **b**,**c**, Images (left) and quantification (right) of v-ATPase inhibition (**b**) and lysosomal localization of AXIN (**c**). Scale bars, 10 μm. **d**, The acetylation state of V1E1 controls AMPK activation. MEFs stably expressing V1E1(3KR) or V1E1(3KQ) (mimicking the constitutively acetylated state) were treated with 1 μM LCA for 4 h, followed by determination of AMPK activation. **e**–**g**,**i**–**k**, Images (left) and quantification (right) showing that CR or LCA treatment causes V1E1 deacetylation. MEFs were treated with 1 μM LCA for 4 h (**e**) or cultured in DMEM with FBS supplemented in the medium replaced with an equal volume of serum from mice subjected to CR for 4 months (**k**). Mice were subjected to CR for 4 months (**i**,**j**) and fed with 1 g l^{-1} (2-hydroxypropyl)-β-cyclodextrin-coated LCA in drinking water for 1 month (**f**,**g**). V1E1(K99)ac levels were measured in MEFs (**e**,**k**), muscles (**f**,**i**) and livers (**g**,**j**). **h**, Image (top) and quantification (bottom) showing that V1E1(K99)ac is inversely correlated with AMPK activation during LCA treatment. MEFs were treated with 1 μM LCA for the indicated times followed by determination of AMPK activation (top and middle) and V1E1(K99)ac (bottom). Statistical results are shown as the mean ± s.e.m. Specific numbers of samples or cells used are labelled on each panel. *P* values (shown on the charts) were calculated using one-way analysis of variance (ANOVA) followed by Kruskal–Wallis test (**a**), two-way ANOVA followed by Tukey's test (**h**), two-sided Mann–Whitney test (**b**), two-sided Student's *t*-test with Welch's correction (**c**) or two-sided Student's *t*-test (**d**–**g**,**i**–**k**). Experiments were performed three (**b**–**k**) or five (**a**) times.

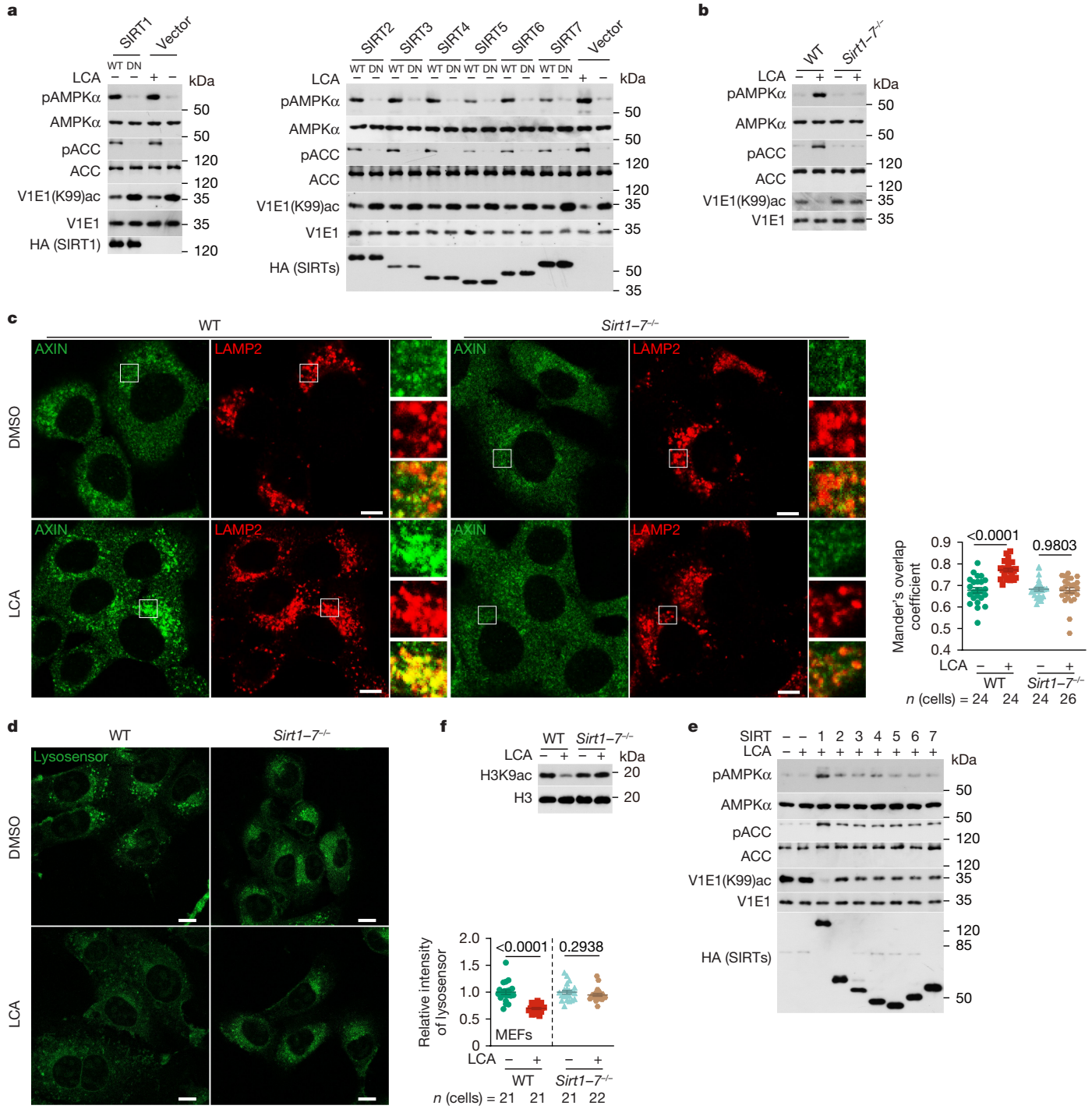

Fig. 2 | Sirtuins are required for the deacetylation of v-ATPase. a, Sirtuins are responsible for V1E1 deacetylation and AMPK activation. HEK293T cells were infected with lentiviruses carrying individual wild-type (WT) sirtuins (HA-tagged SIRT1–SIRT7) or their dominant negative (DN) forms, followed by determination of V1E1 acetylation and AMPK activity. **b**–**d**, Sirtuins are required for LCA-induced V1E1 deacetylation. *Sirt1–7*$^{-/-}$ MEFs were treated with 1 μM LCA for 4 h, followed by determination of AMPK activation (**b**), v-ATPase activity (**d**; assessed by imaging (left) and quantifying (right) intensities of the lysosensor), and lysosomal localization of AXIN (**c**; assessed by imaging (left) and quantifying (right) the co-localization of AXIN with the lysosomal marker LAMP2). Scale bars, 6 μm (**c**) or 10 μm (**d**). **e**, Sirtuin members have complementary roles in mediating LCA-induced V1E1 deacetylation and AMPK activation. *Sirt1–7*$^{-/-}$ MEFs were individually infected with lentivirus carrying seven members of the sirtuin family, followed by treatment with 1 μM LCA for 4 h. AMPK activity and V1E1 acetylation were then determined. **f**, LCA stimulates the activity of sirtuins. WT and *Sirt1–7*$^{-/-}$ MEFs were treated with 1 μM LCA for 4 h, followed by determination of H3K9 acetylation (H3K9ac). Statistical results are shown as the mean ± s.e.m. Specific numbers of cells used are labelled on each panel. *P* values (shown on the charts) were calculated using two-sided Student's *t*-test with Welch's correction (WT, **d**), two-sided Mann–Whitney test (*Sirt1–7*$^{-/-}$, **d**), or two-way ANOVA followed by Tukey's text (**c**). Experiments were performed three (**a**,**c**–**f**) or four (**b**) times.

deacetylating V1E1. Indeed, a non-nuclear fraction of SIRT1 (Extended Data Fig. 5f) was identified to form interactions with V1E1 (Extended Data Fig. 5g). Similarly, partial amounts of SIRT3, SIRT4 and SIRT5 were localized outside mitochondria (Extended Data Fig. 5h,i; for validation data for MEFs with HA-tag knock-in before *Sirt3*, *Sirt4* or *Sirt5*, see Supplementary Table 2 and Extended Data Fig. 5j), where they are mainly

localized[24–26]. Such generated non-mitochondrial SIRT3–SIRT5 also participated in LCA-induced AMPK activation and V1E1 deacetylation, as LCA activated AMPK and deacetylated V1E1 in MEFs expressing only SIRT3–SIRT5 (Extended Data Fig. 5k–m; in the context of quadruple knockout of *Sirt1*, *Sirt2*, *Sirt6* and *Sirt7*, referred to as SIRT1/2/6/7-QKO, see validation data in Supplementary Table 2). The LCA-enhanced activity of sirtuins was seen with other substrates, such as acetylated histone H3 (on residue K9), which can be deacetylated by SIRT1, SIRT2 and SIRT6 (refs. 27–29) (Fig. 2f).

We then explored how LCA activates sirtuins. We first determined the levels of NAD^+, which is a co-substrate of sirtuins[27]. Intracellular NAD^+ levels were increased only after 16 h of LCA treatment, although LCA treatment for 4 h significantly stimulated sirtuin activity in MEFs (Extended Data Fig. 6a,b). These results indicated that sirtuins are activated by LCA before increases in NAD^+ levels. Mutation of SIRT1, as a representative sirtuin, at E230 to lysine (SIRT1(E230K)), which is unable to be activated by allosteric activators such as resveratrol[30], also prevented LCA-induced SIRT1 activation when re-introduced into *Sirt1–7*$^{-/-}$ MEFs (Extended Data Fig. 6c–f). Moreover, the induction of NAD^+ by LCA depended on AMPK (Extended Data Fig. 6a), a result consistent with previous findings that NAD^+ upregulation is a downstream event of AMPK activation[31]. We next tested whether LCA can directly activate sirtuins by using a cell-free system in which purified bacterially expressed SIRT1 was incubated with LCA at various concentrations. LCA did not activate SIRT1 in such a reconstituted condition (Extended Data Fig. 7a; for validation of the SIRT1 activity assay, see Extended Data Fig. 7b). In addition, LCA did not bind to bacterially expressed SIRT1, as determined by an affinity pull-down experiment using a synthetic LCA probe (Extended Data Fig. 7c,d; for the synthesis procedure, see Supplementary Fig. 3, for validation of the LCA probe, see Extended Data Fig. 7e). However, after pre-incubation with lysates from MEFs, SIRT1 activity was increased after LCA addition (Fig. 3a). These observations suggested that LCA activates sirtuins through unknown partners in the cell lysate. We therefore wondered whether such an unknown component might interact with SIRT1. We pulled down HA-tagged SIRT1 from cell lysates and performed MS analyses on the pulled-down proteins. As listed in Supplementary Table 3, a total of 1,655 potential SIRT1-binding proteins were identified as hits. We engineered expression plasmids for all 1,655 proteins and verified that 157 of them could be co-immunoprecipitated by HA-tagged, MYC-tagged or Flag-tagged SIRT1 when individually expressed in HEK293T cells (Supplementary Table 3). We then individually knocked down these 157 proteins in MEFs through lentivirus-mediated short hairpin RNA silencing. Knockdown of *Tulp3*, formerly known as a bipartite transcription regulator[32] and identified as a hit among the SIRT1-interacting proteins[2,33], rendered the cells insensitive to LCA treatment. This result was confirmed by assessing levels of pAMPKα, acetylation of V1E1 and histone H3, and the activity of v-ATPase (Extended Data Fig. 7f,g). MEFs with *Tulp3* knocked out confirmed the requirement of TULP3 for the LCA-induced activation of AMPK and sirtuins (Fig. 3b–d and Extended Data Fig. 7h; see Supplementary Table 2 for validation of *Tulp3* knockout MEFs). The association between TULP3 and SIRT1 was constitutive and independent of LCA (Extended Data Fig. 7i). Indeed, after incubation, purified bacterially expressed TULP3 and SIRT1 co-eluted on size-exclusion chromatography columns regardless of LCA addition (Extended Data Fig. 7j). TULP3 interacted with all seven members of the sirtuin family independent of LCA (Extended Data Fig. 7i). Additionally, in the presence of TULP3, LCA activated bacterially expressed SIRT1 but not its E230K mutant (Fig. 3e and Extended Data Fig. 8a), which indicated that TULP3 bridges LCA to SIRT1. TULP3 bound LCA with a dissociation constant (K_d) value of 15 μM in competition assays (Extended Data Fig. 8b; in which the binding of the LCA probe to TULP3 was competed by LCA to completion at approximately 40 μM). As a control, isolithocholic acid (iso-LCA), a derivative of LCA that is unable to activate AMPK[1], failed to compete with TULP3 for binding to LCA (Extended Data Fig. 8c–e). In silico docking assays revealed four residues of TULP3 (Y193, P195, K333 and P336) that constitute a potential binding pocket for LCA (Extended Data Fig. 8f). Indeed, mutation of these residues to glycine (TULP3(4G)) blocked the LCA-mediated activation of sirtuins and AMPK in MEFs (Fig. 3f and Extended Data Fig. 8g–k; for validation data of expression levels of TULP3(4G), see Extended Data Fig. 8l). Notably, TULP3(4G) showed a similar secondary structure to TULP3, with unchanged thermal stability (Extended Data Fig. 8m) or interactions with SIRT1 (Extended Data Fig. 8n). In contrast to TULP3, other known binding partners or targets of LCA or derivatives did not mediate the activation of AMPK by LCA, as knockout of any of these in MEFs did not impair AMPK activation by LCA[34–51] (summarized in Extended Data Fig. 9a–n; for validation data, see Supplementary Table 4). As an additional control, because some of the receptors share highly similar ligand-binding pocket structures[52,53], we generated MEFs in which genes encoding LXRα and LXRβ were knocked out. LCA could still activate AMPK in these cells (Extended Data Fig. 9o). For a similar reason, we generated paired knockouts in which FXR and FXRβ[37], PXR and CAR[54], and CHRM2 and CHRM3 (ref. 45,46) were depleted in MEFs, and AMPK activation was maintained by LCA (Extended Data Fig. 9p–r). Next, we conducted a domain-mapping assay to pinpoint the regions of TULP3 responsible for binding to SIRT1. TULP3(1–60), a region containing 1–60 amino acids, was sufficient to bind SIRT1 (Extended Data Fig. 10a). Moreover, this region was necessary for binding to other sirtuins (Extended Data Fig. 10b–e; for validation data of the SIRT1 antibody, see Extended Data Fig. 5f). In line with this result, a deletion mutant of TULP3 lacking amino acids 1–60 (TULP3(Δ1–60)), despite an equivalent ability to bind LCA (Extended Data Fig. 10f), failed to complement the roles of full-length TULP3 in mediating the LCA-induced activation of sirtuins and AMPK when re-introduced into *Tulp3*$^{-/-}$ MEFs (Fig. 3g and Extended Data Fig. 10g,h). In addition, a previously reported truncation mutant of SIRT1 (mini-SIRT1)[55,56], which retains deacetylase activity[56], also failed to interact with TULP3 (Extended Data Fig. 11a), and consequently blocked LCA-induced sirtuin and AMPK activation (Fig. 3h and Extended Data Fig. 11b,c). Together, these results show that TULP3 binds LCA to activate SIRT1.

We next determined whether the TULP3–sirtuin–v-ATPase axis mediates the rejuvenating and anti-ageing effects of LCA and CR in animal models. Muscle-specific expression of V1E1(3KR), a deacetylated version of the V1E1 subunit of v-ATPase, led to AMPK activation (Extended Data Fig. 12a) and improved muscle function in aged mice by facilitating the transition of glycolytic fibres to oxidative fibres (Fig. 4a), independently of LCA. V1E1(3KR) also increased muscular NAD^+ levels (Fig. 4b) and muscular mitochondrial content. In detail, the following parameters were increased in aged mice: the mitochondrial DNA-to-nuclear DNA ratios (Extended Data Fig. 12b); the expression of mitochondrial genes and oxidative phosphorylation (OXPHOS) proteins (Extended Data Fig. 12c); and respiratory function (assessed by measuring the oxygen consumption rate (OCR) (Extended Data Fig. 12d). In turn, a significant increase in energy expenditure (Extended Data Fig. 12e–g), running distance, running duration and grip strength were observed in these mice (Fig. 4c,d). Muscle-specific knockout of *Ampk* impaired all benefits brought about by the expression of V1E1(3KR) (Fig. 4a–d and Extended Data Fig. 12a–g). By comparison, muscle-specific re-introduction of TULP3(4G) into mice with muscle-specific knockout of *Tulp3* blocked the CR-mediated rejuvenating effects in muscle (Fig. 4e–g and Extended Data Fig. 12h; for validation data of these mice, see Extended Data Fig. 12i,j).

We then used *Caenorhabditis elegans* and *Drosophila melanogaster* as models to test for the dependency of TULP3 and sirtuins in the regulation of lifespan by LCA. Knockout of *tub-1* (the TULP3 homologue in *C. elegans*) in wild-type (N2) nematodes impaired AMPK activation by LCA (Supplementary Fig. 4a; LCA was absorbed into nematodes as effectively as into mouse muscles, as validated in extended data figure 7a of ref. 1) and abrogated the effects of LCA in lifespan extension

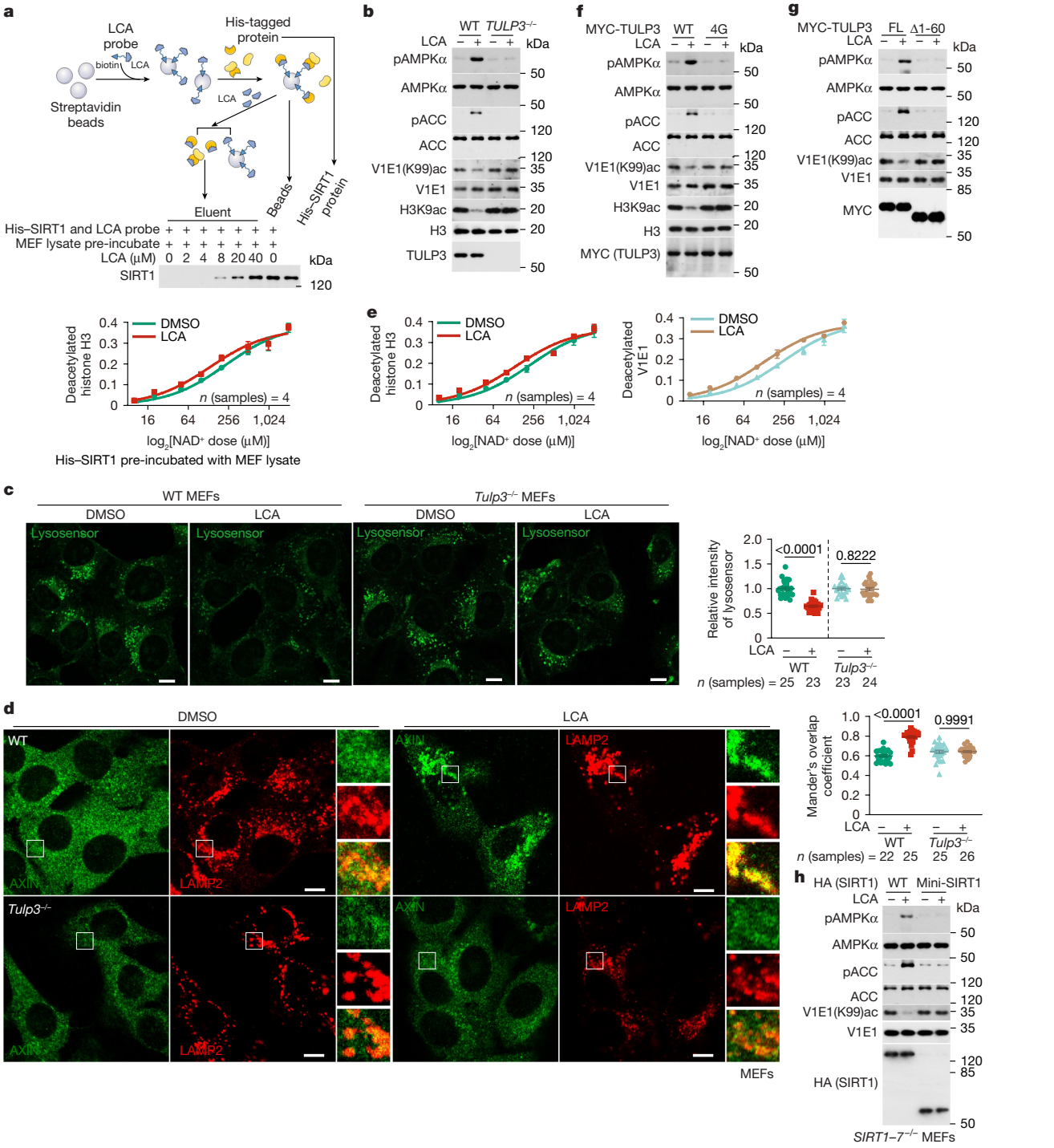

Fig. 3 | TULP3 is the binding protein of LCA for activation of sirtuins. **a**, Purified bacterially expressed SIRT1 requires a cytosolic partner for binding to LCA. Top, schematic of the experiment. His-tagged SIRT1, pre-incubated with cellular lysates from MEFs, was incubated with 5 μM LCA. Bottom, the deacetylase activities of such pre-incubated SIRT1 towards histone H3 and the affinity of SIRT1 towards LCA were determined. **b**–**d**, TULP3 is required for SIRT1-mediated AMPK activation by LCA. MEFs with *Tulp3* knocked out (clone 1 of *Tulp3*$^{-/-}$ MEFs, and the same hereafter for all *Tulp3* knockout experiments) were treated with 1 μM LCA for 4 h. **b**, Determination of AMPK activation and of V1E1 and histone H3 acetylation. **c**, Images (left) and quantification (right) of v-ATPase activity. **d**, Images (left) and quantification (right) of lysosomal localization of AXIN. Scale bars, 10 μm (**c**,**d**). **e**, TULP3 binds LCA and mediates SIRT1 activation. Experiments were performed as in **a**, except that the bacterially expressed His-tagged SIRT1 was co-eluted with bacterially expressed His-tagged TULP3 on a Superdex column before the experiment. **f**, TULP3(4G) is unable to bind LCA and blocks LCA-induced activation of AMPK. *Tulp3*$^{-/-}$ MEFs were infected with lentivirus carrying the TULP3(4G) mutant, followed by treatment with LCA as in **b**. The activities of AMPK were then determined by IB. **g**,**h**, Interaction between TULP3 and sirtuins is required for AMPK activation by LCA. *Tulp3*$^{-/-}$ (**g**) or *SIRT1-7*$^{-/-}$ (**h**) MEFs were infected with lentivirus carrying MYC-tagged TULP3(Δ1–60) (**g**) or HA-tagged mini-SIRT1 (**h**), both of which are mutants that disrupt the interaction between TULP3 and SIRT1. Cells were then treated with LCA as in **b**, followed by determination of AMPK activation. Statistical results are shown as the mean ± s.e.m. Specific numbers of samples used are labelled on each panel. *P* values (shown on the charts) were calculated using two-sided Student's *t*-test (*Tulp3*$^{-/-}$, **c**), two-sided Student's *t*-test with Welch's correction (WT, **c**) or two-way ANOVA followed by Tukey's test (**d**). Experiments were performed three (**a**,**c**–**h**) or four (**b**) times. The schematic in **a** was created using elements from Servier Medical Art under a Creative Commons Attribution 3.0 unported licence.

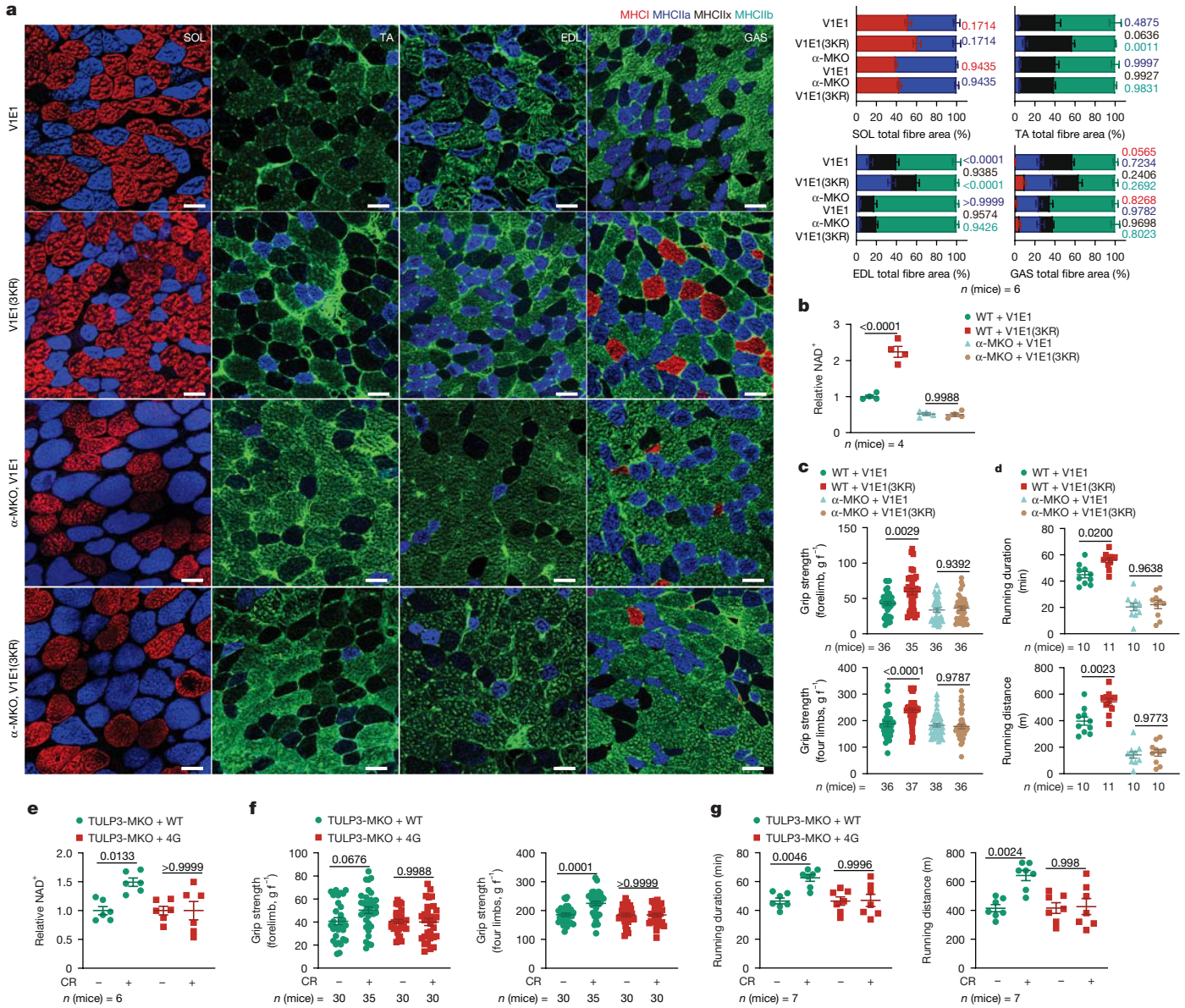

Fig. 4 | The LCA–TULP3–sirtuin–v-ATPase axis exerts rejuvenating effects. **a**, V1E1(3KR) induces oxidative fibre conversion in the muscles of aged mice. Images (left) and quantification (right) of muscle fibre types from WT mice and muscle-specific *Ampka* knockout (α-MKO) mice with muscle-specific expression of V1E1(3KR) (induced by tamoxifen at 16 months old; see the section 'Mouse strains' in the Methods for the procedures for constructing this strain). GAS, gastrocnemius; EDL, extensor digitorum longus; SOL, soleus; TA, tibialis anterior. Scale bars, 50 μm. **b**, V1E1(3KR) induces increases in muscle NAD^+ levels in aged mice. Mice were treated as in **a**, followed by determination of NAD^+ levels in the gastrocnemius muscle. **c**,**d**, V1E1(3KR) promotes muscle strength and running duration in aged mice. Mice were treated as in **a**, followed by determination of the grip strength (**c**) and running duration (**d**). **e**–**g**, TULP3(4G) blocks improvement of muscle function by CR in aged mice. Muscle-specific *Tulp3* knockout (TULP3-MKO) mice with muscle TULP3(4G) (or WT TULP3 expression (induced by tamoxifen at 16 months old, see validation data in Extended Data Fig. 12i) were subjected to CR for 3.5 months, followed by determination of NAD^+ levels (**e**), grip strength (**f**) and running duration and distance (**g**). Statistical results are shown as the mean ± s.e.m. Specific numbers of mice used are labelled on each panel. *P* values (shown on the charts) were calculated using two-way ANOVA followed by Tukey's test. Experiments were performed three times.

(Supplementary Fig. 4b; see also statistical analyses in Supplementary Table 5, and for all the other lifespan data hereafter). Note that knockout of *tub-1* led to an extension of lifespan (Supplementary Fig. 4b) possibly owing to the inhibition of insulin signalling[57]. Similar phenotypes were observed in flies with *ktub* (the TULP3 homologue in *D. melanogaster*) knocked down (Supplementary Fig. 4a,b; flies were able to absorb LCA to a similar level as in mouse muscles, as validated in extended data figure 7b of ref. 1). In addition, both tub-1 and ktub were able to bind LCA (Supplementary Fig. 4c). Notably, structural modelling indicated that tub-1 and ktub contain the three residues that are structurally equivalent to those in TULP3 that are required for LCA binding (Supplementary Fig. 4d). That is, tub-1(P174) and ktub(P219) are equivalent to TULP3(P195), tub-1(P320) and ktub(K353) to TULP3(P336), and tub-1(E172) and ktub(M217) to TULP3(Y193). The three residues in the respective TULP3 family members constitute the hydrophobic cleft for LCA binding (Supplementary Fig. 4d). Mutation of these three residues, tub-1(3G) and ktub(3G) mutants, rendered the respective proteins unable to mediate AMPK activation (Supplementary Figs. 4e and 5a,b; for validation data of these mutants in LCA and SIRT1 binding, see Supplementary Fig. 4f,g) and lifespan extension by LCA (Extended

Data Fig. 13a). Furthermore, re-introduction of wild-type TULP3, but not TULP3(4G), into *tub-1* knockout worms and *ktub* knockout flies restored the extent of lifespan extension by LCA (Extended Data Fig. 13b; see Extended Data Fig. 13c for the data on AMPK activation). Depletion of sirtuins in nematodes (by knocking down *sir-2.3* and *sir-2.4*; *sir-2.1*/*sir-2.2* double knockout nematodes) and flies (by knocking out *Sir2*) impaired LCA-induced AMPK activation (Extended Data Fig. 13d) and lifespan extension (Extended Data Fig. 13e). Regarding the role of v-ATPase deacetylation, both nematodes and flies expressing mammalian V1E1(3KR) showed AMPK activation and extended lifespan (Extended Data Fig. 13f,g). Unlike mammals, nematodes do not possess V1E1; instead, their V1E2 homologue, vha-8, is functionally sufficient for the activity of v-ATPase. The mutant vha-8(2KR) (in which K60 and K117—equivalent to K60 and K118 in V1E2, residues required for LCA-induced AMPK activation—were mutated to arginine; Extended Data Fig. 13h) increased AMPK activation and lifespan extension in nematodes independent of LCA (Extended Data Fig. 13i,j). LCA-mediated extension of healthspan was impaired in nematodes and flies in which TULP3(4G) was expressed or sirtuins were depleted. That is, LCA-induced resistance to oxidative stress and starvation were impaired (Extended Data Fig. 14a–d), as were the increase in mitochondrial content and function (Extended Data Fig. 14e–j) and the increase in NAD^+ levels (Extended Data Fig. 14k,l). By contrast, expression of V1E1(3KR) extended healthspan independent of LCA (Extended Data Fig. 15a–f). Together, these results demonstrate that the TULP3–sirtuin–v–ATPase axis relays the signal of LCA to AMPK activation through deacetylation of the V1E1 subunit of v-ATPase (Extended Data Fig. 15g), which ultimately reproduces the beneficial effects of CR in nematodes, flies and mice.

Discussion

In this study, we delineated how AMPK is activated by physiological, CR-induced levels of LCA. We identified TULP3 as the binding partner for LCA to elicit various benefits. Although the K_d of TULP3 for LCA (approximately 15 μM) is higher than the concentrations of LCA found in serum and muscle during CR (approximately 1 μM), it is possible that TULP3 inside cells may adopt a specific conformation that enables the sensing of physiologically low levels of LCA, as we observed that 1 μM LCA is able to bind to promote sirtuin activity and activate AMPK. It is also possible that local concentrations of LCA can be higher than measured in the serum and muscle of mice. For example, LCA can reach several dozen micromolars during postprandial states in the lumen of the colon[58], and TULP3 in colon epithelial cells may have a role in this process.

Once bound to LCA, TULP3 activates sirtuins before cellular levels of NAD^+ increase, which occurs only after prolonged AMPK activation, as observed in this study (Extended Data Fig. 6a) and others[31]. Therefore, through activating AMPK, LCA–TULP3 creates a positive feedback loop for the production of NAD^+ and the activation of sirtuins, particularly for those sirtuins for which K_m values for NAD^+ are close to the intracellular levels of NAD^+ in tissues of ad libitum-fed animals, such as SIRT1 (ref. 59). As for other sirtuin members that have K_m values for NAD^+ much lower than the regular cellular levels of NAD^+, and are constantly saturated with NAD^+, such as SIRT2 (ref. 60), SIRT4 (ref. 61) and SIRT6 (ref. 62), they can be further allosterically activated by LCA during CR. Nevertheless, TULP3 is required for LCA to activate sirtuins, as shown in cells and animals in which *Tulp3* is knocked out, given that TULP3 is a constitutive component of all seven sirtuins. The common requirement of TULP3 for the activation of sirtuins is in line with previous observations that all members of the sirtuin family participate in the mediation of the physiological effects of CR[63–70].

The importance of sirtuin activation can be supported by the finding that LCA treatment led to deacetylation of the V1E1 subunit of v-ATPase, directly causing the inhibition of v-ATPase, which is a prerequisite for lysosomal AMPK activation. These findings are consistent with previous observations that when v-ATPase holoenzyme is reconstituted with some of the V1 subunits, including V1E1, and expressed and purified from *Escherichia coli*, it showed fivefold lower proton pumping activity compared with the v-ATPase reconstituted with all components purified from calf brain[71]. In addition to acetylation of K52, K99 and K191 in V1E1, we detected phosphorylation on nearby sites such as Y56, S193 and T195 (Supplementary Fig. 6a–c). These nearby phosphorylation sites may additionally regulate v-ATPase.

It is noteworthy that despite an apparent lack of endogenous LCA in nematodes and flies, our results using these animals validated that the conserved signalling route involving sirtuins, NAD^+ and AMPK have a crucial role in extending lifespan. However, it remains to be elucidated how LCA extends lifespan in yeast, as it can benefit from LCA in terms of extending chronological lifespan[72] even though it does not have conserved TULP3 orthologues. Finally, it must also be noted that CR or LCA treatment, at least as far as the late stage of CR is concerned, does not decrease blood glucose to below 5 mM, a low level that gives rise to significant AMPK activation, as seen during fasting or starvation of ad libitum-fed mice. Such a notion is also supported by the observations that disruption of the step from low glucose-sensing aldolase to TRPV, through the expression of the constitutively FBP-bound ALDOA(D34S) or knockout of TRPV receptors, does not affect LCA-mediated AMPK activation. The absence of hypoglycaemia in CR-treated mice has also been observed by other research groups[73,74], and this effect may be due to enhanced gluconeogenesis and decreased glucose oxidation at the expense of increased fat and protein oxidation[75].

In summary, we identified that TULP3 is a receptor of LCA. After binding to LCA, TULP3 activates sirtuins, which in turn deacetylate and inhibit v-ATPase to transmit the LCA signal to activate the lysosomal AMPK pathway and further increase NAD^+ levels. Together, this cascade leads to anti-ageing effects in metazoans.

Online content

Any methods, additional references, Nature Portfolio reporting summaries, source data, extended data, supplementary information, acknowledgements, peer review information; details of author contributions and competing interests; and statements of data and code availability are available at https://doi.org/10.1038/s41586-024-08348-2.

1. Qu, Q. et al. Lithocholic acid phenocopies anti-ageing effects of calorie restriction. *Nature* https://doi.org/10.1038/s41586-024-08329-5 (2024).
2. Armour, S. M. et al. A high-confidence interaction map identifies SIRT1 as a mediator of acetylation of USP22 and the SAGA coactivator complex. *Mol. Cell. Biol.* **33**, 1487–1502 (2013).
3. Green, C. L., Lamming, D. W. & Fontana, L. Molecular mechanisms of dietary restriction promoting health and longevity. *Nat. Rev. Mol. Cell Biol.* **23**, 56–73 (2022).
4. Speakman, J. R. & Mitchell, S. E. Caloric restriction. *Mol. Aspects Med.* **32**, 159–221 (2011).
5. Burkewitz, K., Zhang, Y. & Mair, W. B. AMPK at the nexus of energetics and aging. *Cell Metab.* **20**, 10–25 (2014).
6. Salt, I. P., Johnson, G., Ashcroft, S. J. H. & Hardie, D. G. AMP-activated protein kinase is activated by low glucose in cell lines derived from pancreatic β cells, and may regulate insulin release. *Biochem. J.* **335**, 533–539 (1998).
7. Carling, D., Zammit, V. A. & Hardie, D. G. A common bicyclic protein kinase cascade inactivates the regulatory enzymes of fatty acid and cholesterol biosynthesis. *FEBS Lett.* **223**, 217–222 (1987).
8. Hawley, S. A. et al. 5′-AMP activates the AMP-activated protein kinase cascade, and Ca^{2+}/calmodulin activates the calmodulin-dependent protein kinase I cascade, via three independent mechanisms. *J. Biol. Chem.* **270**, 27186–27191 (1995).
9. Lin, S. C. & Hardie, D. G. AMPK: sensing glucose as well as cellular energy status. *Cell Metab.* **27**, 299–313 (2017).
10. Zhang, C. S. et al. Fructose-1,6-bisphosphate and aldolase mediate glucose sensing by AMPK. *Nature* **548**, 112–116 (2017).
11. Zhang, C. S. et al. The lysosomal v-ATPase–Ragulator complex is a common activator for AMPK and mTORC1, acting as a switch between catabolism and anabolism. *Cell Metab.* **20**, 526–540 (2014).
12. Li, M. et al. Transient receptor potential V channels are essential for glucose sensing by aldolase and AMPK. *Cell Metab.* **30**, 508–524.e12 (2019).
13. Zhang, C. S. et al. Metformin activates AMPK through the lysosomal pathway. *Cell Metab.* **24**, 521–522 (2016).
14. Chen, J. et al. Metformin extends *C. elegans* lifespan through lysosomal pathway. *eLife* **6**, e31268 (2017).
15. Ma, T. et al. Low-dose metformin targets the lysosomal AMPK pathway through PEN2. *Nature* https://doi.org/10.1038/s41586-022-04431-8 (2022).

16. Zong, Y. et al. Hierarchical activation of compartmentalized pools of AMPK depends on severity of nutrient or energy stress. *Cell Res.* **29**, 460–473 (2019).
17. Chia, I. V. & Costantini, F. Mouse axin and axin2/conductin proteins are functionally equivalent in vivo. *Mol. Cell. Biol.* **25**, 4371–4376 (2005).
18. Li, J. et al. *AXIN1* knockout does not alter AMPK/mTORC1 regulation and glucose metabolism in mouse skeletal muscle. *J. Physiol.* **599**, 3081–3100 (2021).
19. Morris, A. J. & Tolan, D. R. Site-directed mutagenesis identifies aspartate 33 as a previously unidentified critical residue in the catalytic mechanism of rabbit aldolase A. *J. Biol. Chem.* **268**, 1095–1100 (1993).
20. Sun-Wada, G. H. et al. A proton pump ATPase with testis-specific E1-subunit isoform required for acrosome acidification. *J. Biol. Chem.* **277**, 18098–18105 (2002).
21. Caron, C., Boyault, C. & Khochbin, S. Regulatory cross-talk between lysine acetylation and ubiquitination: role in the control of protein stability. *Bioessays* **27**, 408–415 (2005).
22. Mostoslavsky, R. et al. Genomic instability and aging-like phenotype in the absence of mammalian SIRT6. *Cell* **124**, 315–329 (2006).
23. Moynihan, K. A. et al. Increased dosage of mammalian Sir2 in pancreatic β cells enhances glucose-stimulated insulin secretion in mice. *Cell Metab.* **2**, 105–117 (2005).
24. Schwer, B., North, B. J., Frye, R. A., Ott, M. & Verdin, E. The human silent information regulator (Sir)2 homologue hSIRT3 is a mitochondrial nicotinamide adenine dinucleotide-dependent deacetylase. *J. Cell Biol.* **158**, 647–657 (2002).
25. Michishita, E., Park, J. Y., Burneskis, J. M., Barrett, J. C. & Horikawa, I. Evolutionarily conserved and nonconserved cellular localizations and functions of human SIRT proteins. *Mol. Biol. Cell* **16**, 4623–4635 (2005).
26. Park, J. et al. SIRT5-mediated lysine desuccinylation impacts diverse metabolic pathways. *Mol. Cell* **50**, 919–930 (2013).
27. Imai, S., Armstrong, C. M., Kaeberlein, M. & Guarente, L. Transcriptional silencing and longevity protein Sir2 is an NAD-dependent histone deacetylase. *Nature* **403**, 795–800 (2000).
28. Zhang, F., Wang, L., Ko, E. E., Shao, K. & Qiao, H. Histone deacetylases SRT1 and SRT2 interact with ENAP1 to mediate ethylene-induced transcriptional repression. *Plant Cell* **30**, 153–166 (2018).
29. Michishita, E. et al. SIRT6 is a histone H3 lysine 9 deacetylase that modulates telomeric chromatin. *Nature* **452**, 492–496 (2008).
30. Hubbard, B. P. et al. Evidence for a common mechanism of SIRT1 regulation by allosteric activators. *Science* **339**, 1216–1219 (2013).
31. Canto, C. et al. AMPK regulates energy expenditure by modulating NAD^+ metabolism and SIRT1 activity. *Nature* **458**, 1056–1060 (2009).
32. Boggon, T. J., Shan, W. S., Santagata, S., Myers, S. C. & Shapiro, L. Implication of tubby proteins as transcription factors by structure-based functional analysis. *Science* **286**, 2119–2125 (1999).
33. Kerek, E. M. et al. A conserved acetylation switch enables pharmacological control of tubby-like protein stability. *J. Biol. Chem.* **296**, 100073 (2021).
34. Makishima, M. et al. Identification of a nuclear receptor for bile acids. *Science* **284**, 1362–1365 (1999).
35. Parks, D. J. et al. Bile acids: natural ligands for an orphan nuclear receptor. *Science* **284**, 1365–1368 (1999).
36. Wang, H., Chen, J., Hollister, K., Sowers, L. C. & Forman, B. M. Endogenous bile acids are ligands for the nuclear receptor FXR/BAR. *Mol. Cell* **3**, 543–553 (1999).
37. Otte, K. et al. Identification of farnesoid X receptor β as a novel mammalian nuclear receptor sensing lanosterol. *Mol. Cell. Biol.* **23**, 864–872 (2003).
38. Staudinger, J. L. et al. The nuclear receptor PXR is a lithocholic acid sensor that protects against liver toxicity. *Proc. Natl Acad. Sci. USA* **98**, 3369–3374 (2001).
39. Xie, W. et al. An essential role for nuclear receptors SXR/PXR in detoxification of cholestatic bile acids. *Proc. Natl Acad. Sci. USA* **98**, 3375–3380 (2001).
40. Han, S. & Chiang, J. Y. Mechanism of vitamin D receptor inhibition of cholesterol 7α-hydroxylase gene transcription in human hepatocytes. *Drug Metab. Dispos.* **37**, 469–478 (2009).
41. Zhang, J., Huang, W., Qatanani, M., Evans, R. M. & Moore, D. D. The constitutive androstane receptor and pregnane X receptor function coordinately to prevent bile acid-induced hepatotoxicity. *J. Biol. Chem.* **279**, 49517–49522 (2004).
42. Saini, S. P. et al. A novel constitutive androstane receptor-mediated and CYP3A-independent pathway of bile acid detoxification. *Mol. Pharmacol.* **65**, 292–300 (2004).
43. Lehmann, J. M. et al. Activation of the nuclear receptor LXR by oxysterols defines a new hormone response pathway. *J. Biol. Chem.* **272**, 3137–3140 (1997).
44. Studer, E. et al. Conjugated bile acids activate the sphingosine-1-phosphate receptor 2 in primary rodent hepatocytes. *Hepatology* **55**, 267–276 (2012).
45. Sheikh Abdul Kadir, S. H. et al. Bile acid-induced arrhythmia is mediated by muscarinic M_2 receptors in neonatal rat cardiomyocytes. *PLoS ONE* **5**, e9689 (2010).
46. Raufman, J. P. et al. Selective interaction of bile acids with muscarinic receptors: a case of molecular mimicry. *Eur. J. Pharmacol.* **457**, 77–84 (2002).
47. Pongracz, J., Clark, P., Neoptolemos, J. P. & Lord, J. M. Expression of protein kinase C isoenzymes in colorectal cancer tissue and their differential activation by different bile acids. *Int. J. Cancer* **61**, 35–39 (1995).
48. Faubion, W. A. et al. Toxic bile salts induce rodent hepatocyte apoptosis via direct activation of Fas. *J. Clin. Invest.* **103**, 137–145 (1999).
49. Ferrari, C., Macchiarulo, A., Costantino, G. & Pellicciari, R. Pharmacophore model for bile acids recognition by the FPR receptor. *J. Comput. Aided Mol. Des.* **20**, 295–303 (2006).
50. Reinehr, R., Becker, S., Wettstein, M. & Haussinger, D. Involvement of the Src family kinase yes in bile salt-induced apoptosis. *Gastroenterology* **127**, 1540–1557 (2004).
51. Maruyama, T. et al. Identification of membrane-type receptor for bile acids (M-BAR). *Biochem. Biophys. Res. Commun.* **298**, 714–719 (2002).
52. Repa, J. J. et al. Regulation of mouse sterol regulatory element-binding protein-1c gene (*SREBP-1c*) by oxysterol receptors, LXRα and LXRβ. *Genes Dev.* **14**, 2819–2830 (2000).
53. Svensson, S. et al. Crystal structure of the heterodimeric complex of LXRα and RXRβ ligand-binding domains in a fully agonistic conformation. *EMBO J.* **22**, 4625–4633 (2003).
54. Xie, W. et al. Reciprocal activation of xenobiotic response genes by nuclear receptors SXR/PXR and CAR. *Genes Dev.* **14**, 3014–3023 (2000).
55. Cao, D. et al. Structural basis for allosteric, substrate-dependent stimulation of SIRT1 activity by resveratrol. *Genes Dev.* **29**, 1316–1325 (2015).
56. Dai, H. et al. Crystallographic structure of a small molecule SIRT1 activator-enzyme complex. *Nat. Commun.* **6**, 7645 (2015).
57. Mukhopadhyay, A., Deplancke, B., Walhout, A. J. & Tissenbaum, H. A. *C. elegans* tubby regulates life span and fat storage by two independent mechanisms. *Cell Metab.* **2**, 35–42 (2005).
58. Hamilton, J. P. et al. Human cecal bile acids: concentration and spectrum. *Am. J. Physiol. Gastrointest. Liver Physiol.* **293**, G256–G263 (2007).
59. Smith, B. C., Hallows, W. C. & Denu, J. M. A continuous microplate assay for sirtuins and nicotinamide-producing enzymes. *Anal. Biochem.* **394**, 101–109 (2009).
60. Borra, M. T., Langer, M. R., Slama, J. T. & Denu, J. M. Substrate specificity and kinetic mechanism of the Sir2 family of NAD^+-dependent histone/protein deacetylases. *Biochemistry* **43**, 9877–9887 (2004).
61. Laurent, G. et al. SIRT4 coordinates the balance between lipid synthesis and catabolism by repressing malonyl CoA decarboxylase. *Mol. Cell* **50**, 686–698 (2013).
62. Pan, P. W. et al. Structure and biochemical functions of SIRT6. *J. Biol. Chem.* **286**, 14575–14587 (2011).
63. Cohen, H. Y. et al. Calorie restriction promotes mammalian cell survival by inducing the SIRT1 deacetylase. *Science* **305**, 390–392 (2004).
64. Wang, F., Nguyen, M., Qin, F. X. & Tong, Q. SIRT2 deacetylates FOXO3a in response to oxidative stress and caloric restriction. *Aging Cell* **6**, 505–514 (2007).
65. Hirschey, M. D. et al. SIRT3 regulates mitochondrial fatty-acid oxidation by reversible enzyme deacetylation. *Nature* **464**, 121–125 (2010).
66. Someya, S. et al. Sirt3 mediates reduction of oxidative damage and prevention of age-related hearing loss under caloric restriction. *Cell* **143**, 802–812 (2010).
67. Yang, H. et al. Nutrient-sensitive mitochondrial NAD^+ levels dictate cell survival. *Cell* **130**, 1095–1107 (2007).
68. Nakagawa, T., Lomb, D. J., Haigis, M. C. & Guarente, L. SIRT5 deacetylates carbamoyl phosphate synthetase 1 and regulates the urea cycle. *Cell* **137**, 560–570 (2009).
69. Kanfi, Y. et al. SIRT6 protects against pathological damage caused by diet-induced obesity. *Aging Cell* **9**, 162–173 (2010).
70. Shin, J. et al. SIRT7 represses Myc activity to suppress ER stress and prevent fatty liver disease. *Cell Rep.* **5**, 654–665 (2013).
71. Xie, X. S. Reconstitution of ATPase activity from individual subunits of the clathrin-coated vesicle proton pump. The requirement and effect of three small subunits. *J. Biol. Chem.* **271**, 30980–30985 (1996).
72. Goldberg, A. A. et al. Chemical genetic screen identifies lithocholic acid as an anti-aging compound that extends yeast chronological life span in a TOR-independent manner, by modulating housekeeping longevity assurance processes. *Aging* **2**, 393–414 (2010).
73. Masoro, E. J., McCarter, R. J., Katz, M. S. & McMahan, C. A. Dietary restriction alters characteristics of glucose fuel use. *J. Gerontol.* **47**, B202–B208 (1992).
74. Ham, D. J. et al. Distinct and additive effects of calorie restriction and rapamycin in aging skeletal muscle. *Nat. Commun.* **13**, 2025 (2022).
75. Most, J. & Redman, L. M. Impact of calorie restriction on energy metabolism in humans. *Exp. Gerontol.* **133**, 110875 (2020).

Methods

Data reporting

The chosen sample sizes were similar to those used in this field: $n = 4–5$ samples were used to evaluate the levels of metabolites in serum[76,77], cells[10,78], tissues[10,16,78,79], nematodes[80–82] and flies[83–85]; $n = 4–5$ samples to determine OCRs in tissues[78,86] and nematodes[87–89]; $n = 3–4$ samples to determine the mRNA levels of a specific gene[11]; $n = 2–6$ samples to determine the expression levels and phosphorylation levels of a specific protein[11]; $n = 20–33$ cells to determine AXIN translocation and lysosomal pH[10,12]; $n = 4$ replicates to determine SIRT1 activity[30,90]; $n = 200$ worms to determine lifespan[91–93]; $n = 60$ worms to determine healthspan[94–96]; $n = 200$ flies, male or female, to determine lifespan[97–99]; $n = 60$ flies, male or female, to determine healthspan[100–102]; $n = 4–8$ mice for energy expenditure (EE) and respiratory quotient (RQ) calculations[78]; $n = 5$ mice for body composition anaylses[78]; $n = 6$ mice for muscle fibre type analyses[74,103,104]; $n = 10–11$ mice for running duration analyses[12,78]; and $n = 35–38$ mice for grasp strength analyses[78]. No statistical methods were used to predetermine the sample sizes. All experimental findings were repeated as stated in the figure legends, and all additional replication attempts were successful. For animal experiments, mice, nematodes and flies were housed under the same condition or place. For cell experiments, cells of each genotype were cultured in the same CO_2 incubator and were seeded in parallel. Each experiment was designed and performed along with proper controls, and samples for comparison were collected and analysed under the same conditions. Randomization was applied wherever possible. For example, during MS analyses (for metabolites and proteins), samples were processed and analysed in random order. For animal experiments, sex-matched (for mice and flies) and age-matched littermate animals in each genotype were randomly assigned to LCA or vehicle treatments. In cell experiments, cells of each genotype were parallel seeded and randomly assigned to different treatments. Otherwise, randomization was not performed. For example, when performing IB, samples needed to be loaded in a specific order to generate the final figures. Blinding was applied wherever possible. For example, samples, cages or agar plates or vials during sample collection and processing were labelled as code names that were later revealed by the individual who picked and treated the animals or cells but did not participate in sample collection or processing until assessing the outcome. Similarly, during microscopy data collection and statistical analyses, the fields of view were chosen on a random basis and were often performed by different operators, thereby preventing potentially biased selection for desired phenotypes. Otherwise, blinding was not performed, such as the measurement of OCR and SIRT1 activity in vitro, as different reagents were added for particular reactions.

Mouse strains

WT C57BL/6J mice (000664) were obtained from the Jackson Laboratory. *AXIN*$^{F/F}$ (*AXIN1*$^{F/F}$) and *LAMTOR1*$^{F/F}$ mice were generated and validated as previously described[11]. *AMPKA1*$^{F/F}$ (014141) and *AMPKA2*$^{F/F}$ mice (014142) were obtained from the Jackson Laboratory, provided by S. Morrison, and *PKCZ*$^{F/F}$ mice (024417) were provided by R. Huganir. *AXIN2*$^{F/F}$ mice (T008456) were purchased from Shanghai Model Organisms Center. The muscle-specific *LAMTOR1*-knockout (*LAMTOR1*-MKO) mice and the liver-specific *LAMTOR1*-knockout (*LAMTOR1*-LKO) mice were generated by crossing *LAMTOR1*$^{F/F}$ mice with *Mck-cre* and *Alb-cre* mice as previously described and validated[11], *AXIN*-LKO mice were generated by crossing *AXIN*$^{F/F}$ mice with *Alb-cre* mice (validated in ref. 13), and *AXIN1/2*-MKO mice were generated by crossing *AXIN1/2*$^{F/F}$ mice with *HSA-creERT2* mice (025750; Jackson Laboratory). AXIN1 and AXIN2 from *AXIN1/2*$^{F/F}$, *HSA-creERT2* mice were removed from muscle by intraperitoneally injecting mice with tamoxifen (dissolved in corn oil) at 200 mg kg^{-1}, 4 times a week for 1 week. *TULP3*$^{F/F}$ mice (S-CKO-17725) were purchased from Cyagen.

WT V1E1 or V1E1(3KR) was introduced to the muscle of *AMPKA1/2*$^{F/F}$ mice through the *Rosa26*-LSL(*loxP*-Stop-*loxP*) system[105], followed by crossing with *HSA-creERT2* mice. The removal of the muscular *AMPK* gene and the LSL cassette ahead of introduced V1E1 and V1E1(3KR) (to trigger the expression of introduced V1E1) was achieved by intraperitoneally injecting mice with tamoxifen. To introduce V1E1 or V1E1(3KR) into *AMPKA1/2*$^{F/F}$ mice, cDNA fragments encoding V1E1 or V1E1(3KR) were inserted into a *Rosa26*-CTV vector[106], followed by purification of the plasmids using the CsCl density gradient ultracentrifugation method. Next, 100 μg plasmid was diluted with 500 μl di-distilled water, followed by concentrating by centrifugation at 14,000*g* at room temperature in a 30-kDa cut-off filter (UFC503096, Millipore) to 50 μl solution. The solution was diluted with 450 μl di-distilled water, followed by another two rounds of dilution–concentration cycles. The plasmid was then mixed with 50 μl di-distilled water to a final volume of 100 μl, followed by mixing with 10 μl sodium acetate solution (3 M stock concentration, pH 5.2). This sample was then mixed with 275 μl ethanol, followed by incubating at room temperature for 30 min to precipitate the plasmid. The precipitated plasmid was collected by centrifugation at 16,000*g* for 10 min at room temperature, followed by washing with 800 μl of 75% (v/v) ethanol (in di-distilled water) twice. After evaporating the ethanol by placing the plasmid next to an alcohol burner lamp for 10 min, the plasmid was dissolved in 100 μl nuclease-free water. The plasmid, along with *SpCas9* mRNA and the sgRNAs against the mouse *Rosa26* locus, was microinjected into in vitro fertilization (IVF) embryos of *AMPKA1/2*$^{F/F}$ mice. To generate the *SpCas9* mRNA, 1 ng pcDNA3.3-hCas9 plasmid (constructed by inserting the *Cas9* fragment released from Addgene 41815 (ref. 107), into the pcDNA3.3 vector; diluted to 1 ng μl^{-1}) was amplified using a Phusion High-Fidelity DNA Polymerase kit on a thermocycler (T100, Bio-Rad) with the following programs: pre-denaturing at 98 °C for 30 s; denaturing at 98 °C for 10 s, annealing at 68 °C for 25 s, then extending at 72 °C for 2 min in each cycle; and final extending at 72 °C for 2 min; cycle number: 33. The following primer pairs were used: 5′-CACCGACTGAGCTCCTTAAG-3′ and 5′-TAGTCAAGCTTCCATGGCTCGA-3′. The PCR product was then purified using a MinElute PCR Purification kit following the manufacturer's instructions. The purified *SpCas9* PCR product was subjected to in vitro transcription using a mMESSAGE mMACHINE T7 Transcription kit following the manufacturer's instruction (with minor modifications). In brief, 5.5 μl (300 ng μl^{-1}) of *SpCas9* PCR product as the template was mixed with 10 μl of 2× NTP/ARCA solution, 2 μl of 10× T7 reaction buffer, 0.5 μl RNase inhibitor, 2 μl T7 enzyme mix and 4.5 μl nuclease-free water, followed by incubating at 37 °C for 2 h. This sample was then mixed with 1 μl Turbo DNase, followed by incubating at 37 °C for 20 min to digest the template. The sample was then mixed with 20 μl of 5× *E*-PAP buffer, 10 μl of 25 mM $MnCl_2$, 10 μl of 10 mM ATP, 4 μl *E*-PAP enzyme and 36 μl nuclease-free water, followed by incubating at 37 °C for 20 min for poly(A) tailing. The tailed product was then purified using a MEGAclear Transcription Clean-Up kit following the manufacturer's instructions (with minor modifications). In brief, 20 μl tailed RNA was mixed with 20 μl elution solution, followed by mixing with 350 μl binding solution concentrate. Next, 250 μl ethanol was added to the mixture, followed by passing it through a filter cartridge and washing with 250 μl wash solution twice. The RNA was then eluted with 50 μl pre-warmed (at 90 °C) elution solution. The sgRNAs were prepared as for *SpCas9* mRNA preparation, except that the gRNA cloning vector (Addgene, 41824, ref. 107) was used as the template, and the following program was used: pre-denaturing at 98 °C for 30 s; denaturing at 98 °C for 10 s, annealing at 60 °C for 25 s, then extending at 72 °C for 20 s in each cycle; and final extending at 72 °C for 2 min; cycle number: 33. The following primers were used: 5′-GAAATTAATACGACTCACTATAGGCGCCCATCTTCTAGAAAGACGTTTTAGAGCTAGAAATAGC-3′, and 5′-AAAAGCACCGACTCGGTGCC-3′. In addition, in vitro transcription was performed using a MEGAshortscript T7 Transcription kit, in which a mixture containing 7.5 μl (100 ng μl^{-1}) purified PCR product, 2 μl T7

10× T7 reaction buffer, 2 μl T7 ATP solution, 2 μl T7 CTP solution, 2 μl T7 GTP solution, 2 μl T7 UTP solution, 0.5 μl RNase inhibitor, 2 μl T7 enzyme mix and 7.5 μl nuclease-free water was prepared. Also, the poly(A) tailing assay was not performed.

The prepared *Rosa26*-CTV-V1E1, *SpCas9* mRNA and *Rosa26* sgRNA plasmids were then microinjected into each zygote from *AMPKA1/2*$^{F/F}$ mice. To prepare the zygotes, *AMPKA1/2*$^{F/F}$ mice (according to ref. 108, with modifications) were first subjected to IVF. In brief, 4-week-old *AMPKA1/2*$^{F/F}$ female mice were intraperitoneally injected with pregnant mare's serum gonadotrophin (PMSG) at a dose of 10 U per mouse. At 46 h after PMSG injection, 10 U per mouse of human chorionic gonadotrophin (hCG) was intraperitoneally injected. At 12 h after hCG injection, oocytes from the oviducts of female mice, along with sperms from cauda epididymides and vasa deferentia of 16-week-old, proven stud *AMPKA1/2*$^{F/F}$ male mice, were isolated. To isolate oocytes, oviducts were briefly left on a filter paper, followed by incubating in a human tubal fluid medium (HTF)–GSH drop on an IVF dish (prepared by placing 200 μl HTF solution supplemented with 125 mM GSH on a 35-mm dish to form a drop, followed by covering the drop with mineral oil and pre-balancing in a humidified incubator containing 5% CO_2 at 37 °C for 0.5 h before use). The ampulla was then torn down by forceps, and the cumulus oocyte masses inside were collected and transferred to another HTF–GSH drop. To isolate sperm, cauda epididymides and vasa deferentia were briefly left on a filter paper, followed by penetrating with a 26 G needle on the cauda epididymides 5 times. Sperm were then released onto a HTF drop on a sperm capacitation dish (prepared by placing 200 μl HTF solution on a 35-mm dish to form a drop, followed by covering the drop with mineral oil and pre-balancing in a humidified incubator containing 5% CO_2 at 37 °C for 12 h before use) by slightly pressing or squeezing the cauda epididymides, followed by incubation in a humidified incubator containing 5% CO_2 at 37 °C for 0.5 h. The capacitated, motile sperm (located on the edge of each HTF drop) were then collected, followed by adding them to the oocyte masses soaked in the HTF–GSH drop, 8 μl per drop. The IVF dishes containing oocyte masses and sperm were then cultured in a humidified incubator containing 5% CO_2 at 37 °C for 4 h, followed by collecting and washing oocytes in a KSOM drop (freshly prepared by placing 20 μl KSOM medium on a 35-mm dish to form a drop, followed by covering the drop with mineral oil and pre-balancing in a humidified incubator containing 5% CO_2 at 37 °C for 0.5 h) twice. The oocytes were then cultured in a HTF–GSH drop on an IVF dish for another 12 h in a humidified incubator containing 5% CO_2 at 37 °C. The presumptive zygotes (in which two pronuclei and an extruded, second polar body could be observed) were then picked up. Next, 10 pl DNA mixture containing *Rosa26*-CTV-V1E1 plasmid (20 ng μl^{-1} final concentration), *SpCas9* mRNA (120 ng μl^{-1} final concentration) and *Rosa26* sgRNA (100 ng μl^{-1}) was microinjected into each of the zygotes and were cultured in KSOM medium at 37 °C in a humidified incubator containing 5% CO_2 for 16 h. Zygotes (20 per mouse) at the 2-cell stage were picked and transplanted into pseudo-pregnant ICR female mice (8–10 weeks old, >26 g; prepared by breeding the in-oestrus female with a 14-week-old, vasectomized male at 1 day before the transplantation), and offspring carrying the LSL-V1E1 or LSL-V1E1(3KR) allele were further outcrossed 6 times to C57BL/6 mice before crossing with *HSA-creERT2* mice. Mice were validated by genotyping. For genotyping the *Rosa26* locus, the following programs were used: pre-denaturing at 98 °C for 300 s; denaturing at 95 °C for 30 s, annealing at 64 °C for 30 s, then extending at 72 °C for 45 s in each cycle for 5 cycles; denaturing at 95 °C for 30 s, annealing at 61 °C for 30 s, then extending at 72 °C for 45 s in each cycle for 5 cycles; denaturing at 95 °C for 30 s, annealing at 58 °C for 30 s, then extending at 72 °C for 45 s in each cycle for 5 cycles; denaturing at 95 °C for 30 s, annealing at 55 °C for 30 s, then extending at 72 °C for 45 s in each cycle for 5 cycles; and final extending at 72 °C for 10 min. For genotyping other genes and elements, the following programs were used: pre-denaturing at 95 °C for 300 s; denaturing at 95 °C for 30 s, annealing at 58 °C for 40 s, then extending at 72 °C for 30 s in each cycle; and final extending at 72 °C for 10 min; cycle number: 35. The following primers were used: 5′-CAGGTAGGGCAGGAGTTGG-3′ and 5′-TTTGCCCCCTCCATATAACA-3′ for *HSA-cre*; 5′-AGTGGCCTCTTCCAGAAATG-3′ and 5′-TGCGACTGTG TCTGATTTCC-3′ for the control of *HSA-cre*; 5′-CCCACCATCACTCCATC TCT-3′ and 5′-AGCCTGCTTGGCACACTTAT-3′ for *Prkaa1*, 5′-GCAGGC GAATTTCTGAGTTC-3′ and 5′-TCCCCTTGAACAAGCATACC-3′ for *Prkaa2*, 5′-TCTCCCAAAGTCGCTCTGAG-3′, 5′-AAGACCGCGAAGAGTTTGTC-3′, and 5′-ATGCTCTGTCTAGGGGTTGG-3′ for *Rosa26*, 5′-CCACACAGGC ATAGAGTGTCT-3′ and 5′-TTTGCACAAGCCGACCTTTC-3′ for the 5′ terminus of *Rosa26-V1E1* (the presence of *Rosa26-V1E1* recombination), and 5′-CTCCACACAGGCATAGAGTGT-3′ and 5′-TTGCACAAGC CGACCTTTCT-3′ for the 3′ terminus of *Rosa26-V1E1*, 5′-AGAGAATTCGG ATCCATGGCTCTCAGCGATGCTGA-3′ and 5′-CTTCCATGGCTCGAG GTCCAAAAACTTCCTGTTGGC-3′ for generating PCR products for sequencing V1E1.

To generate mice with muscular knockout of *Tulp3* and with re-introduction of TULP3 or TULP3(4G), MYC-tagged TULP3 or TULP3(4G) was introduced to *TULP3*$^{F/F}$ mice under the *Rosa26*-LSL system as described above, followed by crossing with *HSA-creERT2* mice and intraperitoneal injection of tamoxifen into the mice. Mice were validated by genotyping using the programs and primers described above, except that primers 5′-TTAAACTAACCAGGGTCTCACTGT-3′ and 5′-GTT CCAGTACAATGGAAAGGAAAGG-3′ were used for *Tulp3*, 5′- CCACA CAGGCATAGAGTGTCT-3′ and 5′- AGCTTAGCCTGTCGCATCTT-3′ were used for *Rosa26-TULP3*, and 5′- AGAGAATTCGGATCCATGGAGGC TTCGCGCTGC-3′ and 5′- CTTCCATGGCTCGAGTTCACACGCCAGCTTA CTGT-3′ were used for generating PCR products for sequencing *Tulp3*.

CR and fasting treatments of mice

Protocols for all mouse experiments were approved by the Institutional Animal Care and the Animal Committee of Xiamen University (XMULAC20180028 and XMULAC20220050). Unless stated otherwise, mice were housed with free access to water and standard diet (65% carbohydrate, 11% fat, 24% protein) under specific pathogen-free conditions. The light was on from 8:00 to 20:00, with the temperature kept at 21–24 °C and humidity at 40–70%. Only male mice were used in the study, and male littermate controls were used throughout.

Mice were individually caged for 1 week before each treatment. For fasting, the diet was withdrawn from the cage at 17:00, and mice were killed at indicated time points by cervical dislocation. For CR, each mouse was fed 2.5 g standard diet (approximately 70% of ad libitum food intake for a mouse at 4 months old and older) at 17:00 each day.

The following ages of mice were used for analyses: (1) for IB and the measurement of adenylates, WT mice aged 5 weeks (treated with LCA for 1 week starting from 4 weeks old), and *AXIN*-LKO, *AXIN*-MKO, *LAMTOR1*-LKO and *LAMTOR1*-MKO mice aged 7 weeks (treated with LCA for 1 week starting from 6 weeks old); (2) for immunohistochemistry (IHC), V1E1(3KR)-expressing mice and WT V1E1-expressing mice aged 18 months (into which tamoxifen was injected at 16 months old, and treated with LCA for 1 month starting from 17 months old), and TULP3(4G)-expressing mice and WT TULP3-expressing mice aged 20.5 months (into which tamoxifen was injected at 16 months old and subjected to CR for 3.5 months starting from 17 months old); (3) for determination of the rejuvenating effect of LCA in mice, V1E1(3KR)-expressing mice and WT V1E1-expressing mice aged 18 months (into which tamoxifen was injected at 16 months old and treated with LCA for 1 month starting from 17 months old), and TULP3(4G)-expressing mice and WT TULP3-expressing mice aged 20.5 months (into which tamoxifen was injected at 16 months old and subjected to CR for 3.5 months starting from 17 months old); and (4) for all the other experiments, mice aged 4 weeks.

Formulation of LCA

LCA was formulated as previously described[1]. In brief, for cell-based experiments, LCA powder was dissolved in DMSO to a stock

concentration of 500 mM and was aliquoted and stored at −20 °C. The solution was placed at room temperature for 10 min (until no precipitate was visible) before adding to the culture medium. Note that any freeze–thaw cycle was not allowed to avoid the re-crystallization of LCA (which otherwise formed sheet-like, insoluble crystals) in the stock solution.

For mouse experiments, LCA was coated with (2-hydroxypropyl)-β-cyclodextrin before given to animals. To coat LCA, LCA powder was dissolved in 100 ml methanol to a concentration of 0.01 g ml^{-1}, followed by mixing with 308 ml (2-hydroxypropyl)-β-cyclodextrin solution (by dissolving (2-hydroxypropyl)-β-cyclodextrin in 30% (v/v, in water) methanol to 0.04 g ml^{-1}, followed by a 30 min of sonication). The control vehicle was similarly prepared but with no LCA added to the (2-hydroxypropyl)-β-cyclodextrin solution. After evaporating at 50 °C and 90 r.p.m. in a rotary evaporator (Rotavator R-300, Vacuum Pump V-300, BUCHI), the coated powder was stored at 4 °C for no more than 2 weeks and was freshly dissolved in drinking water to 1 g l^{-1} before given to mice.

For nematode experiments, LCA at desired concentrations was freshly dissolved in DMSO and was added to warm (cooled to approximately 60 °C after autoclaving) nematode growth medium[109] (NGM; containing 0.3% (w/v) NaCl, 0.25% (w/v) bacteriological peptone, 1 mM $CaCl_2$, 1 mM $MgSO_4$, 25 mM KH_2PO_4-K_2HPO_4, pH 6.0, 0.02% (w/v) streptomycin and 5 μg ml^{-1} cholesterol). The medium was used to make NGM plates by adding 1.7% (w/v) agar. The plates were stored at 20 °C for no more than 3 days.

For fly experiments, LCA was coated and dissolved in water as for the mouse experiments and was added to Bloomington *Drosophila* Stock Center (BDSC) standard cornmeal medium[110] (for regular culture). The BDSC standard cornmeal medium was prepared as previously described but with minor modifications[110]. In brief, 60.5 g dry yeast, 35 g soy flour, 255.5 g cornmeal, 20 g agar and 270 ml corn syrup were mixed with 3,500 ml water in a stockpot. The mixture was thoroughly stirred using a long-handled soup spoon and then boiled, during which lumps formed were pressed out using the back of the spoon. After cooling to approximately 60 °C, 16.8 ml propionic acid was added to the medium followed by stirring with the spoon. The medium was then dispensed into culture vials (6 ml each). The vials of medium were covered with a single-layer gauze, followed by gentle blowing with air using a fan at room temperature overnight. Next, 100 μl LCA solution (dissolved in (2-hydroxypropyl)-β-cyclodextrin as for mice) at the desired concentration was then layered (added dropwise) onto the surface of the medium of each vial, followed by blowing with breeze from the fan for another 8 h at room temperature. The vials of medium were kept at 4 °C (for no more than 3 days) before the experiment.

Determination of mouse running capacity and grip strength

The maximal running capacity was determined as previously described[12,111], but with minor modifications. In brief, mice were trained on a Rodent Treadmill NG (UGO Basile, 47300) for 3 days during the normal light–dark cycle, and tests were performed during the dark period. Before the experiment, mice were fasted for 2 h. The treadmill was set at a 5° incline, and the speed of the treadmill was set to increase in a ramp mode (commencing at a speed of 5 m min^{-1} followed by an increase to a final speed of 25 m min^{-1} within 120 min). Mice were considered to be exhausted and removed from the treadmill following 5 or more shocks (0.1 mA) per min for 2 consecutive minutes. The distances travelled were recorded as the running capacity.

Grip strength was determined using a grip strength meter (Ugo Basile, 47200) following a previously described protocol[96]. In brief, the mouse was held by its tail and lowered ('landed') until the forelimb or all four limbs grasped the T-bar connected to a digital force gauge. The mouse was further lowered to the extent that the body was horizontal to the apparatus and was then slowly, steadily drawn away from the T-bar until the forelimb or all four limbs were removed from the bar, which gave rise to the peak force in grams. Each mouse was tested 5 times with 5-min intervals between measurements.

Determination of body composition

Lean and fat body mass were measured using quantitative magnetic resonance (EchoMRI-100H Analyzer; Echo Medical Systems) as previously described[78]. In brief, the system was calibrated with an oil standard before measurement. Mice were individually weighed and inserted into a restrainer tube and were immobilized by gently inserting a plunger. The mouse was then positioned so that it curled up like a doughnut, with its head against the end of the tube. The body composition of each mouse was measured with three repeated runs, and the average values were taken for further analysis.

Determination of EE

Mouse EE was determined using a metabolic cage system (Promethion Line, CAB-16-1-EU; Sable Systems International) as previously described[112]. In brief, the system was maintained in a condition identical to that for housing mice. Each metabolic cage in the 16-cage system consisted of a cage with standard bedding, a food hopper and a water bottle connected to load cells for continuous monitoring. To minimize stress to the new environment, mice were acclimated (by individual housing in the gas-calibrated chamber) for 1 week before data collection. Mice treated with LCA or vehicle control were randomly assigned and housed to prevent systematic errors in measurement. Body weights and fat proportion of mice were determined before and after the acclimation period, and the food intake and water intake were measured daily. Mice that did not acclimate to the metabolic cage (for example, they resisted eating or drinking) were removed from the study. Data acquisition (5-min intervals in each cage) and instrument control were performed using MetaScreen software (v.2.3.15.12, Sable Systems) and raw data were processed using Macro Interpreter (v.2.32, Sable Systems). Ambulatory activity and position were monitored using *xyz* beam arrays with a beam spacing of 0.25 cm (beam breaks), and the mouse distance walked within the cage was calculated accordingly. Respiratory gases were measured using a GA-3 gas analyser (Sable Systems) equipped with a pull-mode, negative-pressure system. Air flow was measured and controlled using a FR-8 (Sable Systems), with a set flow rate of 2,000 ml min^{-1}. Oxygen consumption (VO_2) and carbon dioxide production (VCO_2) are reported in ml min^{-1} values. Water vapour was measured continuously, and its dilution effect on O_2 and CO_2 was compensated mathematically in the analysis stream. EE was calculated using kcal $h^{-1} = 60 \times (0.003941 \times VO_2 + 0.001106 \times VCO_2)$ (Weir equation). Differences in average EE were analysed by analysis of covariance using body weight as the covariate. The RQ was calculated as VCO_2/VO_2.

Histology

Muscle fibre types were determined as previously described[74,113]. In brief, muscle tissue samples were excised, followed by freezing in isopentane (pre-chilled in liquid nitrogen) for 2 min (until they appeared chalky white). The tissue samples were then quickly transferred to embedding moulds containing OCT compound and were frozen in liquid nitrogen for another 10 min. The embedded tissue samples were then sectioned into 6-μm slices at −20 °C using a CM1950 Cryostat (Leica), followed by fixing in 4% paraformaldehyde for 10 min and washing with running water for 5 min at room temperature. After incubating with PBST (PBS supplemented with 5% (v/v) Triton X-100) for 10 min, the sections were blocked with BSA solution (PBS containing 5% (m/v) BSA) for 30 min at room temperature. Muscle fibres were stained with an antibody against MHCIIb (6 μg ml^{-1}, diluted in BSA solution) overnight at 4 °C, followed by washing with PBS 3 times, 5 min each at room temperature. The sections were then incubated with Alexa Fluor 488-conjugated, goat anti-mouse IgM antibody (1:200 diluted in BSA solution) for 1 h at room temperature in a dark humidified chamber,

followed by washing with PBS for 3 times, 5 min each, incubating in 4% paraformaldehyde for 2 min and then washing with PBS twice, 5 min each, all at room temperature. The sections were then incubated with an antibody against MHCI (6 μg ml^{-1}, diluted in BSA solution) for 3 h at room temperature in a dark humidified chamber, followed by washing with PBS buffer 3 times, 5 min each at room temperature and then incubated with Alexa Fluor 594-conjugated, goat anti-mouse IgG2b antibody (1:200 diluted in BSA solution) for another 1 h at room temperature in a dark humidified chamber, followed by washing with PBS buffer for 3 times, 5 min each at room temperature. After fixing in 4% paraformaldehyde for 2 min and washing with PBS twice, 5 min each at room temperature, the sections were incubated with an antibody against MHCIIa (6 μg ml^{-1}, diluted in BSA solution) for 3 h at room temperature in a dark humidified chamber, followed by washing with PBS buffer 3 times, 5 min each at room temperature and then incubating in Alexa Fluor 647-conjugated goat anti-mouse IgG1 antibody (1:200 diluted in BSA solution) for another 1 h at room temperature in a dark humidified chamber, followed by washing with PBS buffer for 3 times, 5 min each at room temperature. Tissue sections were mounted in 90% glycerol and visualized on a LSM980 microscope (Zeiss). Images were processed and analysed using Zen 3.4 software (Zeiss) and formatted using Photoshop 2023 software (Adobe).

C. elegans strains

Nematodes (hermaphrodites) were maintained on NGM plates spread with *E. coli* OP50 as standard food. All worms were cultured at 20 °C. WT (N2 Bristol) and *sir-2.1* (VC199) strains were obtained from the *Caenorhabditis* Genetics Center, and *sir-2.2* (tm2673) was from the National BioResource Project. All mutant strains were outcrossed six times to N2 before experiments. Unless stated otherwise, worms were maintained on NGM plates spread with *E. coli* OP50 as standard food. The administration of LCA was initiated at the L4 stage.

The *sir-2.1*/*sir-2.2* double-knockout strain was generated by crossing *sir-2.1* knockout with *sir-2.2* knockout strains. Before crossing, *sir-2.1* knockout hermaphrodites were synchronized. Worms were washed off from agar plates with 15 ml M9 buffer (22.1 mM KH_2PO_4, 46.9 mM Na_2HPO_4, 85.5 mM NaCl and 1 mM $MgSO_4$) supplemented with 0.05% (v/v) Triton X-100 per plate, followed by centrifugation at 1,000*g* for 2 min. The worm sediment was suspended with 6 ml M9 buffer containing 50% synchronizing bleaching solution (by mixing 25 ml NaClO solution (5% active chlorine), 8.3 ml of 25% (w/v) NaOH and 66.7 ml M9 buffer for a total of 100 ml), followed by vigorous shaking for 2 min and centrifugation for 2 min at 1,000*g*. The sediment was washed with 12 ml M9 buffer twice, then suspended with 6 ml M9 buffer, followed by rotating at 20 °C, 30 r.p.m. for 12 h. The synchronized worms were then transferred to NGM plates and cultured to the L4 stage, followed by heat-shocking at 28 °C for 12 h. The heat-shocked worms were then cultured at 20 °C for 4 days, and the males were mated with *sir-2.1* knockout hermaphrodites for another 36 h. The mated hermaphrodites were transferred to new NGM plates and allowed to give birth to more *sir-2.1* knockout males for another 4 days at 20 °C. The *sir-2.1* knockout males were then picked and co-cultured with *sir-2.2* knockout hermaphrodites at a 1:2 ratio (for example, 4 males and 8 hermaphrodites on a 10-cm NGM plate) for mating for 36 h at 20 °C, and the mated hermaphrodites (*sir-2.2* knockout) were picked for culturing for another 2 days. The offspring were then picked and were individually cultured on 35-mm NGM plates, followed by being individually subjected to genotyping after egg laying (after culturing for approximately 2 days). For genotyping, individual worms were lysed with 5 μl of single worm lysis buffer (50 mM HEPES, pH 7.4, 1 mM EGTA, 1 mM $MgCl_2$, 100 mM KCl, 10% (v/v) glycerol, 0.05% (v/v) NP-40, 0.5 mM DTT and protease inhibitor cocktail). The lysates were then frozen at −80 °C for 12 h, followed by incubating at 65 °C for 1 h and 95 °C for 15 min on a thermocycler (XP Cycler, Bioer). The lysates were then cooled to room temperature, followed by amplifying genomic DNA on a thermocycler with the following programs: pre-denaturing at 95 °C for 10 min; denaturing at 95 °C for 10 s, then annealing and extending at 60 °C for 30 s in each cycle; cycle number: 35. Primer sequences are as follows: *C. elegans sir-2.1*, 5′-GAATCGGCTCGTTGCAAGTC-3′ and 5′-AGTTGTGGAATGTCATGGATCCT-3′; and *C. elegans sir-2.2*, 5′-TACCGCTCGAAAGATGTGGG-3′ and 5′-CTGGAGCCACGTGTTCTTCT-3′. The offspring generated from *sir-2.1* and *sir-2.2* knockout confirmed individuals were then outcrossed six times to the N2 strain.

The *sir-2.3* and *sir-2.4* genes were then knocked down in the *sir-2.1*/*sir-2.2*-double knockout strain following previously described procedures[15]. In brief, synchronized worms (around the L1 stage) were placed on RNAi plates (NGM containing 1 mg ml^{-1} IPTG and 50 μg ml^{-1} carbenicillin) spread with HT115 *E. coli* stains containing RNAi against *sir-2.3* and *sir-2.4* (well C10 on plate X6, and well K04 on plate I9 from the Ahringer *C. elegans* RNAi Collection) for 2 days. The knockdown efficiency was then examined by determining the levels of *sir-2.3* and *sir-2.4* mRNA levels by qPCR, in which approximately 1,000 worms were washed off from an RNAi plate with 15 ml M9 buffer containing Triton X-100, followed by centrifugation for 2 min at 1,000*g*. The sediment was then washed with 1 ml M9 buffer twice and then lysed with 1 ml of TRIzol. The worms were then frozen in liquid nitrogen, thawed at room temperature and then subjected to repeated freeze–thaw for another two times. The worm lysates were then placed at room temperature for 5 min, then mixed with 0.2 ml chloroform followed by vigorous shaking for 15 s. After 3 min, lysates were centrifuged at 20,000*g* at 4 °C for 15 min, and 450 μl of the aqueous phase (upper layer) was transferred to a new RNase-free centrifuge tube (Biopur, Eppendorf), followed by mixing with 450 μl of isopropanol then centrifuging at 20,000*g* at 4 °C for 10 min. The sediments were washed with 1 ml of 75% ethanol (v/v) followed by centrifugation at 20,000 *g* for 10 min, and then washed with 1 ml anhydrous ethanol followed by centrifugation at 20,000*g* for 10 min. The sediments were then dissolved with 20 μl RNase-free water after the ethanol had evaporated. The dissolved RNA was then reverse-transcribed to cDNA using ReverTra Ace qPCR RT master mix with a gDNA Remover kit, followed by performing real-time qPCR using Maxima SYBR Green/ROX qPCR master mix on a CFX96 thermocycler (Bio-Rad) with the programs as described for genotyping the *sir-2.1*/*2.2* knockout strain. Primer sequences are as follows: *sir-2.3*, 5′-ACTCTCTCGCCTGTGCAAAT-3′ and 5′-ACTTCCAACGATGTCCCAAG-3′; and *sir-2.4*, 5′-GCCGTAAAAAGTTTGAGCCC-3′ and 5′-TTTCCATGCTTTTCGGATT-3′. Data were analysed using CFX Manager software (v.3.1, Bio-Rad). Knockdown efficiency was evaluated according to the CT values obtained.

The *tub-1* knockout nematode strains expressing human TULP3 or TULP3(4G) were established through a three-step strategy as previously described[15], but with minor modifications. (1) TULP3 or TULP3(4G) was first introduced to the N2 strain; (2) such generated strains were then subjected to knockout of the *tub-1* gene; and (3) the *tub-1*-knockout worms were then picked for further outcrossing with the N2 strain. In brief, to generate the N2 strain expressing TULP3 or TULP3(4G), cDNAs were inserted into a pJM1 vector, with GFP as a selection marker, between the Nhe I and Kpn I sites (expressed under control by a *sur-5* promoter), and then injected into the syncytial gonad of the worm (200 ng μl^{-1}, 0.5 μl per worm) following a previously described procedure[15]. The injected worms were then recovered on an NGM plate for 2 days, and the F_1 GFP-expressing hermaphrodites were selected for further culture. The extrachromosomal TULP3 or TULP(S4G) expression plasmid was then integrated into the nematode genome using UV irradiation to establish non-mosaic transgenic strains as previously described[114], but with minor modifications. In brief, 70 TULP3-expressing or TULP3(4G)-expressing worms at the L4 stage were picked and incubated with 600 μl M9 buffer, followed by the addition of 10 μl TMP solution (3 mg ml^{-1} stock concentration in DMSO) and rotating at 30 r.p.m. for 15 min in the dark. Worms were then transferred to a 10-cm NGM plate without OP50 bacteria in the dark,

followed by irradiating with UV at a total dose of 35 J cm^{-2} (exposed for 35 s) on a UV crosslinker (CL-508; UVITEC). The irradiated worms were fed with 1 ml OP50 bacteria at 10^{13} per ml concentration and then cultured at 20 °C for 5 h in the dark, followed by individual culture on a 35-mm NGM plate for 1 week without transferring to any new NGM plate (to ensure that the F_1 generation was under starvation conditions before further selection). The F_1 GFP-expressing hermaphrodites were selected and individually cultured for another 2 days, and the F_2 100% GFP-expressing hermaphrodites were selected for further culture. The genomic sequence encoding *tub-1* was then knocked out from this strain by injecting a mixture of a pDD122 (P*eft-3*::*Cas9* + *ttTi5605* sgRNA) vector carrying sgRNAs targeting *tub-1* (5′-ATAGCTGATCAAAAGTTCTA-3′ for intron 2 and 5′-GAGAGCGGTCAGTGACACGG-3′ for intron 7; inserted into a pDD122 vector with the *ttTi5605* sgRNA sequence replaced), which were designed using the CHOPCHOP website (http://chopchop.cbu.uib.no/), into young adult worms. The F_1 hermaphrodite worms were individually cultured on an NGM plate. After egg laying, worms were lysed using single worm lysis buffer, followed by PCR with the programs as described for genotyping the *sir-2.1/2.2* knockout strain, and the primers 5′-GAGTAATTTTCGGCATTTGTGC-3′ and 5′-CGAGAAGCTCATTTCAAGGTTT-3′ were used. The offspring generated from knockout-confirmed individuals were outcrossed six times to the N2 strain, and the expression levels of TULP3 or TULP3(4G) were examined by IB. Strains expressing TULP3 or TULP3(4G) at similar levels were chosen for further experiments.

Nematode strain (N2) with human V1E1 or V1E1(3KR) expression was constructed as described above, except that cDNAs of human V1E1 or V1E1(3KR) were used, and that the *sur-5* promoter on the pJM1 vector was replaced by the promoter of V1E1 (vha-8) itself (by replacing the sequence between Asc I and Fse I sites with the annealed primer pair 5′-CTGACTGGGCCGGCCCTTAGAGATAGACTGTGGTC-3′ and 5′-CTCTAGAGGCGCGCCGACATTTAATAAAATAATCATTTTTC-3′). The presence of V1E1 or V1E1(3KR) was validated by sequencing using the primer 5′-ATGGCTCTCAGCGATGCTGA-3′.

For all nematode experiments, worms at the L4 stage were used.

Evaluation of lifespan and healthspan in nematodes

To determine the lifespan of nematodes, the worms were first synchronized. Synchronized worms were cultured to the L4 stage before transfer to desired agar plates for determining lifespan. Worms were transferred to new plates every 2 days. Live and dead worms were counted during the transfer. Worms that displayed no movement after gentle touching with a platinum picker were judged as dead. Kaplan–Meier curves were generated using Prism 9 (GraphPad Software), and statistical analysis was performed using SPSS 27.0 (IBM).

The resistance of nematodes to oxidative stress was determined as previously described[94]. In brief, synchronized worms were cultured to the L4 stage, after which LCA was administered. After 2 days of LCA treatment, 20 worms were transferred to a NGM plate containing 15 mM $FeSO_4$. Worms were then cultured at 20 °C, during which the live and dead worms were counted every 1 h.

D. melanogaster strains

All flies were cultured at 25 °C and 60% humidity with a 12-h light–dark cycle. Adult flies were cultured in BDSC standard cornmeal medium (for regular culture) agar diet. Larvae and the crossed fly strains were reared on a semi-defined, rich medium, which was prepared as previously described[115], but with minor modifications. In brief, 10 g agar, 80 g dry yeast, 20 g yeast extract, 20 g peptone, 30 g sucrose, 60 g glucose, 0.5 g $MgSO_4 \cdot 6H_2O$ and 0.5 g $CaCl_2 \cdot 6H_2O$ were dissolved in 1,000 ml di-distilled water and then boiled, followed by cooling to 60 °C. Next, 6 ml propionic acid was added to the medium, and the medium was dispensed into culture vials (6 ml each). The vials of medium were covered with gauze and blown with a breeze as described above and were kept at 20 °C (for no more than 3 days) before experiments. Fly embryos were prepared using grape juice plates. The plates were prepared by mixing 30 g agar in 1 l water, followed by boiling in a microwave for 3 rounds, 3 min per round. Next, 360 ml grape juice, 2 g methyl paraben and 30 g sucrose were then sequentially added to the agar solution, with each component mixed thoroughly on a heated magnetic stirrer. The medium was dispensed into 100-cm Petri dishes, 10 ml each, and was kept at 4 °C (for no more than 1 week) before experiments. The yeast paste used for collecting embryos was freshly prepared by thoroughly mixing 7 g dry yeast with 9 ml water in a 50-ml conical flask with a metal spatula until it reached the consistency of peanut butter. The paste was then dabbed at the centre of each grape juice plate before experiments.

The WT fly strain (w^{1118}; 3605), $Sir2^{4.5}$ strain ($Sirt1^{4.5}$ cn^1/*SM6b*, *P*{$ry^{+t7.2}$=*eve-lacZ8.0*}*SB*^{1}; 32568), $Sir2^{5.26}$ strain ($Sirt1^{5.26}$ cn^1; 32657), Cas9-expressing strain (y^1 sc^* v^1 sev^{21}; *P*{$y^{+t7.7}$ $v^{+t1.8}$=*nanos-Cas9*.R}*attP2*; 78782), Bloomington DB strain (w^{1118}; $wg^{Sp\text{-}1}$/*CyO*; *MKRS*/*TM6B*, Tb^1; 76357) and the *GAL4*-expressing strain (y^1 w^*; *P*{*Act5C-GAL4-w*}*E1/CyO*; 25374) were obtained from the BDSC. The *GAL4*-induced, *ktub* RNAi-carrying strain (w^{1118}; *P*{*GD14210*}*v29111*; 29111) was obtained from the Vienna *Drosophila* Resource Center. The *yw*R13S strain (*yw*; *Sp*/*CyO*; *MKRS*/*TM2*), CAS DB strain (w^{1118}; *BL1*/*CyO*; *TM2*/*TM6B*), *attp*3# (68A4) strain (y^1 *M*{*vas-int.Dm*}*ZH-2A w**; P{*CaryP*}*attP2*) and the *attp*2# (25C6) strain (y^1 *M*{*vas-int.Dm*}*ZH-2A w**; P{*CaryP*}*attP40*) were obtained from the Core Facility of *Drosophila* Resource and Technology, Chinese Academy of Sciences. Files with *Sir2* knockout were obtained by crossing the $Sir2^{4.5}$ and the $Sir2^{5.26}$ strains, followed by picking the F_1 offspring with red eyes and straight wings ($Sir2^{4.5}$/$Sir2^{5.26}$). Flies with *GAL4* expressed on the w^{1118} background (w^{1118}; *P*{*Act5C-GAL4-w*}*E1/CyO*) were first generated as previously described[1] by crossing the y^1 w^*; *P*{*Act5C-GAL4-w*}*E1/CyO* males with w^{1118}; *Sp/CyO* females, followed by crossing the F_1 males with straight wings (w^{1118}; *P*{*Act5C-GAL4-w*}*E1/Sp*) with w^{1118}; *Sp/CyO* females.

To generate *ktub* (*CG9398*) knockout flies, the synchronized (see the section 'Evaluation of lifespan and healthspan of flies' for details), Cas9-expressing flies were housed in a collection cage (59-101; Genesee Scientific) containing a grape juice plate for 2 days. Flies were then allowed to lay embryos for 3 rounds, with each round lasting for 1 h, on a fresh grape juice plate that contained a dab of yeast paste at the centre. Next, 800 embryos were collected by filling each grape juice plate with water, followed by gently dislodging the embryos with a paintbrush and then filtering the solution by passing through a 70-μm cell strainer (350350; Falcon). The embryos in the strainer were then vigorously rinsed with tap water at 2 ml s^{-1} 3 times, 30 s each, followed by rough drying on a paper towel. The embryos were then dechorionated by dipping the strainer into freshly prepared 50% bleach solution (diluted in water) filled in a 10-cm Petri dish for 1 min, followed by rinsing with tap water at 2 ml s^{-1} for 3 times, 30 s each. After roughly drying on a paper towel, embryos were aligned with their ventral side sitting on a segment of double-sided tape (665; 3M Scotch) that was stuck onto a slide, followed by covering with a drop of mineral oil (1:1; Halocarbon oil 700 to Halocarbon oil 27). Next, 2 nl of 500 ng μl^{-1} gRNAs targeting exon 3 of *ktub* (5′-CGCATTACGCGGGACAGGAA-3′ and 5′-CGGAGATCTCATCGCACGAGT-3′) were then injected into the posterior pole of the embryo following previously described procedures[15]. The injected embryos were cultured at 18 °C for 48 h on a IHC transparent humidified chamber, and the larvae were then transferred to the semi-defined, rich medium and cultured at 25 °C for another week for the F_0 adults. The F_0 adults were then individually mated with *yw*R13S adults, and any F_1 offspring with straight wings were discarded. The remaining F_1 female offspring with curled wings were then screened for the presence of *ktub* knockout through genotyping following the procedures outlined in the section 'Analysis of mitochondrial DNA copy numbers in mice, nematodes and flies', with the following primers: 5′-AGATCAATCGACCCATGTCCG-3′ and 5′-CTTGCCGTAGTCACGTTCCA-3′. The F_1 male, curled-wing offspring (possibly with the *yw*; $ktub^{-/-}$/*CyO*; +/*TM2* genotype) from those female counterparts with *ktub* knockout were individually mated with virgin

females of the CAS DB strain. After 4 days of mating, each F_1 male was subjected to genotyping with the *ktub* knockout, and the F_2 male offspring (possibly the w^{1118}; $ktub^{-/-}$/*CyO*; +/*TM6B* genotype) generated from those *ktub*-knockout-confirmed F_1 males were picked and mated again with virgin females of the CAS DB strain. The F_3 male, curled-wing offspring (possibly the w^{1118}; $ktub^{-/-}$/*CyO*; +/*TM6B* genotype) were then individually mated with virgin females of F_3 curled-wing offspring. After 10 days of mating, each pair of F_3 male and female flies were subjected to examination for *ktub* knockout, and the F_4 offspring generated from the breeding of these F_3 males and females with *ktub* knockout were selected to breed with each other, leading to the generation of $ktub^{-/-}$ (w^{1118}; $ktub^{-/-}$/$ktub^{-/-}$) flies.

Human TULP3(4G) was re-introduced to the $ktub^{-/-}$ flies by expressing TULP3(4G) in the *attp*3# flies (with TULP3 inserted into chromosome III). The modified flies were then sequentially crossed with *yw*R13S and DB flies to backcross to a w^{1118} background, followed by crossing with the $ktub^{-/-}$ flies. In brief, to generate *attp*3# flies with TULP3(4G) expression, cDNA encoding TULP3(4G) was inserted into a pUAST-attB vector between the Xho I and Xba I sites. The construct was then injected into the embryos of *attp*3# flies as for sgRNA injection, except that the concentration was 300 ng μl^{-1}. The F_0 adults were then individually mated with *yw*R13S flies, and the F_1 males with curled wings and orange eyes (possibly the *yw*; +/*CyO*; *TULP3-4G*/*TM2* genotype) were mated with the virgin females of the CAS DB strain. The F_2 males with curled wings and white eyes (w^{1118}; +/*CyO*; *TULP3-4G*/*TM6B*) were mated with virgin females of the CAS DB strain again, followed by crossing the F_3 males with curled wings and white eyes with F_3 virgin females with curled wings and white eyes to generate the TULP3(4G)-expressing (w^{1118}; +/+; *TULP3-4G*/*TM6B*) flies. The TULP3(4G)-expressing strains and the $ktub^{-/-}$ strains were separately crossed with Bloomington DB flies. The F_1 offspring of TULP3(4G) with curled wings (w^{1118}; +/*CyO*; *TULP3-4G*/*MKRS*) and the F_1 offspring of $ktub^{-/-}$ with additional bristles in the humerus (w^{1118}; $ktub^{-/-}$/$wg^{Sp\text{-}1}$; +/*TM6B*, Tb^1), were then mated together, and the F_2 offspring with curled wings and additional bristles in the humerus (possibly the w^{1118}; $ktub^{-/-}$/*Cyo*; *TULP3-4G*/*TM6B*, Tb^1) were picked. The expression of TULP3(4G) was achieved by crossing the picked F_2 offspring with the *GAL4*-expressing strain (w^{1118}; *P{Act5C-GAL4-w}E1/CyO*), and the F_3 offspring with straight wings and regular bristles (w^{1118}; *P{Act5C-GAL4-w}E1*/$ktub^{-/-}$; *TULP3-4G*/+) were used for further experiments. The TULP3-re-introduced, $ktub^{-/-}$ flies were similarly generated, except that *TULP3* cDNA was used.

The human V1E1(3KR) was introduced to the WT flies as for TULP3, except that the *attp*2# strain (with V1E1 inserted into chromosome II) was used as the acceptor. The F_0 adults were then sequentially mated with *yw*R13S flies, CAS DB flies, the F_2 offspring themselves and the *GAL4*-expressing strain as for TULP3. The w^{1118}; *P{Act5C-GAL4-w}E1/V1E1-3KR* flies were used for further experiments.

Evaluation of lifespan and healthspan of flies

Fly lifespan was determined as previously described[116], but with minor modifications. Before the experiment, flies were synchronized. Approximately 200 pairs of flies, housed 10 pairs per tube, were cultured in semi-defined, rich medium and allowed to lay eggs for a day. After discarding the parent flies, the embryos were cultured for another 10 days, and the flies that eclosed at day 12 were anaesthetized and collected with CO_2 (those that emerged before day 12 were discarded), followed by transferring to BDSC standard cornmeal medium and cultured for another 2 days. The male and female adults were then sorted by briefly anaesthetizing with CO_2 on an anaesthetic pad using a homemade feather brush (by attaching the apical region of a vane from the secondary coverts of an adult goose to a plastic balloon stick), and 200 adults of each group and sex were randomly assigned to BDSC standard cornmeal medium, with or without LCA, with 20 flies per tube. The files were transferred to new medium tubes every 2 days without anaesthesia until the last survivor was dead. During each tube transfer, the sum of dead flies in the old tubes and the dead flies carried to the new tubes were recorded as the numbers of deaths, and the escaped or accidentally killed flies (that is, died within 3 days of same-sex culturing or squeezed by the tube plugs) were censored from the experiments. Kaplan–Meier curves were generated using Prism 9 (GraphPad Software), and statistical analysis was performed using SPSS 27.0 (IBM).

The resistance of flies to oxidative stress was determined as previously described[117]. In brief, synchronized adults were treated with LCA for 30 days, followed by transfer to vials (20 flies each), each containing a filter paper soaked with 20 mM paraquat or 5% (m/v) H_2O_2 dissolved or diluted in 5% (w/v, in water) glucose solution. To determine the resistance of flies to starvation (food deprivation), flies treated with LCA for 30 days were transferred to vials with culture medium replaced by the same volume of 1.5% agarose to remove the food supply. Dead files were recorded every 2 h until the last survivor was dead.

Quantification of mRNA levels of mitochondrial genes in mice, nematodes and flies

Mice treated with LCA were killed by cervical dislocation, immediately followed by dissecting the gastrocnemius muscle. The muscle tissue was roughly sliced into cubes (with edge lengths of approximately 2 mm) and then soaked in RNAprotect tissue reagent (1 ml per 100 mg of tissue) for 24 h at room temperature. The tissue was then incubated in 1 ml TRIzol, followed by three rounds of freeze–thaw cycles and was then homogenized. The homogenate was centrifuged at 12,000*g* for 15 min at 4 °C, and 900 µl of clear supernatant (not the lipid layer on the top) was transferred to a RNase-free tube. Next, 200 µl chloroform was added to the supernatant, followed by a vigorous vortex for 15 s. After centrifugation at 12,000*g* for 15 min at 4 °C, 450 µl of the upper aqueous layer was transferred to a RNase-free tube. The RNA was then precipitated by adding 450 µl isopropanol, followed by centrifugation at 12,000*g* for 30 min at 4 °C. The pellet was washed twice with 75% ethanol and once with 100% ethanol, and was dissolved with 20 µl DEPC-treated water. The concentration of RNA was determined using a NanoDrop 2000 spectrophotometer (Thermo). Next, 1 µg of RNA was diluted with DEPC-treated water to a final volume of 10 µl, heated at 65 °C for 5 min and immediately chilled on ice. Random primer mix, enzyme mix and 5× RT buffer (all from the ReverTra Ace qPCR RT master mix) were added to the RNA solution, followed by incubation at 37 °C for 15 min and then at 98 °C for 5 min on a thermocycler. The reverse-transcribed cDNA was quantified using Maxima SYBR Green/ROX qPCR master mix on a LightCycler 480 II system (Roche) with the following programs: pre-denaturing at 95 °C for 10 min; denaturing at 95 °C for 10 s, then annealing and extending at 65 °C for 30 s in each cycle (determined according to the amplification curves, melting curves and bands on agarose gel of serial pilot reactions (in which a serial annealing temperature was set according to the estimated annealing temperature of each primer pair) of each primer pair, and same hereafter), for a total of 45 cycles. Primer pairs for mouse *Nd1*, *Nd2*, *Nd3*, *Nd4*, *Nd4l*, *Nd5*, *Nd6*, *Ndufab1*, *Cytb*, *Uqcrc1*, *Uqcrc2*, *Atp5f1b*, *Cox6a1*, *Atp6*, *Atp8*, *Cox1* and *Cox3* were generated as previously described[118], and others were generated using the Primer-BLAST website (https://www.ncbi.nlm.nih.gov/tools/primer-blast/index.cgi). Mouse primer sequences are as follows: *Gapdh*, 5′-GACTTCAACAGCAACTCCCAC-3′ and 5′-TCCACCACCCTGTTGCTGTA-3′; *Nd1*, 5′-TGCACCTACCCTATCACTCA-3′ and 5′-C GGCTCATCCTGATCATAGAATGG-3′; *Nd2*, 5′-ATACTAGCAATTACTTCTATTTTCATAGGG-3′ and 5′-GAGGGATGGGTTGTAAGGAAG-3′; *Nd3*, 5′-AAGCAAATCCATATGAATGCGG-3′ and 5′-GCTCATGGTAGTGGAAGTAGAAG-3′; *Nd4*, 5′-CCTCAGACCCCCTATCCACA-3′ and 5′-GTTTGGTTCCCTCATCGGGT-3′; *Nd4l*, 5′-CCAACTCCATAAGCTCCATACC-3′ and 5′-GATTTTGGACGTAATCTGTTCCG-3′; *Nd5*, 5′-ACGAAAATGACCCAGACCTC-3′ and 5′-GAGATGACAAATCCTGCAAAGATG-3′; *Nd6*, 5′-TGTTGGAGTTATGTTGGAAGGAG-3′ and 5′-CAAAGATCACCCAGCTACTACC-3′; *Tfam*, 5′-GGTCGCATCCCCTCGTCTAT-3′ and 5′-TTGGGTAGCTGTTCTGTGGAA-3′; *Cs*, 5′-CTCTACTCACTGCAGC

AACCC-3′ and 5′-TTCATGCCTCTCATGCCACC-3′; *Ndufs8*, 5′-TGGCGGCA ACGTACAAGTAT-3′ and 5′-GTAGTTGATGGTGGCAGGCT-3′; *Ndufab1*, 5′-GGACCGAGTTCTGTATGTCTTG-3′ and 5′-AAACCCAAATTCGTCTTCC ATG-3′; *Ndufb10*, 5′-TGCCAGATTCTTGGGACAAGG-3′ and 5′-GTCG TAGGCCTTCGTCAAGT-3′; *Ndufv3*, 5′-GTGTGCTCAAAGAGCCCGAG-3′ and 5′-TCAGTGCCGAGGTGACTCT-3′; *Ndufa8*, 5′-GCGGAGCCTTT CACAGAGTA-3′ and 5′-TCAATCACAGGGTTGGGCTC-3′; *Ndufs3*, 5′-CTG ACTTGACGGCAGTGGAT-3′ and 5′-CATACCAATTGGCCGCGATG-3′; *Ndufa9*, 5′-TCTGTCAGTGGAGTTGTGGC-3′ and 5′-CCCATCAGACGA AGGTGCAT-3′; *Ndufa10*, 5′-CAGCGCGTGGGACGAAT-3′ and 5′-ACTCT ATGTCGAGGGGCCTT-3′; *Sdha*, 5′-AGGGTTTAATACTGCATGCCTTA-3′ and 5′-TCATGTAATGGATGGCATCCT-3′; *Sdhb*, 5′-AGTGCGGACCT ATGGTGTTG-3′ and 5′- AGACTTTGCTGAGGTCCGTG-3′; *Sdhc*, 5′-TGAG ACATGTCAGCCGTCAC-3′ and 5′-GGGAGACAGAGGACGGTTTG-3′; *Sdhd*, 5′-TGGTACCCAGCACATTCACC-3′ and 5′-GGGTGTCCCCATG AACGTAG-3′; *Cytb*, 5′-CCCACCCCATATTAAACCCG-3′ and 5′-GAGGT ATGAAGGAAAGGTATTAGGG-3′; *Uqcrc1*, 5′-ATCAAGGCACTGTCCA AGG-3′ and 5′-TCATTTTCCTGCATCTCCCG-3′; *Uqcrc2*, 5′-TTCCAGTGCA GATGTCCAAG-3′ and 5′-CTGTTGAAGGACGGTAGAAGG-3′; *Atp5f1b*, 5′-CCGTGAGGGCAATGATTTATAC-3′ and 5′-GTCAAACCAGTCAGAGC TACC-3′ *Cox6a1*, 5′-GTTCGTTGCCTACCCTCAC-3′ and 5′- TCTCTTT ACTCATCTTCATAGCCG-3′; *Atp6*, 5′-TCCCAATCGTTGTAGCCATC-3′ and 5′-TGTTGGAAAGAATGGAGTCGG-3′; *Atp8*, 5′-GCCACAACTAGATA CATCAACATG-3′ and 5′-TGGTTGTTAGTGATTTTGGTGAAG-3′; *Atp5f1a*, 5′-CATTGGTGATGGTATTGCGC-3′ and 5′-TCCCAAACACGACAACTCC-3′; *Cox1*, 5′-CCCAGATATAGCATTCCCACG-3′ and 5′- ACTGTTCATCCTGTT CCTGC-3′; *Cox2*, 5′-TCTACAAGACGCCACATCCC-3′ and 5′-ACGGGGT TGTTGATTTCGTCT-3′; *Cox3*, 5′-CGTGAAGGAACCTACCAAGG-3′ and 5′-CGCTCAGAAGAATCCTGCAA-3′; *Cox5b*, 5′-AGCTTCAGGC ACCAAGGAAG-3′ and 5′-TGGGGCACCAGCTTGTAATG-3′. The mRNA level was then calculated using the comparative ΔΔct method and LightCycler software (v.96 1.1, Roche; same hereafter for all qPCR experiments).

Nematodes at the L4 stage treated with LCA for 1 day were used for the analysis of mitochondrial gene expression. About 1,000 worms were collected with 15 ml M9 buffer containing 0.05% Triton X-100 (v/v), followed by centrifugation for 2 min at 1,000*g*. The sediment was washed with 1 ml M9 buffer twice and then lysed with 1 ml TRIzol. Worms were then frozen in liquid nitrogen, thawed at room temperature and the freeze–thaw process was repeated for another 2 times. The worm lysates were then placed at room temperature for 5 min, mixed with 0.2 ml of chloroform, followed by vigorous shaking for 15 s. After centrifugation at 12,000*g* for 15 min at 4 °C, 450 µl of the upper aqueous layer was transferred to a RNase-free tube. The RNA was then precipitated by adding 450 µl of isopropanol, followed by centrifugation at 12,000*g* for 30 min at 4 °C. The pellet was washed twice with 75% ethanol and once with 100% ethanol, and was dissolved with 20 µl DEPC-treated water. The concentration of RNA was determined using a NanoDrop 2000 spectrophotometer (Thermo). Next, 1 µg of RNA was diluted with DEPC-treated water to a final volume of 10 µl, heated at 65 °C for 5 min and immediately chilled on ice. Random primer mix, enzyme mix and 5× RT buffer (all from the ReverTra Ace qPCR RT master mix) were then added to the RNA solution, followed by incubation at 37 °C for 15 min and then at 98 °C for 5 min on a thermocycler. The reverse-transcribed cDNA was quantified using Maxima SYBR Green/ROX qPCR master mix on a LightCycler 480 II System (Roche) with the following programs: pre-denaturing at 95 °C for 10 min; denaturing at 95 °C for 10 s, then annealing and extending at 65 °C for 30 s in each cycle (determined according to the amplification curves, melting curves, and bands on agarose gel of serial pilot reactions (in which a serial annealing temperature was set according to the estimated annealing temperature of each primer pair) of each primer pair, and same hereafter), for a total of 45 cycles. Primer pairs used for qPCR were as previously described[119,120], except that *C. elegans ctb-1* was designed using the Primer-BLAST website. *C. elegans* primer sequences are as follows: *ama-1*, 5′-GAC ATTTGGCACTGCTTTGT-3′ and 5′-ACGATTGATTCCATGTCTCG-3′; *nuo-6*, 5′-CTGCCAGGACATGAATACAATCTGAG-3′ and 5′-GCTATGAG GATCGTATTCACGACG-3′; *nuaf-1*, 5′-GAGACA TAACGAGGCTCGTGT TG-3′ and 5′-GAAGCCTTCTTTCCAATCACTATCG-3′; *sdha-1*, 5′-TTAC CAGCGTGCTTTCGGAG-3′ and 5′-AGGGTGTGGAGAAGAGAATGACC-3′; *sdhb-1*, 5′-GCTGAACGTGATCGTCTTGATG-3′ and 5′-GTAGGATGGGC ATGACGTGG-3′; *cyc-2.1*, 5′-CGGA GTTATCGGACGTACATCAG-3′ and 5′-GTCTCGCGGGTCCAGACG-3′; *isp-1*, 5′-GCAGAAAGATGAATGGTCC GTTG-3′ and 5′-ATCCGTGACAAGGGCAGTAATAAC-3′; *cco-1*, 5′-GCTG GAGATGATCGTTACGAG-3′ and 5′-GCATCCAATGATTCTGAAGTCG-3′; *cco-2*, 5′-GTGATACCGTCTACGCCTACATTG-3′ and 5′-GCTCTGGC ACGAAGAATTCTG-3′; *atp-3*, 5′-GTCCTCGACCCAACTCTCAAG-3′ and 5′-GTCCAAGGAAG TTTCCAGTCTC-3′; *nduo-1*, 5′-AGCGTCATTTAT TGGGAAGAAGAC-3′ and 5′-AAGCTTGTGCTAATCCCATAAATGT-3′; *nduo-2*, 5′-TCTT TGTAGAGGAGGTCTATTACA-3′ and 5′-ATGTTAAAAA CCACATTAGCCCA-3′; *nduo-4*, 5′-GCACACGGTTATACATCTACACT TATG-3′ and 5′-GATGTATGATAAAATTCACCAATAAGG-3′; *nduo-5*, 5′-AGATGAGATTTATTGGGTATTTCTAG-3′ and 5′-CACCTAGACGATT AGTTAATGCTG-3′; *ctc-1*, 5′-GCAGCAGGGTTAAGATCTATCTTAG-3′ and 5′-CTGTTACAAATACAGTTCAAACAAAT-3′; *ctc-2*, 5′-GTAGTTT ATTGTTGGGAGTTTTAGTG-3′ and 5′-CACAATAATTCACCAAACTGATA CTC-3′; *atp-6*, 5′-TGCTGCTGTAGCGTGATTAAG-3′ and 5′-ACTGT TAAAGCAAGTGGACGAG-3′; *ctb-1*, 5′-TGGTGTTACAGGGGCAAC AT-3′ and 5′-TGGCCTCATTATAGGGTCAGC-3′. The mRNA level was then calculated using the comparative ΔΔct method and LightCycler software (v.96 1.1, Roche; same hereafter for all qPCR experiments).

Drosophila adults treated with LCA for 30 days were used to determine the expression of mitochondrial genes. For each sample, 20 adults were used. The adults were anaesthetized, transferred to a 1.5-ml Eppendorf tube, followed by quickly freezing in liquid nitrogen and then homogenized using a pellet pestle (Z359963-1EA, Sigma). The homogenate was then lysed in 1 ml TRIzol for 5 min at room temperature, followed by centrifugation at 12,000*g* for 15 min at 4 °C. Next, 900 µl of supernatant (without the lipid layer) was transferred to a RNase-free tube, followed by mixing with 200 µl chloroform. After vigorous vortexing for 15 s, the mixture was centrifuged at 12,000*g* for 15 min at 4 °C, and 450 µl of the upper aqueous layer was transferred to a RNase-free tube. The RNA was then precipitated by adding 450 µl isopropanol, followed by centrifugation at 12,000*g* for 30 min at 4 °C. The pellet was washed twice with 75% (v/v, in water) ethanol and was dissolved with 20 µl of DEPC-treated water. The concentration of RNA was determined using a NanoDrop 2000 spectrophotometer (Thermo). Next, 1 µg of RNA was diluted with DEPC-treated water to a final volume of 10 µl, heated at 65 °C for 5 min and immediately chilled on ice. Random primer mix, enzyme mix and 5× RT buffer (all from the ReverTra Ace qPCR RT master mix) were then added to the RNA solution, followed by incubation at 37 °C for 15 min and then at 98 °C for 5 min on a thermocycler. The reverse-transcribed cDNA was quantified using Maxima SYBR Green/ROX qPCR master mix on a LightCycler 480 II system (Roche) with the following programs: pre-denaturing at 95 °C for 5 min; denaturing at 95 °C for 10 s, then annealing at 60 °C for 20 s, and then extending at 72 °C for 20 s in each cycle, for a total of 40 cycles. *D. melanogaster* primer pairs used for qPCR were as previously described[121], and are as follows: *CG9172*, 5′-CGTGGCTGCGATAGGATAAT-3′ and 5′-ACCACATCTGGAGCGTCTTC-3′; *CG9762*, 5′-AGTCACCGCATTGGTTCTCT-3′ and 5′-GAGATGGGGTGCTTC TCGTA-3′; *CG17856*, 5′-ACCTTTCCATGACCAAGACG-3′ and 5′-CTCCATT CCTCACGCTCTTC-3′; *CG18809*, 5′-AAGTGAAGACGCCCAATGAGA-3′ and 5′-GCCAGGTACAACGACCAGAAG-3′; *CG5389*, 5′-ATGGCTACAG CATGTGCAAG-3′ and 5′-GACAGGGAGGCATGAAGGTA-3′; and *Act5c*, 5′-GCAGCAACTTCTTCGTCACA-3′ and 5′-CATCAGCCAGCAGTCGTCTA-3′.

Analysis of mitochondrial DNA copy numbers in mice, nematodes and flies

Mouse mitochondrial DNA copy numbers were determined as previously described[78]. In brief, mouse tissue DNA was extracted using a Biospin tissue genomic DNA extraction kit (BioFlux) following the manufacturer's

instruction, but with minor modifications. In brief, mice treated with LCA were killed by cervical dislocation, quickly followed by dissecting the gastrocnemius muscle. The muscle tissue was then ground in a ceramic mortar in liquid nitrogen. Next, 50 mg of ground tissue was transferred to a 1.5-ml Eppendorf tube, followed by the addition of 600 µl FL buffer and 10 µl PK solution containing 2 µl of 100 mg ml^{-1} RNase A. The mixture was incubated at 56 °C for 15 min, followed by centrifugation at 12,000 *g* for 3 min. Next, 500 µl of supernatant was transferred to a 2-ml Eppendorf tube, followed by mixing with 700 µl binding buffer and 300 µl absolute ethanol. The mixture was then loaded onto a Spin column and was centrifuged at 10,000*g* for 1 min. The flowthrough was discarded and 500 µl of the PW buffer was added to the Spin column, followed by centrifugation at 10,000*g* for 30 s. Next, 600 µl washing buffer was added to the Spin column, followed by centrifugation at 10,000*g* for 30 s, and the process was repeated again. The Spin column was then centrifuged for 1 min at 10,000*g* to completely remove the washing buffer, and DNA on the column was eluted with 100 µl of elution buffer (added to the Spin column, followed by incubation at room temperature for 5 min, and then centrifuged at 12,000*g* for 1 min). Total DNA was quantified using Maxima SYBR Green/ROX qPCR master mix on a LightCycler 480 II system (Roche) with the following programs: 70 ng of DNA was pre-denatured at 95 °C for 10 min and then subjected to PCR for a total of 45 cycles: denaturing at 95 °C for 10 s, annealing and extending at 65 °C for 30 s in each cycle. Mouse primer pairs used for qPCR were as previously described[122] (*Hk2*, 5′-GCCAGC CTCTCCTGATTTTAGTGT-3′ and 5′-GGGAACACAAAAGACCTCTTCT GG-3′; and *Nd1*, 5′-CTAGCAGAAACAAACCGGGC-3′ and 5′-CCGGCT GCGTATTCTACGTT-3′).

Nematode mitochondrial DNA copy numbers were determined from worm lysates as previously described[78]. In brief, 30 synchronized early L4 worms were collected and were lysed with 10 µl single worm lysis buffer. The worm lysate was frozen at −80 °C overnight, followed by incubating at 65 °C for 1 h and 95 °C for 15 min. Nematode DNA was then quantified using Maxima SYBR Green/ROX qPCR master mix on a LightCycler 480 II system (Roche) with the following programs: pre-denaturing at 95 °C for 10 min and then for a total of 45 cycles of denaturing at 95 °C for 10 s, and annealing and extending at 65 °C for 30 s in each cycle. *C. elegans* primer pairs used for qPCR were designed as previously described[95] (*nd-1*, 5′-AGCGTCATTTATTGGGAAGAAGAC-3′ and 5′-AAG CTTGTGCTAATCCCATAAATGT-3′; and *act-3*, 5′-TGCGACATTGATA TCCGTAAGG-3′ and 5′-GGTGGTTCCTCCGGAAAGAA-3′).

Drosophila DNA copy numbers were determined as previously described[123], but with minor modifications. In brief, 20 anaesthetized adults were homogenized in 100 µl fly lysis buffer (75 mM NaCl, 25 mM EDTA and 25 mM HEPES, pH7.5) containing proteinase K (100 µg ml^{-1}). The homogenate was then frozen at −80 °C for 12 h, followed by incubation at 65 °C for 1 h and 95 °C for another 15 min. The fly DNA was then quantified using Maxima SYBR Green/ROX qPCR master mix on a LightCycler 480 II system (Roche) with the following programs: pre-denaturing at 95 °C for 5 min and then for a total of 40 cycles of denaturing at 95 °C for 10 s, and annealing 60 °C for 20 s and extending at 72 °C for 20 s in each cycle. *D. melanogaster* primer pairs used for qPCR were as previously described[123] (*16S rRNA*, 5′-TCGTCCAACCATTCATTCCA-3′ and 5′-TGGCCGCAGTATTTTGACTG-3′; and *RpL32*, 5′-AGGCCCAAGATC GTGAAGAA-3′ and 5′-TGTGCACCAGGAACTTCTTGAA-3′).

Measurement of adenylates and NAD^+

ATP, ADP, AMP and NAD^+ from cells, tissues or flies were analysed by capillary–MS (CE–MS) as previously described[10], but with minor modifications[124]. In brief, each measurement required MEFs collected from one 10-cm dish (60–70% confluence), 100 mg of liver or muscle tissue dissected by freeze-clamping, or 20 anesthetized adult flies. Before CE–MS analysis, cells were rinsed with 20 ml of 5% (m/v) mannitol solution (dissolved in water) and instantly frozen in liquid nitrogen. Cells were then lysed with 1 ml methanol containing IS1 (50 µM L-methionine sulfone, 50 µM D-campher-10-sulfonic acid, dissolved in water; 1:500 (v/v) added to the methanol and used to standardize the metabolite intensity and to adjust the migration time), and were scraped from the dish. For analysis of metabolites in liver and muscle, mice were anaesthetized after indicated treatments. The tissue was then quickly excised by freeze-clamping and then ground in 1 ml methanol with IS1. For analysis of metabolites in flies, 20 adult flies were anesthetized, followed by grinding in 1 ml methanol with IS1 after freezing by liquid nitrogen. The lysate was then mixed with 1 ml chloroform and 400 µl water by 20 s of vortexing. After centrifugation at 15,000 *g* for 15 min at 4 °C, 450 µl of aqueous phase was collected and was then filtrated through a 5-kDa cut-off filter (OD003C34, PALL) by centrifuging at 12,000*g* for 3 h at 4 °C. In parallel, quality control samples were prepared by combining 10 µl of the aqueous phase from each sample and then filtered alongside the samples. The filtered aqueous phase was then freeze-dried in a vacuum concentrator at 4 °C and then dissolved in 100 µl water containing IS2 (50 µM 3-aminopyrrolidine dihydrochloride, 50 µM *N*,*N*-diethyl-2-phenylacetamide, 50 µM trimesic acid, 50 µM 2-naphtol-3,6-disulfonic acid disodium salt, dissolved in methanol; used to adjust the migration time). A total of 20 µl of re-dissolved solution was then loaded into an injection vial (9301-0978, Agilent; equipped with a snap cap (5042-6491, Agilent)). Before CE–MS analysis, the fused-silica capillary (TSP050375, i.d. 50 µm × 80 cm; Polymicro Technologies) was installed in a CE–MS cassette (G1603A, Agilent) on a CE system (Agilent Technologies 7100). The capillary was then pre-conditioned with conditioning buffer (25 mM ammonium acetate and 75 mM diammonium hydrogen phosphate, pH 8.5) for 30 min, followed by balancing with running buffer (50 mM ammonium acetate, pH 8.5; freshly prepared) for another 1 h. CE–MS analysis was run in anion mode, during which the capillary was washed with conditioning buffer, followed by injection of the samples at a pressure of 50 mbar for 25 s, and then separation with a constant voltage at −30 kV for another 40 min. Sheath Liquid (0.1 µM hexakis(1*H*,1*H*,3*H*-tetrafluoropropoxy) phosphazine, 10 µM ammonium trifluoroacetate, dissolved in methanol and water (50% v/v); freshly prepared) was flowed at 1 ml min^{-1} through a 1:100 flow splitter (Agilent Technologies 1260 Infinity II; actual flow rate to the MS: 10 µl min^{-1}) throughout each run. The parameters of MS (Agilent Technologies 6545) were set as follows: ion source, dual AJS ESI; polarity, negative; nozzle voltage, 2,000 V; fragmentor voltage, 110 V; skimmer voltage, 50 V; OCT RFV, 500 V; drying gas (N_2) flow rate, 7 l min^{-1}; drying gas (N_2) temperature, 300 °C; nebulizer gas pressure, 8 psig; sheath gas temperature, 125 °C; sheath gas (N_2) flow rate, 4 l min^{-1}; capillary voltage (applied onto the sprayer), 3,500 V; reference (lock) masses, *m/z* of 1,033.988109 for hexakis(1*H*,1*H*, 3*H*-tetrafluoropropoxy)phosphazine and *m/z* of 112.985587 for trifluoroacetic acid; scanning range: 50–1,100 *m/z*; and scanning rate, 1.5 spectra per s. Data were collected using MassHunter LC/MS acquisition (v.10.1.48; Agilent Technologies) and were processed using Qualitative Analysis B.06.00 (Agilent Technologies). Levels of AMP, ADP, ATP and NAD^+ were measured using full scan mode with *m/z* values of 346.0558, 426.0221, 505.9885 and 662.1019, respectively. Note that a portion of ADP and ATP could lose one phosphate group during in-source fragmentation, thus leaving the same *m/z* ratios as AMP and ADP, and were corrected according to their different retention times in the capillary. Therefore, the total amount of ADP is the sum of the latter peak of the *m/z* 346.0558 spectrogram and the former peak of the *m/z* 426.0221 spectrogram, and the same was applied for ATP. Note that the retention time of each metabolite could vary between each run, which was adjusted by using isotope-labelled standards (dissolved in individual cell or tissue lysates) run between each sample, as do IS1 and IS2.

Levels of ATP, ADP, AMP and NAD^+ in nematodes were analysed using high-performance liquid chromatography (HPLC)–MS as previously described[78]. In brief, 150 nematodes maintained on NGM (with or without LCA) for 2 days were washed with ice-cold M9 buffer containing Triton X-100, followed by removal of bacteria by quickly centrifuging

the slurry at 100*g* for 5 s and then instantly lysing in 1 ml methanol. The lysates were then mixed with 1 ml chloroform and 400 µl water (containing 4 µg ml^{-1} [U-^{13}C]-glutamine), followed by 20 s of vortexing. After centrifugation at 15,000*g* for another 15 min at 4 °C, 800 µl of aqueous phase was collected, lyophilized in a vacuum concentrator at 4 °C and then dissolved in 30 µl of 50% (v/v, in water) acetonitrile. Next, 30 µl of supernatant was loaded into an injection vial (5182-0714, Agilent Technologies; with an insert (HM-1270, Zhejiang Hamag Technology)) equipped with a snap cap (HM-2076, Zhejiang Hamag Technology). Measurements of adenylate and NAD^+ levels were based on ref. 125 using a QTRAP MS (QTRAP 5500, SCIEX) interfaced with a UPLC system (ExionLC AD, SCIEX). A total of 2 µl of each sample was loaded onto a HILIC column (ZIC-pHILIC, 5 µm, 2.1 × 100 mm, PN: 1.50462.0001, Millipore). The mobile phase consisted of 15 mM ammonium acetate containing 3 ml l^{-1} ammonium hydroxide (>28%, v/v) in LC–MS grade water (mobile phase A) and LC–MS grade 90% (v/v) acetonitrile in LC–MS grade water (mobile phase B) run at a flow rate of 0.2 ml min^{-1}. Metabolites were separated with the following HPLC gradient elution program: 95% B held for 2 min, then to 45% B in 13 min, held for 3 min, and then back to 95% B for 4 min. The MS was run on a Turbo V ion source in negative mode with a spray voltage of −4,500 V, source temperature of 550 °C, gas no.1 at 50 psi, gas no.2 at 55 psi, and curtain gas at 40 psi. Metabolites were measured using the multiple reactions monitoring mode, and declustering potentials and collision energies were optimized using analytical standards. The following transitions were used for monitoring each compound: 505.9/158.9 and 505.9/408.0 for ATP; 425.9/133.9, 425.9/158.8 and 425.9/328.0 for ADP; 345.9/79.9, 345.9/96.9 and 345.9/133.9 for AMP, 662.0/540.1 for NAD^+; and 149.9/114 for [U-^{13}C]-glutamine. Data were collected using Analyst software (v.1.7.1, SCIEX), and the relative amounts of metabolites were analysed using MultiQuant software (v.3.0.3, SCIEX). Similar to CE–MS analysis, a portion of ADP and ATP could lose one or two phosphate groups during in-source-fragmentation, thus leaving the same *m/z* ratios as AMP and ADP, which was corrected according to their different retention times in the column.

Reagents

Rabbit polyclonal antibody against V1E1(K99)ac (1:1,000 dilution for IB) was raised using the peptide CARDDLITDLLNEA(AcK) of human V1E1 conjugated to the KLH immunogen (linked to the cysteine residue). A rabbit was then biweekly immunized with 300 µg KLH-conjugated antigen, which was pre-incubated with 1.5 mg manganese adjuvant (provided by Z. Jiang[126]) for 5 min and then mixed with PBS to a total volume of 1.5 ml for 4 times followed by collection of antiserum. The V1E1(K99)ac antibody was then purified from the antiserum using a CARDDLITDLLNEA(AcK) peptide-conjugated SulfoLink Coupling resin/column supplied in a SulfoLink Immobilization kit. To prepare the column, 1 mg of the peptide was first dissolved with 2 ml coupling buffer followed by the addition of 0.1 ml TCEP (25 mM stock concentration) and then incubation at room temperature for 30 min. The mixture was then incubated with SulfoLink Resin in a column, which was pre-calibrated with 2 ml coupling buffer 2 times on a rotator at room temperature for 15 min, followed by incubating at room temperature for 30 min without rotating. The excess peptide was then removed, and the resin was washed with 2 ml of wash solution 3 times, followed by 2 ml coupling buffer 2 times. The nonspecific-binding sites on the resin were then blocked by incubating with 2 ml cysteine solution (by dissolving 15.8 mg of L-cysteine-HCl in 2 ml coupling buffer to make a concentration of 50 mM cysteine) on a rotator for 15 min at room temperature, followed by incubating for another 30 min without rotating at room temperature. After removing the cysteine solution, the resin was washed with 6 ml binding/wash buffer, followed by incubating with 2 ml of antiserum mixed with 0.2 ml of binding/wash buffer for 2 h on a rotator. The resin was then washed with 1 ml of binding/wash buffer 5 times, and the antibody was eluted with 2 ml elution buffer. The eluent was then mixed with 100 µl neutralization buffer. The antibody against basal V1E1 that exists in the crude antibody eluent was then removed through a previously described membrane-based affinity purification method[127]. In brief, the bacterially purified, His-tagged V1E1 was subjected to SDS–PAGE, followed by transferring to a PVDF membrane (see details in the section "Immunoprecipitation and IB assays"). The V1E1-bound-membrane was incubated in 5% (w/v) nonfat milk dissolved in TBST (40 mM Tris, 275 µM NaCl and 0.2% (v/v) Tween-20, pH 7.6) for 2 h, then incubated with the crude antibody preparation for 2 days, and the process was repeated for another 2 times.

The following antibodies were purchased from Cell Signaling Technology: rabbit anti-phospho-AMPKα-Thr172 (2535, RRID: AB_331250; 1:1,000 for IB); anti-AMPKα (2532, RRID: AB_330331; 1:1,000 for IB); anti-phospho-ACC-Ser79 (3661, RRID: AB_330337; 1:1,000 for IB); anti-ACC (3662, RRID: AB_2219400; 1:1,000 for IB); anti-LKB1 (3047, RRID: AB_2198327; 1:1,000 for IB); anti-His-tag (12698, RRID: AB_2744546; 1:1,000 for IB); anti-Myc-tag (2278, RRID: AB_490778; 1:120 for immunofluorescence (IF)); anti-AXIN1 (2074, RRID: AB_2062419; 1:1,000 for IB); anti-SIRT1 (9475, RRID: AB_2617130; 1:1,000 for IB and 1:100 for IF); anti-SIRT2 (12650, RRID: AB_2716762; 1:1,000 for IB); anti-SIRT3 (5490, RRID: AB_10828246; 1:1,000 for IB); anti-SIRT5 (8782, RRID: AB_2716763; 1:1,000 for IB); anti-SIRT6 (12486, RRID: AB_2636969; 1:1,000 for IB); anti-SIRT7 (5360, RRID: AB_2716764; 1:1,000 for IB); anti-histone H3 (4499, RRID: AB_10544537; 1:1,000 for IB); anti-acetyl-histone H3-Lys9 (9649, RRID: AB_823528; 1:1,000 for IB); anti-LAMTOR1 (8975, RRID: AB_10860252; 1:1,000 for IB); anti-GAPDH (5174; RRID: AB_10622025; 1:1,000 for IB); mouse anti-Myc-tag (2276, RRID: AB_331783; 1:120 for IF); and HRP-conjugated mouse anti-rabbit IgG (conformation-specific, 5127, RRID: AB_10892860; 1:2,000 for IB); and anti-ubiquitin (Ub; 3936, RRID: AB_331292; 1:1,000 for IB). The following antibodies were purchased from Santa Cruz Biotechnology: mouse anti-HA-tag (sc-7392, RRID: AB_2894930; 1:500 for IP or 1:120 for IF); anti-LKB1 (sc-32245, RRID: AB_627890, 1:100 for IF); goat anti-AXIN (sc-8567, RRID: AB_22277891; 1:100 for IP (immunoprecipitation) and 1:120 for IF); rabbit anti-VDR (sc-13133, RRID: AB_628040, 1:1,000 for IB); and mouse anti-goat IgG-HRP (sc-2354, RRID: AB_628490; 1:2,000 for IB). The following antibodies were purchased from Abcam: mouse anti-total OXPHOS (ab110413, RRID: AB_2629281; 1:5,000 for IB); rat anti-LAMP2 (ab13524, RRID: AB_2134736; 1:120 for IF); rabbit anti-laminin (ab11575, RRID: AB_298179; 1:200 for IF); anti-phospho-AMPKα2-Ser345 (ab129081, 1:1,000 for IB); anti-transferrin (ab1223, RRID: AB_298951; 1:500 for IB); anti-ATP6V1B2 (ab73404, RRID: AB_1924799; 1:1,000 for IB); anti-PEN2 (ab154830, 1:1,000 for IB); and goat anti-SIRT4 (ab10140, RRID: AB_2188769; 1:1,000 for IB). The following antibodies were purchased from Developmental Studies Hybridoma Bank: mouse anti-eMHC (BF-G6, RRID: AB_10571455; 1:100 for IHC); anti-Pax7 (Pax-7, RRID: AB_2299243; 1:100 for IHC); anti-MHCIIa (SC71, RRID: AB_2147165; 1:100 for IHC); anti-MHCIIb (BF-F3, RRID: AB_2266724; 1:100 for IHC); and anti-MHCI (C6B12, RRID: AB_528351; 1:100 for IHC). The following antibodies were purchased from Proteintech: rabbit anti-tubulin (10068-1-AP, RRID: AB_2303998; 1:1,000 for IB nematode tubulin); anti-ATP6V1E1 (15280-1-AP, RRID: AB_2062545; 1:1,000 for IB); anti-TULP3 (13637-1-AP, RRID: AB_2211547, 1:20,000 for IB); anti-TOMM20 (11802-1-AP, RRID: AB_2207530; 1:1,000 for IB); anti-YES 20243-1-AP, RRID: AB_10697656; 1:1,000 for IB); mouse anti-tubulin (66031-1-Ig, RRID: AB_11042766; 1:20,000 for IB mammalian tubulin); and anti-HA-tag (66006-2-Ig, RRID: AB_2881490; 1:20,000 for IB). Rabbit anti-ATP6v0c (NBP1-59654, RRID: AB_11004830; 1:1,000 for IB) was purchased from Novus Biologicals. Mouse anti β-actin (A5316, RRID: AB_476743; 1:1,000 for IB) and anti-Flag M2 affinity gel (A2220, 1:500 for IP) were purchased from Sigma. The following antibodies were purchased from Thermo: donkey anti-goat IgG (H+L) highly cross-adsorbed secondary antibody, Alexa Fluor Plus 488 (A-32814, RRID: AB_2762838; 1:100 for IF); donkey anti-rat IgG (H+L) highly cross-adsorbed secondary antibody, Alexa Fluor 594 (A-21209, RRID: AB_2535795; 1:100 for IF);

goat anti-mouse IgM (heavy chain) cross-adsorbed secondary antibody, Alexa Fluor 488 (A-21042, RRID: AB_2535711; 1:200 for IHC); goat anti-mouse IgG2b cross-adsorbed secondary antibody, Alexa Fluor 594 (A-21145, RRID: AB_2535781; 1:200 for IHC); goat anti-mouse IgG1 cross-adsorbed secondary antibody, Alexa Fluor 647 (A-21240, RRID: AB_2535809; 1:200 for IHC); goat anti-mouse IgG1 cross-adsorbed secondary antibody, Alexa Fluor 488 A-21121, RRID: AB_2535764; 1:200 for IHC); goat anti-rabbit IgG (H+L) highly cross-adsorbed secondary antibody, Alexa Fluor 488 (A11034, RRID: AB_2576217; 1:200 for IF); and goat anti-rabbit IgG (H+L) cross-adsorbed secondary antibody, Alexa Fluor 594 (A-11012, RRID: AB_2534079; 1:200 for IHC). Horseradish peroxidase (HRP)-conjugated goat anti-mouse IgG (115-035-003, RRID: AB_10015289; 1:5,000 dilution for IB) and goat anti-rabbit IgG (111-035-003, RRID: AB_2313567; 1:5,000 dilution for IB) were purchased from Jackson ImmunoResearch.

The following reagents were purchased from Sigma (catalogue numbers in parentheses): DMSO (D2650), LCA (L6250), (2-hydroxypropyl)-β-cyclodextrin (C0926), methanol (646377), ethanol (459836), chloroform (C7559), PBS (P5493), Triton X-100 (T9284), sodium acetate (NaAc; S5636), nuclease-free water (W4502), human tubal fluid (HTF) medium (MR-070-D), KSOM medium (MR-121-D), L-glutathione reduced (GSH; G4251), NaCl (S7653), $CaCl_2$ (C5670), $MgSO_4$ (M2643), KH_2PO_4 (P5655), K_2HPO_4 (P9666), streptomycin (85886), cholesterol (C3045), agar (A1296), propionic acid (P5561), sucrose (S7903), glucose (G7021), 2-methylbutane (isopentane; M32631), paraformaldehyde (158127), Canada balsam (C1795), BSA (A2153), glycerol (G5516), Na_2HPO_4 (S7907), sodium hypochlorite solution (NaClO; 239305), NaOH (S8045), Iron(II) sulfate heptahydrate ($FeSO_4$; F8633), HEPES (H4034), EDTA (E6758), EGTA (E3889), $MgCl_2$ (M8266), KCl (P9333), IGEPAL CA-630 (NP-40; I3021), dithiothreitol (DTT; 43815), IPTG (I6758), carbenicillin (C1613), D-mannitol (M4125), glycine (G8898), isopropanol (34863), diethylpyrocarbonate (DEPC)-treated water (693520), trioxsalen (TMP; T6137), methyl 4-hydroxybenzoate (methyl paraben; H3647), mineral oil (M5310), halocarbon oil 700 (H8898), halocarbon oil 27 (H8773), paraquat (36541), H_2O_2 (H1009), agarose (A9539), proteinase K (P6556), L-methionine sulfone (M0876), D-campher-10-sulfonic acid (1087520), acetonitrile (34888), ammonium acetate (73594), ammonium hydroxide solution (338818), 3-aminopyrrolidine dihydrochloride (404624), *N*,*N*-diethyl-2-phenylacetamide (384011), trimesic acid (482749), diammonium hydrogen phosphate (1012070500), ammonium trifluoroacetate (56865), formic acid (5.43804), diammonium hydrogen phosphate (1012070500), ammonium trifluoroacetate (56865), Tween-20 (P9416), hexadimethrine bromide (polybrene; H9268), octyl β-D-glucopyranoside (ODG; O8001), Trizma base (Tris; T1503), sodium pyrophosphate (P8135), β-glycerophosphate (50020), SDS (436143), sodium deoxycholate (S1827), β-mercaptoethanol (M6250), formaldehyde solution (formalin; F8775), chloroform-*d* (with 0.05% (v/v) tetramethylsilane (TMS); 612200), *N*,*N*-dimethylformamide (DMF; 33120), *N*,*N*-diisopropylethylamine (DIEA; 199818), dichloromethane (DCM; 650463), Na_2SO_4 (746363), $NaHCO_3$ (S5761), ATP (A7699), IPTG (I6758), imidazole (I5513), HIS-select nickel affinity gel (P6611), Coomassie Brilliant Blue R-250 (1.12553), acetic acid (27225), TCEP (C4706), TBTA (678937), $CuSO_4$ (C1297), trichloroacetic acid (91228), ammonium formate (70221), FCCP (C2920), sodium azide (NaN_3; S2002), gentamycin (345814), collagenase A (11088793001), oligomycin A (75351), concanamycin A (conA; C9705), fluorescein isothiocyanate–dextran (FITC-dextran; FD10S), lysosome isolation kit (LYSISO1) and Duolink In Situ Red Starter kit (Mouse/Rabbit; DUO92101). The following reagents were purchased from Thermo: TRIzol (15596018), Phusion High-Fidelity DNA Polymerase kit (F530N), mMESSAGE mMACHINE T7 Transcription kit (AM1344), MEGAclear Transcription Clean-Up kit (AM1908), MEGAshortscript T7 Transcription kit (AM1354), Maxima SYBR Green/ROX qPCR master mix (K0223), SulfoLink Immobilization kit for Peptides (44999), DMEM, high glucose (DMEM; 12800082), FBS (10099141C), penicillin–streptomycin (15140163), Lipofectamine 2000 (11668500), MEM non-essential amino acids solution (11140050), GlutaMAX (35050061), sodium pyruvate (11360070), ProLong Diamond antifade mountant (P36970), ProLong Live Antifade reagent (P36975), streptavidin magnetic beads (88817; 1:100 for IP), prestained protein MW marker (26612), and LysoSensor Green DND-189 (L7535). MinElute PCR Purification kit (28004) was purchased from Qiagen. EX-527 (S1541) and MG-132 (S2619) were purchased from Selleck. Biospin Tissue Genomic DNA Extraction kit (BSC04M1) was purchased from BioFlux. hCG (110900282) and PMSG (110904564) were purchased from Sansheng Biological Technologyk. WesternBright ECL and peroxide solutions (210414-73) were purchased from Advansta. Bacteriological peptone (LP0037) and yeast extract (LP0021) were purchased from Oxoid. Protease inhibitor cocktail (70221) was purchased from Roche. 3-Hydroxynaphthalene-2,7-disulfonic acid disodium salt (2-naphtol-3,6-disulfonic acid disodium salt; H949580) was purchased from Toronto Research Chemicals. Hexakis(1*H*,1*H*,3*H*-perfluoropropoxy)phosphazene (hexakis(1*H*,1*H*,3*H*-tetrafluoropropoxy)phosphazine; sc-263379) was purchased from Santa Cruz Biotechnology. Polyethylenimine (PEI; 23966) was purchased from Polysciences. Nonfat dry milk (9999) and normal goat serum (NGS; 5425) were purchased from Cell Signaling Technology. 2-(3-(but-3-*yn*-1-*yl*)-3*H*-diazirin-3-yl)Ethan-1-amine and 1*H*-benzotriazol-1-yloxytris(dimethylamino)phosphonium hexafluorophosphate (BOP) were purchased from Bidepharm. OCT compound (4583) was purchased from Sakura. ReverTra Ace qPCR RT master mix with gDNA remover (FSQ-301) was purchased from Toyobo. PrimeSTAR HS polymerase (R40A) was purchased from Takara. Dry yeast (FLY804020F) and cornmeal (FLY801020) were purchased from LabScientific. Soy flour (62116) was purchased from Genesee Scientific. Light corn syrup was purchased from Karo. Grape juice was purchased from Welch's. Cell Counting Kit-8 (CCK-8) was purchased from ApexBio. [U-^{13}C]-glutamine (184161-19-1) was purchased from Cambridge Isotope Laboratories. rProtein A Sepharose Fast Flow (17127904), Protein G Sepharose 4 Fast Flow (17061806) and Superdex 200 Increase 10/300 GL (28990944) were purchased from Cytiva.

Cell lines

In this study, no cell lines used are on the list of known misidentified cell lines maintained by the International Cell Line Authentication Committee (https://iclac.org/databases/cross-contaminations/). HEK293T cells (CRL-3216) were purchased from the American Type Culture Collection. *LAMTOR1*$^{F/F}$, *AXIN*$^{F/F}$ and *PKCZ*$^{F/F}$ MEFs were established by introducing SV40 T antigen using lentivirus into cultured primary embryonic cells from mouse litters. *LAMTOR1*$^{-/-}$ MEFs were generated by infecting *LAMTOR1*$^{F/F}$ MEFs with adenoviruses expressing the Cre recombinase for 12 h, as for *AXIN*$^{-/-}$ MEFs and *PKCZ*$^{-/-}$ MEFs. The infected cells were then incubated in fresh DMEM for another 12 h before further treatments. The *ALDO*-TKD[10], *TRPV*-QKO[12], *PEN2*$^{-/-}$ (ref. 15), *ATP6AP1*$^{-/-}$ (ref. 15) and *AMPKA1/2*$^{-/-}$ (ref. 128) MEFs, and si*ATP6V0C*[11] HEK293T cells were generated and validated as previously described. HEK293T cells and MEFs were maintained in DMEM supplemented with 10% FBS, 100 IU penicillin and 100 mg ml^{-1} streptomycin at 37 °C in a humidified incubator containing 5% CO_2. All cell lines were verified to be free from mycoplasma contamination. HEK293T cells and MEFs were authenticated by STR sequencing performed by Immocell Biotechnology. PEI at a final concentration of 10 μM was used to transfect HEK293T cells (ectopic expression). Total DNA to be transfected for each plate was adjusted to the same amount by using relevant empty vector. Transfected cells were collected at 24 h after transfection.

Lentiviruses, including those for knockdown or stable expression (expressed at close-to-endogenous levels), were packaged in HEK293T cells by transfection using Lipofectamine 2000. At 30 h after transfection, medium (DMEM supplemented with 10% FBS and MEM non-essential amino acids; approximately 2 ml) was collected and centrifuged at 5,000*g* for 3 min at room temperature.

The supernatant was mixed with 10 μg ml^{-1} polybrene and was added to MEFs or HEK293T cells, followed by centrifuging at 3,000*g* for 30 min at room temperature (spinfection). Cells were incubated for another 24 h (MEFs) or 12 h (HEK293T cells) before further treatments. The sequence of each siRNA used to knockdown mouse *Tulp3* is: 5′-GCATCTTGAGTAGTGTGAACTATGA-3′ (1), 5′-CCAGCTTGGAGAAGTGGAGAATTTA-3′ (2), and 5′-GAGAATTTAGAGGACTTTGCGTATA-3′ (3).

Genes encoding SIRT1–SIRT7, FXR, FXRβ, PXR, VDR, CAR, LXRα, LXRβ, S1PR2, CHRM2, CHRM3, FAS, FPR1, YES1 and TULP3 were deleted from MEFs using the CRISPR–Cas9 system. Nucleotides were annealed to their complements containing the cloning tag aaac and inserted into the back-to-back BsmB I restriction sites of the lentiCRISPRv2 vector. The sequence for each sgRNA is as follows: 5′-CGGTATCTATGCTCGCCTTG-3′ and 5′-CAAGGCGAGCATAGATACCG-3′ for *Sirt1*, 5′-AAGGACGGGGAACTTACACG-3′ and 5′-CGTGTAAGTTCCCCGTCCTT-3′ for *Sirt2*, 5′-AACATCGACGGGCTTGAGAG-3′ and 5′-CTCTCAAGCCCGTCGATGTT-3′ for *Sirt3*, 5′-GGCGGCACAAATAACCCCGA-3′ and 5′-TCGGGGTTATTTGTGCCGCC-3′ for *Sirt4*, 5′-CATTGACGAGTTGCATCGCA-3′ and 5′-TGCGATGCAACTCGTCAATG-3′ for *Sirt5*, 5′-CGAGGGCCGAGCATTCTCGA-3′ and 5′-TCGAGAATGCTCGGCCCTCG-3′ for *Sirt6*, 5′-CCGACTTCGACCCTGCAGCT-3′ and 5′-AGCTGCAGGGTCGAAGTCGG-3′ for *Sirt7*, 5′-ACCAGTCTTCCGGTTGTTGG-3′ and 5′-CCAACAACCGGAAGACTGGT-3′ for *Fxr* (1), 5′-CGAATGGCCGCGGCATCGGC-3′ and 5′-GCCGATGCCGCGGCCATTCGC-3′ for *Fxr* (2), 5′-ACCAGTCTTCCGGTTGTTGG-3′ and 5′-CCAACAACCGGAAGACTGGT-3′ for *Fxrb* (1), 5′-GGACTCGACGCTCGAGAATC-3′ and 5′-GATTCTCGAGCGTCGAGTCC-3′ for *Fxrb* (2), 5′-TGAAACGCAATGTCCGGCTG-3′ and 5′-CAGCCGGACATTGCGTTTCA-3′ for *Pxr* (1), 5′-GATCATGTCCGATGCCGCTG-3′ and 5′-CAGCGGCATCGGACATGATC-3′ for *Pxr* (2), 5′-ACTTTGACCGGAATGTGCCT-3′ and 5′-AGGCACATTCCGGTCAAAGT-3′ for *Vdr* (1), 5′-TGGAGATTGCCGCATCACCA-3′ and 5′-TGGTGATGCGGCAATCTCCA-3′ for *Vdr* (2), 5′-CGGCCCATATTCTTCTTCAC-3′ and 5′-GTGAAGAAGAATATGGGCCG-3′ for *Car* (1), 5′-GGGGCCCACACTCGCCATGT-3′ and 5′-ACATGGCGAGTGTGGGCCCC-3′ for *Car* (2), 5′-TTCCGCCGCAGTGTCATCAA-3′ and 5′- TTGATGACACTGCGGCGGAA -3′ for *Lxra*, 5′-GCCGGGCGCTATGCCTGTCG-3′ and 5′-CGACAGGCATAGCGCCCGGC-3′ for *Lxrb* (1), 5′-CATAGCGCCCGGCCCCACCG-3′ and 5′-CGGTGGGGCCGGGCGCTATG-3′ for *Lxrb* (2), 5′-CGTGCAGTGGTTTGCCCGAG-3′ and 5′-CTCGGGCAAACCACTGCACG-3′ for *S1pr2* (1), 5′-AAGACGGTCACCATCGTACT-3′ and 5′-AGTACGATGGTGACCGTCTT-3′ for *S1pr2* (2), 5′-GCATGATGATTGCAGCTGCG-3′ and 5′-CGCAGCTGCAATCATCATGC-3′ for *Chrm2*, 5′-GCCGTGCCGAAGGTGATGGT-3′ and 5′-ACCATCACCTTCGGCACGGC-3′ for *Chrm3* (1), 5′-AGCCGGTGTGATGATTGGTC-3′ and 5′-GACCAATCATCACACCGGCT-3′ for *Chrm3* (2), 5′-TCTCCGAGAGTTTAAAGCTG-3′ and 5′-CAGCTTTAAACTCTCGGAGA-3′ for *Fas* (1), 5′-TGCTCAGAAGGATTATATCA-3′ and 5′-TGATATAATCCTTCTGAGCA-3′ for *Fas* (2), 5′-AGAAGGTAATCATCGTACCC-3′ and 5′-GGGTACGATGATTACCTTCT-3′ for *Fpr1* (1), 5′-GGGCAACGGGCTCGTGATCT-3′ and 5′-AGATCACGAGCCCGTTGCCC-3′ for *Fpr1* (2), 5′-TCTAGTCGCAATGATTCTCG-3′ and 5′-CGAGAATCATTGCGACTAGA-3′ for *Yes1*, 5′-CTCCCCGTCGGCTCGCTCAG-3′ and 5′-CTGAGCGAGCCGACGGGGAG-3′ for *Tulp3* (1), 5′-ACGTCGCTGCGAGGCATCTG-3′ and 5′-CAGATGCCTCGCAGCGACGT-3′ for *Tulp3* (2). The constructs were then subjected to lentivirus packaging using HEK293T cells that were transfected with 2 μg of DNA in Lipofectamine 2000 transfection reagent per well of a 6-well plate. At 30 h after transfection, the virus (approximately 2 ml) was collected for infecting MEFs as described above, except cells cultured to 15% confluence were incubated with the virus for 72 h. When cells were approaching to confluence, they were single-cell sorted into 96-well dishes. Clones were expanded and evaluated for knockout status by sequencing.

To knock in the HA-tag in front of the first exon of *Sirt3*, *Sirt4* and *Sirt5* in MEFs, the 3×HA sequence (insert) flanked by 150-bp 5′ and 3′ sequences of *Sirt3*, *Sirt4* or *Sirt5* (5′ and 3′ homology arms), was synthesized and cloned into a pBluescript II KS (+) vector as a template. MEFs grown in a 10-cm dish to 80% confluence were trypsinized and resuspended with 2 ml DMEM, followed by determining the cell density using a CountStar (IC 1000) cell counter equipped with a chamber slide (12-0005-50). About 10^6 cells were then suspended with 400 μl of electroporation buffer (freshly prepared by mixing 80 μl of solution A (362.88 mM ATP and 590.26 mM $MgCl_2$ in di-distilled water, sterilized by passing through a 0.22-μm filter) with 4 ml of solution B (88.18 mM KH_2PO_4, 14.284 mM $NaHCO_3$ and 2.2 mM glucose, pH 7.4 in di-distilled water, sterilized by passing through a 0.22-μm filter)) in a Gene Pulser/MicroPulser electroporation cuvette (0.4-cm gap; 1652088, Bio-Rad), followed by mixing with 2 μg of *Cas9* mRNA (synthesized as previously described[129] and dissolved with DEPC water to a 1.5 μg μl^{-1} stock solution), 2 μg of sgRNA (synthesized and chemically modified by the EasyEdit sgRNA synthetic service provided by GenScript, dissolved with DEPC water to a 1 μg μl^{-1} stock solution) and 6 μg of the template. Cells were then electroporated on a Nucleofector II (Lonza) electroporator using the T-020 programme, followed by incubating in 2 ml DMEM in a 6-well dish at 37 °C in a humidified incubator containing 5% CO_2 for 30 min. The presence of the HA-tag was validated by sequencing. The sequence for each sgRNA is as follows: 5′-CATGACCACCACCCTACTGC-3′ for *Sirt3*, 5′-ATTGACTTTCAGGCCGACAA-3′ for *Sirt4*, and 5′-CAATCAGGAGAGGTCGCATC-3′ for *Sirt5*.

Plasmids

Full-length cDNAs used in this study were obtained either by PCR using cDNA from MEFs or by purchasing from Origene or Sino Biological. The DN mutants of SIRT1–SIRT7, that is, SIRT1(H363Y)[130], SIRT2(H150Y)[131], SIRT3(H248Y)[65], SIRT4(H161Y)[132], SIRT5(H158Y)[133], SIRT6(H133Y)[29] and SIRT7(H187Y)[70], were generated according to previous reports. Mutations of V1E1, SIRT1–SIRT7 and TULP3 were performed by PCR-based site-directed mutagenesis using PrimeSTAR HS polymerase. Expression plasmids for various epitope-tagged proteins were constructed in a pcDNA3.3 vector (K830001, Thermo) for transfection (ectopic expression) in mammalian cells, in a pBOBI vector for lentivirus packaging (stable expression) in mammalian cells, in a in pLVX-IRES (for ALDOA; 631849, Takara) for doxycycline-inducible expression in mammalian cells, or in a pET-28a vector (69864-3, Novagen) for bacterial expression. PCR products were verified by sequencing (Invitrogen). All expression plasmids constructed in this study have been deposited into Addgene (https://www.addgene.org/Sheng-cai_Lin/). The lentivirus-based vector pLV-H1-EF1a-puro (SORT-B19, Biosettia) was used for the expression of siRNA in MEFs. *E. coli* strain DH5α (PTA-1977) was purchased from the American Type Culture Collection, and Stbl3 (C737303) was from Thermo. All plasmids were amplified in *E. coli* strain DH5α, except those for mutagenesis in Stbl3. All plasmids used in this study were purified by using CsCl density gradient ultracentrifugation method.

Immunoprecipitation and IB assays

For determining the formation of the AMPK-activating complex, endogenous AXIN was immunoprecipitated and analysed as previously described[11]. In brief, four 15-cm dishes of MEFs (grown to 80% confluence) were collected for immunoprecipitation of AXIN. Cells were lysed with 750 μl per dish of ice-cold ODG buffer (50 mM Tris-HCl, pH 8.0, 50 mM NaCl, 1 mM EDTA, 2% (w/v) ODG, 5 mM β-mercaptoethanol with protease inhibitor cocktail), followed by sonication and centrifugation at 4 °C for 15 min. Cell lysates were incubated with anti-AXIN antibody overnight. Overnight protein aggregates were pre-cleared by centrifugation at 20,000 *g* for 10 min, and protein A/G beads (1:250, balanced with ODG buffer) were then added into the lysate–antibody mixture for another 3 h at 4 °C. The beads were centrifuged and washed with 100 times the volume of ODG buffer 3 times (by centrifuging at 2,000*g*) at 4 °C and then mixed with an equal volume of 2× SDS sample buffer and boiled for 10 min before IB.

To determine the interaction between ectopically expressed TULP3 and sirtuins, a 6 cm-dish of HEK293T cells was transfected with different expression plasmids. At 24 h after transfection, cells were collected and lysed in 500 µl of ice-cold Triton lysis buffer (20 mM Tris-HCl, pH 7.5, 150 mM NaCl, 1 mM EDTA, 1 mM EGTA, 1% (v/v) Triton X-100, 2.5 mM sodium pyrophosphate, 1 mM β-glycerophosphate, with protease inhibitor cocktail), followed by sonication and centrifugation at 4 °C for 15 min. Anti-HA-tag (1:100) or anti-MYC-tag (1:100) antibodies, along with protein A/G beads (1:100, pre-balanced in Triton lysis buffer) were added into the supernatant and mixed for 4 h at 4 °C. The beads were washed with 200 times the volume of ice-cold Triton lysis buffer wash buffer 3 times at 4 °C and then mixed with an equal volume of 2× SDS sample buffer and boiled for 10 min before IB.

The ubiquitination of V1E1 was determined as previously described[134]. In brief, a 6 cm-dish of HEK293T cells were transfected with 6 µg HA-tagged V1E1 and 6 µg Flag-tagged ubiquitin. At 12 h after transfection, cells were treated with 20 nM MG-132 for another 12 h. The culture medium was then aspirated, and the cells were lysed by quick addition of 500 µl of RIPA buffer containing 1% SDS (25 mM Tris-HCl, pH 7.6, 150 mM NaCl, 1% (v/v) NP-40, 1% (w/v) sodium deoxycholate, 1% (w/v) SDS) into the dish, followed by boiling in water for 15 min. The lysates were then diluted with 9-fold volumes of RIPA buffer without SDS, and 500 µl of the diluent was used for immunoprecipitation of HA-tag as described above. The levels of V1E1 ubiquitination were then determined by IB.

To analyse the levels of pAMPKα, pACC and V1E1(K99)ac in HEK293T cells and MEFs, cells grown to 70–80% confluence in a well of a 6-well dish were lysed with 250 µl of ice-cold Triton lysis buffer. The lysates were then centrifuged at 20,000*g* for 10 min at 4 °C and an equal volume of 2× SDS sample buffer was added to the supernatant. Samples were then boiled for 10 min and then directly subjected to IB. To analyse the levels of pAMPKα, pACC and V1E1(K99)ac in muscle and liver tissues, mice were anaesthetized after indicated treatments. Freeze-clamped tissues were immediately lysed with ice-cold Triton lysis buffer (10 µl mg^{-1} tissue weight for liver, and 5 µl mg^{-1} tissue weight for muscle), followed by homogenization and centrifugation as described above. The lysates were then mixed with 2× SDS sample buffer, boiled and subjected to IB. To analyse the levels of p-AMPKα and pACC in flies, 20 adults or third instar larvae were lysed with 200 µl ice-cold RIPA buffer (50 mM Tris-HCl, pH 7.5, 150 mM NaCl, 1% NP-40, 0.5% sodium deoxycholate, with protease inhibitor cocktail) containing 0.1% SDS, followed by homogenization and centrifugation as described above. The lysates were then mixed with 5× SDS sample buffer, boiled and subjected to IB. To analyse the levels of pAMPKα and pACC in nematodes, 150 nematodes cultured on NGM plates were collected for each sample. Worms were quickly washed with ice-cold M9 buffer containing Triton X-100 and were lysed with 150 µl of ice-cold lysis buffer. The lysates were then mixed with 5× SDS sample buffer, followed by homogenization and centrifugation as described above and then boiled before being subjected to IB.

All samples were subjected to IB on the same day of preparation, and any freeze–thaw cycles were avoided.

For IB, the SDS–PAGE were prepared in house, as previously described[15]. The thickness of the gels used in this study was 1.0 mm. Samples of less than 10 µl were loaded into wells, and electrophoresis was run at 100 V (using a PowerPac HC High-Current Power Supply, Bio-Rad) in a Mini-PROTEAN Tetra Electrophoresis Cell (Bio-Rad). In this study, all samples were resolved on 8% resolving gels, except those for H3, H3K9ac, LAMTOR1, OXPHOS proteins and ATP6V0C, which were on 15% gels (prepared as those for 8%, except that a final concentration of 15% Acryl–Bis was added to the resolving gel solution), and β-actin, GAPDH, ALDOA, V1E1 and V1E1(K99)ac, which were on 10% gels. The resolved proteins were then transferred to the PVDF membrane (0.45 µm, IPVH00010, Merck) as previously described[15]. The PVDF membrane was then blocked by 5% (w/v) BSA (for all antibodies against phosphorylated proteins) or 5% (w/v) nonfat milk (for all antibodies against total proteins) dissolved in TBST for 2 h on an orbital shaker at 60 r.p.m. at room temperature, followed by rinsing with TBST for twice, 5 min each. The PVDF membrane was then incubated with the desired primary antibody overnight at 4 °C on an orbital shaker at 60 r.p.m., followed by rinsing with TBST 3 times, 5 min each at room temperature, and then the secondary antibodies for 3 h at room temperature with gentle shaking. The secondary antibody was then removed, and the PVDF membrane was further washed with TBST 3 times, 5 min each, at room temperature. The PVDF membrane was incubated in an ECL mixture (by mixing equal volumes of ECL solution and peroxide solution for 5 min), then life with medical X-ray film (Fujifilm). The films were then developed using X-OMAT MX developer (Carestream), and X-OMAT MX fixer and replenisher solutions (Carestream) on a medical X-ray processor (Carestream) using Developer (Model 002, Carestream). The developed films were scanned using a Perfection V850 Pro scanner (Epson) with Epson Scan software (v.3.9.3.4) and were cropped using Photoshop 2023 software (Adobe). Levels of total proteins and phosphorylated proteins were analysed on separate gels, and representative immunoblots are shown. Uncropped immunoblots are shown in Supplementary Fig. 1. The band intensities on developed films were quantified using ImageJ software (v.1.8.0, National Institutes of Health Freeware) and formatted using Illustrator 2022 (Adobe).

Confocal microscopy

For determining the lysosomal localization of AXIN and LKB1, cells grown to 80% confluence on coverslips in 6-well dishes were fixed for 20 min with 4% (v/v) formaldehyde in PBS at room temperature. The coverslips were rinsed twice with PBS and permeabilized with 0.1% (v/v) Triton X-100 in PBS for 5 min at 4 °C. After rinsing twice with PBS, the sections were blocked with PBS containing 5% BSA for 30 min at room temperature. Then the coverslips were incubated with anti-AXIN or anti-LKB1, and anti-LAMP2 antibodies (all at 1:100, diluted in PBS) overnight at 4 °C. The cells were then rinsed 3 times with 1 ml of PBS and then incubated with secondary antibody for 8 h at room temperature in the dark. Cells were washed another 4 times with 1 ml PBS and then mounted on slides using ProLong Diamond antifade mountant. Confocal microscopy images were taken using a STELLARIS 8 FALCON (Leica) system equipped with HyD SMD detectors and a HC PL APO CS2 ×63/1.40 oil objective (Leica). All parameters were kept unchanged between imaging. Images were taken and analysed using LAS X Software (v.3.0.2.16120, Leica) and formatted using Photoshop 2023 software (Adobe).

The localization of SIRT3, SIRT4 and SIRT5 (HA-tagged) was determined as described above, except that antibodies against HA-tag and TOMM20 were used. For SIRT1, MEFs grown to 80% confluence on coverslips in 6-well dishes were fixed for 20 min with 4% (v/v) formaldehyde in PBS at room temperature. The coverslips were rinsed twice with PBS and permeabilized with 0.5% (v/v) NP-40 in PBS for 15 min at room temperature. After rinsing twice with PBS, the sections were blocked with PBS containing 5% BSA for 30 min at room temperature. The coverslips were then incubated with anti-SIRT1 antibodies (1:100, diluted in PBS) for 8 h at room temperature, followed by rinsing 3 times with 1 ml of PBS. Cells were then incubated with Alexa Fluor 488-conjugated, goat anti-rabbit IgG secondary antibody (1:100, diluted in PBS) for 2 h at room temperature and at 37 °C for another 30 min in the dark. Cells were washed another 4 times with 1 ml PBS and then mounted on slides using the Duolink In Situ mounting medium with DAPI (from a Duolink In Situ Red Starter kit). Confocal microscopy images were taken using a STELLARIS 8 FALCON (Leica) system equipped with HyD SMD detectors and a HC PL APO CS2 63x/1.40 oil objective (Leica). All parameters were kept unchanged between imaging. Images were taken and analysed using LAS X Software (v.3.0.2.16120, Leica) and formatted using Photoshop 2023 software (Adobe).

For detecting the pH of lysosomes, cells were grown on a 4-chamber 35-mm glass-bottom dish (D35C4-20-1.5-N, In Vitro Scientific). Cells

were cultured to 60–80% confluence and then treated with LCA or DMSO control in neighbouring chambers in the same 35-mm dish. Cells were treated with 1 μM (final concentration) LysoSensor Green DND-189 (ref. 135) for 30 min, then washed twice with PBS and incubated in fresh medium for another 30 min. In the meantime, ProLong Live antifade reagent was added to the medium before taking images. All cells were stained and processed simultaneously. In particular, any counterstaining, such as using Hoechst dye to stain the nucleus, was avoided in this experiment to prevent nonspecific staining. During imaging, live cells were kept at 37 °C, 5% CO_2 in a humidified incubation chamber (Zeiss, Incubator PM S1). All parameters, such as PMT voltage, offset, pinhole and gain were kept unchanged between each picture taken. Images were taken using a Zeiss LSM 980 with a ×63, 1.4 NA oil objective.

The PLA/Duolink assay was performed using a Duolink In Situ Red Starter kit (Mouse/Rabbit) as previously described[136]. In brief, WT MEFs, or HA-tagged SIRT3-knockin (SIRT3-KI), SIRT4-KI or SIRT5-KI MEFs, all stably expressing MYC-tagged TULP3 (or TULP3(Δ1–60)) were grown to 80% confluence on coverslips in 6-well dishes, followed by fixation for 20 min with 4% (v/v) formaldehyde in PBS, 2 ml per coverslip per well at room temperature. The coverslips were rinsed twice with 2 ml PBS and permeabilized with 2 ml of 0.1% (v/v) Triton X-100 in PBS for 10 min at 4 °C. Cells were then blocked with Duolink blocking solution (50 μl per coverslip) in a humidified chamber at 37 °C for 1 h. Cells were then incubated with primary antibodies (1:100 diluted with Duolink antibody diluent; 50 μl per coverslip) in a humidified chamber at 4 °C for 12 h, followed by washing with 2 changes of 2 ml of wash buffer A, 5 min per change, at room temperature. The coverslip was then incubated with Plus and Minus PLA probe solution (freshly prepared by mixing 10 μl of PLA probe Minus stock, 10 μl of PLA probe Plus stock with 30 μl of Duolink antibody diluent; 50 μl per coverslip) in a humidified chamber at 37 °C for 1 h, followed by washing with 2 changes of 2 ml of wash buffer A, 5 min per change, at room temperature. The coverslip was then incubated with ligation solution (freshly prepared by 1:5 diluting Duolink ligation buffer with water, followed by the addition of ligase stock at a ratio of 1:50; 50 μl per coverslip) in a humidified chamber at 37 °C for 0.5 h, followed by washing with 2 changes of 2 ml of wash buffer A, 5 min per change, at room temperature. The coverslip was then incubated with amplification solution (freshly prepared by 1:5 diluting amplification buffer with water, followed by addition of polymerase stock at a ratio of 1:80; 50 μl per coverslip) in a humidified chamber at 37 °C for 100 min, followed by washing with 2 changes of 2 ml of wash buffer B, 10 min per change, at room temperature. The coverslip was then washed with 2 ml of 0.01× wash buffer B for 1 min at room temperature, followed by mounting with 15 μl of Duolink PLA mounting medium with DAPI for 30 min, and then subjected to imaging using an LSM 980 (Zeiss) as described above, except that a DPSS laser module (Lasos) at 594 nm and a diode laser module (Lasos) at 405 nm were used to excite the PLA and DAPI, respectively.

FRET–FLIM assay

FRET-FLIM experiments were carried out as previously described[136]. In brief, HEK293T cells stably expressing TULP3–GFP ('donor only', as a control), or different combinations of SIRT1–mCherry and TULP3–GFP, or TULP3(Δ1–60)–GFP as a control, were cultured in 35-mm glass-bottom dishes (D35-20-10-N, In Vitro Scientific) to 60–80% confluence in a humidified chamber with 5% CO_2 at 37 °C, followed by determining the fluorescence lifetime of GFP in different cells using a STELLARIS 8 FALCON (Leica) system equipped with HyD X and HyD SMD detectors and a HC PL APO CS2 ×63/1.40 oil objective (Leica). Cells were excited with a 460-nm laser through the system's tuneable white light laser, and photon arrival times were recorded using a HyD X detector covering the GFP emission spectrum (460–510 nm). All parameters were kept unchanged between imaging. Images were taken and analysed using LAS X software (v.3.0.2.16120, Leica). In all experiments, the position of the focal plane was actively stabilized using Leica auto focus control to prevent any focal drift or focus artefacts.

Synthesis of the LCA probe

All reagents and solvents were obtained from commercial suppliers and described in the section 'Reagents'. In this section, the following equipment were used: preparative HPLC (Sail 1000, Welch Materials) equipped with a RD-C18 column (30.0 × 250 mm, 5 μm; Welch Materials) was used for the purification of LCA probe; 3100 Mass Detector (Waters) was used to record MS spectra for each compound; Q-Exactive Orbitrap MS (Thermo) was used to record high-resolution MS spectra for each compound; HPLC with UV detection at 220 nm (HD-C18 column, 5 μm, 4.6 × 250 mm, Agilent Technologies) was used to determine the purity of the LCA probe, and the gradients were as follows: t = 0 min, 20% solvent B (methanol) and 80% solvent A (H_2O); t = 10 min, 100% solvent B (methanol) and 0% solvent A (H_2O); t = 30 min, 100% B (methanol) and 0% solvent A (H_2O) with a constant flow rate at 1 ml min^{-1}); and Bruker Avance III 600 MHz NMR spectrometer (^{1}H: 600 MHz; ^{13}C: 151 MHz) was used to record NMR spectra (spectrometer instrument in chloroform-*d*, with TMS as the internal standard; chemical shifts are reported in δ (ppm), multiplicities (s = singlet, d = doublet, t = triplet, q = quartet, p = pentet, dd = doublet of doublets, td = triplet of doublets, tt = triplet of triplets and m = multiplet), integration and coupling constants (J in Hz), and ^{1}H and ^{13}C chemical shifts are relative to the solvent: δ_H of 7.26 and δ_C of 77.2 for chloroform-*d*).

The biotin-N_3 linker was synthesized as previously described[137], and the LCA probe was synthesized through an amide condensation reaction between LCA and 2-(3-(but-3-*yn*-1-yl)-3*H*-diazirin-3-yl)ethan-1-amine. In brief, LCA (55 mg, 0.146 mmol, 1.0 eq) was dissolved in 2 ml of DMF, followed by mixing with 97.3 mg BOP (0.219 mmol, 1.5 eq). After 30 min of stirring at room temperature, 24 mg of 2-(3-(but-3-*yn*-1-yl)-3*H*-diazirin-3-yl)ethan-1-amine (0.175 mmol, 1.2 eq) and 0.073 ml DIEA (0.438 mmol, 3.0 eq) were added to the mixture, followed by stirring for another 12 h at room temperature. The mixture was then diluted with 20 ml H_2O, followed by extracting with 30 ml of DCM for 3 rounds. The organic phase obtained from the three rounds of extraction was pooled, dried by anhydrous Na_2SO_4 and then evaporated on a rotary evaporator (Rotavapor R-300, BUCHI) at 90 r.p.m. at room temperature. The powder was then dissolved in 1 ml DMSO, followed by purifying using preparative HPLC with the following gradients: t = 0 min, 50% solvent B (methanol) and 50% solvent A (H_2O); t = 15 min, 80% solvent B (methanol) and 2% solvent A (H_2O); t = 25 min, 100% B (methanol) and 0% solvent A (H_2O); t = 45 min, 100% B (methanol) and 0% solvent A (H_2O) with a constant flow rate at 20 ml min^{-1}. The LCA probe was obtained as a white solid with a yield of 80.7% (58.4 mg) and was dissolved in DMSO to a stock concentration of 50 mM. The solution was stored at 4 °C for no more than 1 month.

LCA probe: ^{1}H NMR (600 MHz, chloroform-*d*) δ 5.71 (t, J = 5.9 Hz, 1H), 3.62 (tt, J = 10.6, 4.6 Hz, 1H), 3.10 (q, J = 6.5 Hz, 2H), 2.24 (ddd, J = 14.5, 10.6, 5.1 Hz, 1H), 2.10–2.05 (m, 1H), 2.04–2.01 (m, 3H), 1.98–1.94 (m, 1H), 1.89–1.77 (m, 5H), 1.77–1.72 (m, 1H), 1.69 (t, J = 6.7 Hz, 2H), 1.67–1.63 (m, 3H), 1.60–1.54 (m, 1H), 1.53–1.48 (m, 1H), 1.44–1.35 (m, 6H), 1.35–1.29 (m, 2H), 1.28–1.19 (m, 3H), 1.17–1.12 (m, 1H), 1.09 (dd, J = 11.5, 7.8 Hz, 2H), 1.07–1.03 (m, 2H), 0.97 (td, J = 14.3, 3.5 Hz, 1H), 0.93 (d, J = 6.8 Hz, 3H), 0.92 (s, 3H), 0.64 (s, 3H); ^{13}C NMR (151 MHz, chloroform-*d*) δ 173.7, 82.7, 71.8, 69.4, 56.5, 56.0, 42.8, 42.1, 40.5, 40.2, 36.5, 35.9, 35.5, 35.4, 34.6, 34.3, 33.6, 32.6, 32.2, 31.7, 30.6, 28.2, 27.2, 26.9, 26.4, 24.2, 23.4, 20.8, 18.4, 13.2, 12.1. MS (ESI) m/z: 496 $[M + H]^+$. HRMS (ESI): $[M + H]^+$ calculated for $C_{31}H_{50}O_2N_3$, 496.3898; found, 496.3910. HPLC analysis: retention time = 14.55 min; peak area, 98.02% (λ = 220 nm).

Protein expression

The cDNAs encoding human SIRT1, TULP3, ktub, tub-1 and mutants were inserted into pET-28a vectors for expressing His-tagged recombinant proteins. The pET-28a plasmids were transformed into the *E. coli* strain

BL21 (DE3) (EC0114, Thermo), followed by culturing in LB medium in a shaker at 200 r.p.m. at 37 °C. The cultures of transformed cells were induced with 0.1 mM IPTG at an OD_{600} of 1.0. After incubating for another 12 h at 160 r.p.m. at 16 °C, the cells were collected. Cells were then homogenized in a His-binding buffer (50 mM sodium phosphate, pH 7.0, 150 mM NaCl, 1% Triton X-100, 5% glycerol and 10 mM imidazole). The homogenates were then sonicated on ice and were subjected to ultracentrifugation at 150,000*g* for 30 min at 4 °C, followed by incubating with nickel affinity gel (pre-balanced with His-binding buffer). The nickel affinity gel was then washed with 100 times the volume of ice-cold His-washing buffer (50 mM sodium phosphate, pH 7.0, 150 mM NaCl and 20 mM imidazole), and the proteins were eluted from the resin with His-elution buffer (50 mM sodium phosphate, pH 7.0, 150 mM NaCl and 250 mM imidazole) at 4 °C. Proteins were then concentrated to approximately 3 mg ml^{-1} by ultrafiltration (Millipore, UFC905096) at 4 °C, then purified by gel filtration on a Superdex 200 column (Cytiva) balanced with the Superdex buffer containing 50 mM Tris-HCl, pH 7.0 and 300 mM NaCl.

For determining the interaction between TULP3 and SIRT1 in vitro, the purified His-tagged TULP3 and SIRT1, 4 μg of each, were pre-incubated in 100 μl (final volume) of Superdex buffer on ice for 30 min. The mixtures were then placed into a Superdex 200 column balanced with Superdex buffer. The fraction size was set at 1 ml, with the mobile phase Superdex buffer and a flow rate of 0.5 ml min^{-1}. Samples were mixed with 5× SDS sample buffer, boiled and subjected to SDS–PAGE followed by Coomassie Brilliant Blue staining (see details in the section 'Determination of the binding sites of TULP3 for LCA') or IB.

Determination of the binding affinity of LCA to TULP3

To determine the binding affinity of LCA for TULP3 or SIRT1 using affinity pull-down assays, streptavidin magnetic beads bound with biotinylated LCA probe were first prepared (described in ref. 15, but with minor modifications). In brief, 10 μM LCA probe was dissolved in 100 μl ice-cold Triton lysis buffer at 4 °C, followed by mixing with 1 mM TCEP, 0.1 mM TBTA, 1 mM $CuSO_4$ and 1 mM biotin-N_3 linker (all final concentrations) at 4 °C for another 1 h. After centrifugation for 30 min at 20,000*g*, 4 °C, the supernatant was incubated with 10 μl streptavidin magnetic beads at 4 °C for 30 min, followed by washing with 100× volume of ice-cold Triton lysis buffer 3 times. The biotinylated LCA probe-bound beads were then incubated with 3 μg His-tagged TULP3, SIRT1 or TULP3–SIRT1 complex (prepared as described in the 'Protein expression' section) in 100 μl ice-cold Triton lysis buffer at 4 °C for 2 h, followed by washing with 100× volume of ice-cold Triton lysis buffer for 3 times and then incubating in 100 μl ice-cold Triton lysis buffer containing different concentrations of LCA at 4 °C for 0.5 h. The supernatants were then mixed with an equal volume of 2× SDS sample buffer, followed by IB to determine the amount of TULP3 or SIRT1 inside.

Determination of the binding sites of TULP3 for LCA

The binding sites of TULP3 for LCA were determined through a two-step approach using MS combined with silico docking assays, as previously described[15]. In brief, 10 μM LCA probe was incubated with 3 μg His-tagged TULP3 (purified as described in the section 'Protein expression') in 100 μl ice-cold Triton lysis buffer at 4 °C for 2 h and then exposed to 365-nm wavelength UV (CX-2000, UVP) for 10 min. The mixture was then adjusted to final concentrations of 1 mM TCEP, 0.1 mM TBTA, 1 mM $CuSO_4$ and 1 mM biotin-N_3 linker, and were incubated at 4 °C for another 1 h. Protein aggregates were cleared by centrifugation at 20,000 *g* for 15 min, and 10 μl streptavidin magnetic beads were then added to the supernatant for 2 h with gentle rotation. Beads were then washed with 100× volume of Triton lysis buffer for 3 times at 4 °C, followed by incubating in 100 μl ice-cold Triton lysis buffer containing different concentrations of LCA at 4 °C for 0.5 h. The supernatants were then mixed with an equal volume of 2× SDS sample buffer, followed by SDS–PAGE. After staining with Coomassie Brilliant Blue R-250 dye (5% (m/v) dissolved in 45% (v/v) methanol and 5% (v/v) acetic acid in water), gels were decoloured (in 45% (v/v) methanol and 5% (v/v) acetic acid in water), and the excised gel slices were subjected to in-gel chymotrypsin digestion and then dried. Samples were analysed using a nanoElute (Bruker) coupled to a timsTOF Pro (Bruker) equipped with a CaptiveSpray source. Peptides were dissolved in 10 μl of 0.1% formic acid (v/v) and were loaded onto a home-made C18 column (35 cm × 75 μm, i.d. of 1.9 μm, 100 Å). Samples were then eluted with linear gradients of 3–35% acetonitrile (v/v, in 0.1% formic acid) at a flow rate of 0.3 μl min^{-1} for 60 min. MS data were acquired using a timsTOF Pro MS (Bruker) operated in PASEF mode, and data were analysed using Peaks Studio Xpro software (PEAKS Studio 10.6 build 20201221, Bioinformatics Solutions). The human UniProt Reference Proteome database was used for data analysis, during which the parameters were set as follows: precursor and fragment mass tolerances, 20 ppm and 0.05 Da; semi-specific digest mode, allowed; maximal missed cleavages per peptide, 3; variable modifications, oxidation of methionine, acetylation of protein amino termini and phosphorylation of serine, threonine and tyrosine; fixed modification, carbamidomethylation of cysteine, and 467.3763 for LCA modification.

According to the MS results, the cleft comprising amino acids S194 and K333 might constitute a binding site of TULP3 for LCA. The in silico docking assay was then performed using the AutoDock vina software[138] (v.1.1.2), during which the structure of LCA and the AlphaFold-predicted TULP3 structure (https://alphafold.ebi.ac.uk/entry/O75386)[139,140] were used. Data were then illustrated using PyMOL (ver. 2.5, Schrodinger) software. The amino acid residues Y193, P195, K333 and P336 of TULP3 were then mutated (all to glycine) to generate the TULP3(4G) mutant. Structural alignments were performed as described above, and the following structures, predicted by AlphaFold, were used: TULP3: https://alphafold.ebi.ac.uk/entry/O75386; ktub: https://alphafold.ebi.ac.uk/entry/Q86PC9; tub-1: https://alphafold.ebi.ac.uk/entry/Q09306; V1E2: https://alphafold.ebi.ac.uk/entry/ Q96A05; and vha-8: https://alphafold.ebi.ac.uk/entry/Q95X44.

Determination of the thermal stability of TULP3

The thermal stability of TULP3 was determined by differential scanning calorimetry (DSC) assays performed on a VP-DSC as previously described[15], but with minor modifications. In brief, the VP-DSC was run on a mode without feedback, and 15 min of equilibration at 10 °C was performed before and between each scan. The scanning range was set from 10 to 100 °C, and the heating rate at 90 °C h^{-1}. The instrument was pre-equilibrated by running for five heating–cooling cycles with both the sample cell and the reference cell loaded with His-elution buffer. The sample cell was then loaded with 350 μl of 50 μM His-tagged TULP3 protein or 30 μM His-tagged TULP3(4G) in the His-elution buffer, and curves of heat capacity (C_p) versus temperature were recorded. Data were collected using MicroCal VP-Capillary DSC software and were then corrected for His-elution buffer baselines and normalized for scan rate and protein concentration[141] using Origin 2016.

Determination of SIRT1 activity

The deacetylase activity of SIRT1 was determined using a HPLC–MS-based method as previously described[27], but with some modifications. In brief, 4 μg of His-tagged SIRT1 or SIRT1(E230K) mutant (purified as described in the section 'Protein expression'), either co-eluted with 4 μg of TULP3 or bound on 5 μl of nickel affinity gel and incubated with lysates collected from two 10-cm dishes of MEFs (at 60–70% confluence, lysed in 1 ml Triton lysis buffer as for IB) at 4 °C for 1 h and then washed with 1 ml Triton lysis buffer twice, was incubated in 45 μl of reaction buffer containing 50 mM Tris-HCl, pH 9.0, 4 mM $MgCl_2$, 0.2 mM DTT, 5 μM LCA (for LCA-treatment group only) and NAD^+ at desired concentrations at 25 °C. The reaction was initiated by

adding 5 µl acetylated histone H3 peptide (QTAR(AcK)STGG) or acetylated V1E1 peptide (LNEA(AcK)QRLS), both dissolved in the reaction buffer to a stock concentration of 2 µg µl^{-1} to the mixture, followed by incubating at 25 °C for another 15 min. Next, 25 µl of 100% trichloroacetic acid and 50 µl distilled water were added to the mixture, and the mixture was incubated at −20 °C for 12 h, followed by centrifugation at 18,000*g* at 4 °C for 30 min. The pellets were dissolved with 70 µl of 10% (v/v, in water) acetonitrile, followed by vortexing for 30 s and then centrifuging at 18,000*g* at 4 °C for another 10 min. Next, 30 µl of supernatant was loaded into an injection vial (5182-0714, Agilent Technologies; with an insert (HM-1270, Zhejiang Hamag Technology)) equipped with a snap cap (HM-2076, Zhejiang Hamag Technology), and 4 µl of supernatant was injected into a HILIC column (HILIC Silica 3 µm, 2.1 × 150 mm, SN: 186002015; Atlantis) on a 1290 Infinity II LC system (Agilent Technologies), which was interfaced with a 6545 MS (Agilent Technologies). The mobile phase consisted of 10 mM ammonium formate containing 0.1% (v/v) formic acid in LC–MS grade water (mobile phase A) and LC–MS grade acetonitrile containing 0.1% (v/v) formic acid (mobile phase B) and run at a flow rate of 0.3 ml min^{-1}. The HPLC gradient was as follows: 70% B for 1 min, then to 30% B at the 12th min, hold for 3 min, and then back to 70% B at the 15.4th min, hold for another 2 min. The parameters of 6545 MS (Agilent Technologies) were set as follows: ion source, Dual AJS ESI; polarity, positive; nozzle voltage, 500 V; fragmentor voltage, 175 V; skimmer voltage, 65 V; VCap, 500 V; drying gas (N_2) flow rate, 8 l min^{-1}; drying gas (N_2) temperature, 280 °C; nebulizer gas pressure, 35 psig; sheath gas temperature, 125 °C; sheath gas (N_2) flow rate, 11 l min^{-1}; and scanning range, 50–1,100 *m/z*. The deacetylated-to-acetylated peptide ratios of histone H3 and V1E1 were used to determine the activities of SIRT1 towards these substrates. The peak areas of each type of peptide were calculated using following *m/z* values: acetylated histone H3: 453.2403 + 905.4805; deacetylated histone H3: 453.2403 + 905.4805; acetylated V1E1: 550.8071 + 1100.6064; and deacetylated V1E1: 529.8019 + 1058.5959.

Measurement of v-ATPase activity in vitro

The ATP-dependent proton transport rates were measured using the initial rate of ATP-dependent fluorescent quenching of FITC–dextran, as previously described[12,142,143]. In brief, lysosomes were loaded with FITC–dextran by incubating 60 10-cm dishes of MEFs (60–80% confluence) in DMEM supplemented with 2 mg ml^{-1} FITC–dextran (final concentration) on ice for 5 min, then transferring to a 37 °C incubator for 30 min. Cells were washed with DMEM for 3 times and incubated with DMEM for another 30 min at 37 °C to allow transport of FITC–dextran to lysosomes. Cells were then collected by directly scraping at room temperature, followed by centrifugation for 5 min at 500*g* at 37 °C, and lysosomes were purified using a lysosome isolation kit according to the manufacturer's instructions, but with minor modifications[15]. In brief, cells were resuspended in 7 ml of 1× extraction buffer containing protease inhibitor cocktail at room temperature and were dounced in a 7-ml dounce homogenizer (Sigma, P0610) for 120 strokes on ice followed by centrifugation for 10 min at 1,000*g*, 4 °C, which produced post-nuclear supernatant (PNS). The PNS was then centrifuged for 20 min at 20,000*g* and the pellet was suspended in 1× extraction buffer by gentle pipetting, generating the crude lysosomal fraction (CLF). The volume of CLF was adjusted to 2.4 ml and then equally divided into six 1.5-ml Eppendorf tubes (400 µl per tube). A volume of 253 µl of OptiPrep and 137 µl of 1× OptiPrep dilution buffer were added to each CLF, and mixed by gentle pipetting. The mixture is defined as the diluted OptiPrep fraction (DOF). Each DOF (0.8 ml) was loaded into an 11 × 60 mm centrifuge tube at the top of 27% (0.4 ml) and 22.5% (0.5 ml) OptiPrep solution cushions, and then overlaid with 16% (1 ml), 12% (0.9 ml) and 8% (0.3 ml) OptiPrep solutions. The tube was then centrifuged on a SW60 Ti rotor (Beckman) at 150,000*g* for 4 h at 4 °C, and the fraction at the top of 12% OptiPrep solution was collected as the CLF. The fraction was diluted with two volumes of PBS, followed by centrifugation at 20,000*g* for 20 min. The supernatant was then aspirated, and the sediment was resuspended in assay buffer (125 mM KCl, 1 mM EDTA, 20 mM HEPES, pH 7.5, with KOH) and was balanced on ice for 1 h, then mixed with 5 µM ConA (for calculating the v-ATPase-specific proton transport rates) or DMSO, then warmed at 37 °C for 10 min. The fluorescence of FITC was recorded with excitation at 490 nm and emission at 520 nm using a SpectraMax M5 microplate reader. The initial slope of fluorescence quenching was measured after the addition of 5 mM Mg-ATP (final concentration).

Purification of mitochondria and cytosol

Mitochondria were purified as previously described[144], but with minor modifications[16]. In brief, 40 10-cm dishes of MEFs (60–80% confluence) were collected by scraping at room temperature, followed by centrifugation for 5 min at 500*g* at 37 °C. Cells were then resuspended in 20 ml ice-cold IB_{cells}-1 buffer (225 mM mannitol, 75 mM sucrose, 0.1 mM EGTA and 30 mM Tris-HCl, pH 7.4) and dounced for 100 strokes in a 40-ml dounce homogenizer (using a small clearance pestle, or pestle B; D9188, Sigma), followed by 2 times of centrifugation for 5 min at 600*g* at 4 °C. The supernatants were then collected and centrifuged for 10 min at 7,000*g* at 4 °C. The pellets were then washed twice with 20 ml ice-cold IB_{cells}-2 buffer (225 mM mannitol, 75 mM sucrose and 30 mM Tris-HCl pH 7.4). The suspensions were centrifuged at 7,000*g*, and again at 10,000*g*, both for 10 min at 4 °C. The pellets were then resuspended in 2 ml ice-cold MRB buffer (250 mM mannitol, 5 mM HEPES, pH 7.4 and 0.5 mM EGTA) and were loaded on top of 10 ml of Percoll medium (225 mM mannitol, 25 mM HEPES pH 7.4, 1 mM EGTA and 30% Percoll (v/v)) in 14 × 89-mm centrifuge tubes (344059, Beckman). The tubes were then centrifuged in a SW 41 Ti rotor (Beckman) at 95,000*g* for 0.5 h at 4 °C. After centrifugation, the dense band located near the bottom of each tube was collected as the mitochondrial fraction. The mitochondrial fractions were diluted with 10 volumes of MRB buffer, followed by centrifugation at 6,300*g* for 10 min at 4 °C. The pellets were resuspended and washed with 2 ml of MRB buffer, followed by centrifugation at 6,300*g* for 10 min at 4 °C to obtain pure mitochondria (the pellets).

Cytosol was purified as previously described[145]. In brief, ten 10-cm dishes of cells were homogenized in 800 µl homogenization buffer (HB; 250 mM sucrose and 3 mM imidazole, pH 7.4). Homogenates were then passed through a 22 G needle attached to a 1-ml syringe 6 times and were then centrifuged at 2,000*g* for 10 min to produce PNS. PNS samples were then loaded onto the top of 11 × 60-mm centrifuge tubes that had been sequentially loaded with 1 ml of 40.6% sucrose (dissolved in HB), 1 ml of 35% sucrose (dissolved in HB) and 1 ml of 25% sucrose (dissolved in HB). Tubes were then centrifuged in a SW60 Ti rotor (Beckman) at 35,000 r.p.m. for 1 h at 4 °C, and the top fractions (about 200 µl) were collected as cytosolic fractions.

Protein and peptide MS

To determine the modifications of v-ATPase, the 21 HA-tagged subunits of v-ATPase, including ATP6V1A, ATP6V1B2, ATP6V1C1, ATP6V1C2, ATP6V1D, ATP6V1E1, ATP6V1E2, ATP6V1F, ATP6V1G1, ATP6V1G2, ATP6V1G3, ATP6V1H, ATP6V0A4, ATP6V0A2, ATP6V0B, ATP6V0C, ATP6V0D1, ATP6V0D2, ATP6V0E1, ATP6AP1 and ATP6AP2, were individually expressed in HEK293T cells. The immunoprecipitants (immunoprecipitated from 25 10-cm dishes of HEK293T cells ectopically expressing a certain subunit) were subjected to SDS–PAGE and were processed as described in the section 'Determination of the binding sites of TULP3 for LCA'. Samples were analysed using a nanoElute (Bruker) coupled to a timsTOF Pro (Bruker) equipped with a CaptiveSpray source. Peptides were dissolved in 10 µl of 0.1% formic acid (v/v) and were loaded onto a home-made C18 column (35 cm × 75 µm, i.d. of 1.9 µm, 100 Å). Samples were then eluted with linear gradients of 3–35% acetonitrile (v/v, in 0.1% formic acid) at a flow rate of 0.3 µl min^{-1} for 60 min. MS data were acquired using a timsTOF Pro MS (Bruker)

operated in PASEF mode, and were analysed using Peaks Studio Xpro (PEAKS Studio 10.6 build 20201221, Bioinformatics Solutions). The human UniProt Reference Proteome database was used for data analysis, during which the parameters were set as follows: precursor and fragment mass tolerances, 20 ppm and 0.05 Da; semi-specific digest mode, allowed; maximal missed cleavages per peptide, 3; variable modifications, oxidation of methionine, acetylation of protein amino termini, phosphorylation of serine, threonine and tyrosine, and acetylation of lysine; fixed modification, carbamidomethylation of cysteine.

To identify SIRT1-interacting proteins, HA-tagged SIRT1 immunoprecipitants (immunoprecipitated from 20 10-cm dishes of MEFs stably expressing HA-tagged SIRT1) were subjected to SDS–PAGE and were processed as described above. Data acquisition was performed as described above, except that an EASY-nLC 1200 System (Thermo) coupled to an Orbitrap Fusion Lumos Tribrid spectrometer (Thermo) equipped with an EASY-Spray Nanosource was used. Data were analysed using Proteome Discoverer (v.2.2, Thermo) against the mouse UniProt Reference Proteome database.

Protein levels of each bile acid receptor expressed in MEFs, as shown in Extended Data Fig. 9 and Supplementary Table 4, were quantified by using parallel reaction monitoring (PRM)-based MS. In brief, each bile acid receptor was individually expressed in HEK293T cells, followed by SDS–PAGE and processing as described above. Data acquisition was performed using an Orbitrap Fusion Lumos Tribrid spectrometer (Thermo) equipped with an EASY-Spray Nanosource in data-dependent acquisition mode. Peptides were eluted for 120 min with linear gradients of 3–35% acetonitrile in 0.1% formic acid at a flow rate of 300 nl min^{-1}. The data-dependent acquisition raw files were analysed using Proteome Discoverer software (v.2.5, Thermo), with the UniProt database (*Mus musculus*) utilized, and the quantotypic peptides for each bile acid receptor chosen accordingly (as shown in Supplementary Table 4). Protein levels of endogenous bile acid receptors were then determined through PRM analysis on the same spectrometer using samples prepared from MEFs, with the *m/z*, *z* and start/stop time of each quantotypic peptide applied. During data collection, the automatic gain control was set at 1×10^5, the maximum injection time at 1,000 ms, and the precursor isolation window width of *m/z* at 1 (complete parameter set available in the source data files deposited in the iProX partner repository along with the paper). The PRM data were analysed using Skyline-daily software (21.2.1.424) as previously described[146].

Determination of OCRs

The OCRs of nematodes was measured as previously described[147]. In brief, nematodes were washed with M9 buffer for 3 times. About 15–25 nematodes were suspended in 200 µl M9 buffer and were added to a well on a 96-well Seahorse XF cell culture microplate. Measurements were performed using a Seahorse XFe96 Analyzer (Agilent Technologies) at 20 °C following the manufacturer's instruction, with a Seahorse XFe96 sensor cartridge (Agilent Technologies) pre-equilibrated in Seahorse XF calibrant solution in a CO_2-free incubator at 37 °C overnight. Concentrations of respiratory chain inhibitors used during the assay were as follows: FCCP at 10 µM and sodium azide at 40 mM. At the end of the assay, the exact number of nematodes in each well was determined on a Cell Imaging Multi-Mode reader (Cytation 1, BioTek) and was used for normalizing and correcting OCR results. Data were collected using Wave 2.6.1 Desktop software (Agilent Technologies) and exported to Prism 9 (GraphPad) for further analysis according to the manufacturer's instructions.

The OCRs of intact muscle tissue was measured as previously described[86,148], but with modifications. In brief, mice were starved for desired durations and were killed through cervical dislocation. The gastrocnemius muscles from two hindlegs were then excised, followed by incubating in 4 ml dissociation medium (DM; by dissolving 50 µg ml^{-1} gentamycin, 2% (v/v) FBS, 4 mg ml^{-1} collagenase A in DMEM containing HEPES) in a 35-mm culture dish in a humidified chamber at 37 °C, 5% CO_2 for 1.5 h. The digested muscle masses were then washed with 4 ml pre-warmed collagenase A-free DM, incubated in 0.5 ml of pre-warmed collagenase A-free DM and dispersed by passing through a 20 G needle 6 times. Next, 20 µl of muscle homogenate was transferred to a well of a Seahorse XF24 Islet capture microplate (Agilent Technologies). After placing an islet capture screen by a Seahorse Capture Screen Insert Tool (Agilent Technologies) into the well, 480 µl pre-warmed aCSF medium (120 mM NaCl, 3.5 mM KCl, 1.3 mM $CaCl_2$, 0.4 mM KH_2PO_4, 1 mM $MgCl_2$, 5 mM HEPES, 15 mM glucose, 1× MEM non-essential amino acids, 1 mM sodium pyruvate and 1 mM GlutaMAX; adjust to pH 7.4 before use) was added, followed by equilibrating in a CO_2-free incubator at 37 °C for 1 h. OCR was then measured at 37 °C in an XFe24 Extracellular Flux analyzer (Agilent Technologies), with a Seahorse XFe24 sensor cartridge (Agilent Technologies) pre-equilibrated in Seahorse XF calibrant solution (Agilent Technologies) in a CO_2-free incubator at 37 °C overnight. The respiratory chain inhibitor used during the assay was oligomycin at 10 µM of final concentration. Data were collected using Wave 2.6.3 Desktop software (Agilent Technologies) and exported to Prism 9 (GraphPad) for further analysis according to the manufacturer's instructions.

Statistical analysis

Statistical analyses were performed using Prism 9 (GraphPad Software), except for the survival curves, which were analysed using SPSS 27.0 (IBM) by log-rank (Mantel–Cox) test. Each group of data was subjected to Kolmogorov–Smirnov tests, Anderson–Darling tests, D'Agostino–Pearson omnibus tests or Shapiro–Wilk tests for normal distribution when applicable. An unpaired two-sided Student's *t*-test was used to determine the significance between two groups of normally distributed data. Welch's correction was used for groups with unequal variances. An unpaired two-sided Mann–Whitney test was used to determine the significance between data without a normal distribution. For comparisons between multiple groups with a fixed factor, an ordinary one-way ANOVA was used, followed by Tukey's, Sidak's, Dunnett's or Dunn's test as specified in the legends. The assumptions of homogeneity of error variances were tested using *F*-test ($P > 0.05$). For comparison between multiple groups with two fixed factors, an ordinary two-way ANOVA was used, followed by Tukey's or Sidak's multiple comparisons test as specified in the legends. Geisser–Greenhouse's correction was used where applicable. The adjusted means and s.e.m. or s.d. values were recorded when the analysis met the above standards. Differences were considered significant when $P < 0.05$ or $P > 0.05$ with large differences of observed effects (as suggested in refs. 149,150).

Reporting summary

Further information on research design is available in the Nature Portfolio Reporting Summary linked to this article.

Data availability

The data supporting the findings of this study are available within the paper and its Supplementary Information files. The MS proteomics data have been deposited into the ProteomeXchange Consortium (http://proteomecentral.proteomexchange.org) through the iProX partner repository[151,152] with the dataset identifier IPX0007019000. Materials and reagents are available upon request. Questions regarding the details of experiments are welcome. Full immunoblots are provided in Supplementary Information Fig. 1. Source data are provided with this paper.

Code availability

The analysis was performed using standard protocols with previously described computational tools. No custom code was used in this study.

76. Nguyen, L. N. et al. Mfsd2a is a transporter for the essential omega-3 fatty acid docosahexaenoic acid. *Nature* **509**, 503–506 (2014).
77. Green, C. L. et al. The effects of graded levels of calorie restriction. XIII. Global metabolomics screen reveals graded changes in circulating amino acids, vitamins, and bile acids in the plasma of C57BL/6 mice. *J. Gerontol. A Biol. Sci. Med. Sci.* **74**, 16–26 (2019).
78. Zhang, C. S. et al. The aldolase inhibitor aldometanib mimics glucose starvation to activate lysosomal AMPK. *Nat. Metab.* https://doi.org/10.1038/s42255-022-00640-7 (2022).
79. Garcia-Flores, L. A. et al. The effects of graded calorie restriction XVII: multitissue metabolomics reveals synthesis of carnitine and NAD, and tRNA charging as key pathways. *Proc. Natl Acad. Sci. USA* **118**, e2101977118 (2021).
80. Perez, C. L. & Van Gilst, M. R. A ^{13}C isotope labeling strategy reveals the influence of insulin signaling on lipogenesis in *C. elegans*. *Cell Metab.* **8**, 266–274 (2008).
81. Falk, M. J. et al. Stable isotopic profiling of intermediary metabolic flux in developing and adult stage *Caenorhabditis elegans*. *J. Vis. Exp.* https://doi.org/10.3791/2288 (2011).
82. Vergano, S. S. et al. In vivo metabolic flux profiling with stable isotopes discriminates sites and quantifies effects of mitochondrial dysfunction in *C. elegans*. *Mol. Genet. Metab.* **111**, 331–341 (2014).
83. Liu, Y., Wang, W., Shui, G. & Huang, X. CDP-diacylglycerol synthetase coordinates cell growth and fat storage through phosphatidylinositol metabolism and the insulin pathway. *PLoS Genet.* **10**, e1004172 (2014).
84. Cox, J. E., Thummel, C. S. & Tennessen, J. M. Metabolomic studies in *Drosophila*. *Genetics* **206**, 1169–1185 (2017).
85. Ding, L. et al. Seipin regulates lipid homeostasis by ensuring calcium-dependent mitochondrial metabolism. *EMBO J.* https://doi.org/10.15252/embj.201797572 (2018).
86. Schuh, R. A., Jackson, K. C., Khairallah, R. J., Ward, C. W. & Spangenburg, E. E. Measuring mitochondrial respiration in intact single muscle fibers. *Am. J. Physiol. Regul. Integr. Comp. Physiol.* **302**, R712–R719 (2012).
87. Koopman, M. et al. A screening-based platform for the assessment of cellular respiration in *Caenorhabditis elegans*. *Nat. Protoc.* **11**, 1798–1816 (2016).
88. Sarasija, S. & Norman, K. R. Measurement of oxygen consumption rates in intact *Caenorhabditis elegans*. *J. Vis. Exp.* https://doi.org/10.3791/59277 (2019).
89. Ng, L. F. & Gruber, J. Measurement of respiration rate in live *Caenorhabditis elegans*. *Bio-Protocol* **9**, e3243 (2019).
90. Shao, D. et al. Improved mass spectrometry-based activity assay reveals oxidative and metabolic stress as sirtuin-1 regulators. *Redox Biol.* **22**, 101150 (2019).
91. Espada, L. et al. Loss of metabolic plasticity underlies metformin toxicity in aged *Caenorhabditis elegans*. *Nat. Metab.* **2**, 1316–1331 (2020).
92. Wu, L. et al. An ancient, unified mechanism for metformin growth inhibition in *C. elegans* and cancer. *Cell* **167**, 1705–1718.e13 (2016).
93. Martin-Montalvo, A. et al. Metformin improves healthspan and lifespan in mice. *Nat. Commun.* **4**, 2192 (2013).
94. De Rosa, M. J. et al. The flight response impairs cytoprotective mechanisms by activating the insulin pathway. *Nature* **573**, 135–138 (2019).
95. Yuan, J. et al. Two conserved epigenetic regulators prevent healthy ageing. *Nature* **579**, 118–122 (2020).
96. Zhang, H. et al. NAD^+ repletion improves mitochondrial and stem cell function and enhances life span in mice. *Science* **352**, 1436–1443 (2016).
97. Wood, J. G. et al. Sirtuin activators mimic caloric restriction and delay ageing in metazoans. *Nature* **430**, 686–689 (2004).
98. Libert, S. et al. Regulation of *Drosophila* life span by olfaction and food-derived odors. *Science* **315**, 1133–1137 (2007).
99. Rogina, B. & Helfand, S. L. Sir2 mediates longevity in the fly through a pathway related to calorie restriction. *Proc. Natl Acad. Sci. USA* **101**, 15998–16003 (2004).
100. Broughton, S. J. et al. Longer lifespan, altered metabolism, and stress resistance in *Drosophila* from ablation of cells making insulin-like ligands. *Proc. Natl Acad. Sci. USA* **102**, 3105–3110 (2005).
101. Minois, N. et al. Spermidine promotes stress resistance in *Drosophila melanogaster* through autophagy-dependent and -independent pathways. *Cell Death Dis.* **3**, e401 (2012).
102. Sanchez, J. A. et al. FOXO-mediated repression of Dicer1 regulates metabolism, stress resistance, and longevity in *Drosophila*. *Proc. Natl Acad. Sci. USA* **120**, e2216539120 (2023).
103. Lin, L. et al. Regulation of skeletal muscle oxidative capacity and muscle mass by SIRT3. *PLoS ONE* **9**, e85636 (2014).
104. Liu, Y. et al. TLR9 and beclin 1 crosstalk regulates muscle AMPK activation in exercise. *Nature* **578**, 605–609 (2020).
105. Chu, V. T. et al. Efficient generation of *Rosa26* knock-in mice using CRISPR/Cas9 in C57BL/6 zygotes. *BMC Biotechnol.* **16**, 4 (2016).
106. Xiao, C. et al. Lymphoproliferative disease and autoimmunity in mice with increased miR-17-92 expression in lymphocytes. *Nat. Immunol.* **9**, 405–414 (2008).
107. Mali, P. et al. RNA-guided human genome engineering via Cas9. *Science* **339**, 823–826 (2013).
108. Taft, R. In vitro fertilization in mice. *Cold Spring Harbor Protoc.* **2017**, pdb.prot094508 (2017).
109. Brenner, S. The genetics of *Caenorhabditis elegans*. *Genetics* **77**, 71–94 (1974).
110. Lakovaara, S. Malt as a culture medium for *Drosophila* species. *Drosoph. Inf. Serv.* **44**, 128 (1969).
111. Park, S. J. et al. DNA-PK promotes the mitochondrial, metabolic, and physical decline that occurs during aging. *Cell Metab.* **26**, 447 (2017).
112. Liu, P. et al. Blocking FSH induces thermogenic adipose tissue and reduces body fat. *Nature* **546**, 107–112 (2017).
113. Liu, L. et al. Histone methyltransferase MLL4 controls myofiber identity and muscle performance through MEF2 interaction. *J. Clin. Invest.* **130**, 4710–4725 (2020).
114. Han, M. et al. A systematic RNAi screen reveals a novel role of a spindle assembly checkpoint protein BuGZ in synaptic transmission in *C. elegans*. *Front. Mol. Neurosci.* **10**, 141 (2017).
115. Backhaus, B., Sulkowski, E. & Schlote, F. W. A semi-synthetic, general-purpose medium for *Drosophila melanogaster*. *Drosoph. Inf. Serv.* **60**, 210–212 (1984).
116. Linford, N. J., Bilgir, C., Ro, J. & Pletcher, S. D. Measurement of lifespan in Drosophila melanogaster. *J. Vis. Exp.* https://doi.org/10.3791/50068 (2013).
117. Wu, Q. et al. 2,5-Dimethyl-celecoxib extends *Drosophila* life span via a mechanism that requires insulin and target of rapamycin signaling. *J. Gerontol. A Biol. Sci. Med. Sci.* **72**, 1334–1341 (2017).
118. Gomes, A. P. et al. Declining NAD^+ induces a pseudohypoxic state disrupting nuclear–mitochondrial communication during aging. *Cell* **155**, 1624–1638 (2013).
119. Nargund, A. M., Fiorese, C. J., Pellegrino, M. W., Deng, P. & Haynes, C. M. Mitochondrial and nuclear accumulation of the transcription factor ATFS-1 promotes OXPHOS recovery during the UPR^{mt}. *Mol. Cell* **58**, 123–133 (2015).
120. Zhang, Q. et al. The memory of neuronal mitochondrial stress is inherited transgenerationally via elevated mitochondrial DNA levels. *Nat. Cell Biol.* **23**, 870–880 (2021).
121. Copeland, J. M. et al. Extension of *Drosophila* life span by RNAi of the mitochondrial respiratory chain. *Curr. Biol.* **19**, 1591–1598 (2009).
122. Quiros, P. M., Goyal, A., Jha, P. & Auwerx, J. Analysis of mtDNA/nDNA ratio in mice. *Curr. Protoc. Mouse Biol.* **7**, 47–54 (2017).
123. Rodrigues, A. P. C., Camargo, A. F., Andjelkovic, A., Jacobs, H. T. & Oliveira, M. T. Developmental arrest in *Drosophila melanogaster* caused by mitochondrial DNA replication defects cannot be rescued by the alternative oxidase. *Sci. Rep.* **8**, 10882 (2018).
124. Wu, Y.-Q. et al. Low glucose metabolite 3-phosphoglycerate switches PHGDH from serine synthesis to p53 activation to control cell fate. *Cell. Res.* https://doi.org/10.1038/s41422-023-00874-4 (2023).
125. Bajad, S. U. et al. Separation and quantitation of water soluble cellular metabolites by hydrophilic interaction chromatography–tandem mass spectrometry. *J. Chromatogr. A* **1125**, 76–88 (2006).
126. Fang, R., Jiang, Q., Jia, X. & Jiang, Z. ARMH3-mediated recruitment of PI4KB directs Golgi-to-endosome trafficking and activation of the antiviral effector STING. *Immunity* **56**, 500–515.e6 (2023).
127. Lin, S. C. & Morrison-Bogorad, M. Cloning and characterization of a testis-specific thymosin β_{10} cDNA. Expression in post-meiotic male germ cells. *J. Biol. Chem.* **266**, 23347–23353 (1991).
128. Li, M. et al. Hierarchical inhibition of mTORC1 by glucose starvation-triggered AXIN lysosomal translocation and by AMPK. *Life Metab.* https://doi.org/10.1093/lifemeta/load005 (2023).
129. Feng, Y. et al. Cationic polymer synergizing with a disulfide-containing enhancer achieved efficient nucleic acid and protein delivery. *Biomater. Sci.* **10**, 6230–6243 (2022).
130. Takata, T. & Ishikawa, F. Human Sir2-related protein SIRT1 associates with the bHLH repressors HES1 and HEY2 and is involved in HES1- and HEY2-mediated transcriptional repression. *Biochem. Biophys. Res. Commun.* **301**, 250–257 (2003).
131. Luthi-Carter, R. et al. SIRT2 inhibition achieves neuroprotection by decreasing sterol biosynthesis. *Proc. Natl Acad. Sci. USA* **107**, 7927–7932 (2010).
132. Lang, A. et al. SIRT4 interacts with OPA1 and regulates mitochondrial quality control and mitophagy. *Aging* **9**, 2163–2189 (2017).
133. Du, Z. et al. Targeting a Sirt5-positive subpopulation overcomes multidrug resistance in wild-type *Kras* colorectal carcinomas. *Cell Rep.* **22**, 2677–2689 (2018).
134. Zhang, C. S. et al. RHOBTB3 promotes proteasomal degradation of HIFα through facilitating hydroxylation and suppresses the Warburg effect. *Cell Res.* **25**, 1025–1042 (2015).
135. Cousin, M. A. & Nicholls, D. G. Synaptic vesicle recycling in cultured cerebellar granule cells: role of vesicular acidification and refilling. *J. Neurochem.* **69**, 1927–1935 (1997).
136. Li, M. et al. AMPK targets PDZD8 to trigger carbon source shift from glucose to glutamine. *Cell Res.* https://doi.org/10.1038/s41422-024-00985-6 (2024).
137. Umeda, N., Ueno, T., Pohlmeyer, C., Nagano, T. & Inoue, T. A photocleavable rapamycin conjugate for spatiotemporal control of small GTPase activity. *J. Am. Chem. Soc.* **133**, 12–14 (2011).
138. Trott, O. & Olson, A. J. AutoDock Vina: improving the speed and accuracy of docking with a new scoring function, efficient optimization, and multithreading. *J. Comput. Chem.* **31**, 455–461 (2010).
139. Jumper, J. et al. Highly accurate protein structure prediction with AlphaFold. *Nature* **596**, 583–589 (2021).
140. Varadi, M. et al. AlphaFold Protein Structure Database: massively expanding the structural coverage of protein-sequence space with high-accuracy models. *Nucleic Acids Res.* **50**, D439–D444 (2022).
141. Kurganov, B. I., Lyubarev, A. E., Sanchez-Ruiz, J. M. & Shnyrov, V. L. Analysis of differential scanning calorimetry data for proteins. Criteria of validity of one-step mechanism of irreversible protein denaturation. *Biophys. Chem.* **69**, 125–135 (1997).
142. Liberman, R., Bond, S., Shainheit, M. G., Stadecker, M. J. & Forgac, M. Regulated assembly of vacuolar ATPase is increased during cluster disruption-induced maturation of dendritic cells through a phosphatidylinositol 3-kinase/mTOR-dependent pathway. *J. Biol. Chem.* **289**, 1355–1363 (2014).
143. Trombetta, E. S., Ebersold, M., Garrett, W., Pypaert, M. & Mellman, I. Activation of lysosomal function during dendritic cell maturation. *Science* **299**, 1400–1403 (2003).
144. Wieckowski, M. R., Giorgi, C., Lebiedzinska, M., Duszynski, J. & Pinton, P. Isolation of mitochondria-associated membranes and mitochondria from animal tissues and cells. *Nat. Protoc.* **4**, 1582–1590 (2009).
145. Kobayashi, T. et al. Separation and characterization of late endosomal membrane domains. *J. Biol. Chem.* **277**, 32157–32164 (2002).
146. MacLean, B. et al. Skyline: an open source document editor for creating and analyzing targeted proteomics experiments. *Bioinformatics* **26**, 966–968 (2010).
147. Preez, G. D. et al. Oxygen consumption rate of *Caenorhabditis elegans* as a high-throughput endpoint of toxicity testing using the Seahorse XF®96 Extracellular Flux Analyzer. *Sci. Rep.* **10**, 4239 (2020).

148. Wang, Q. et al. IL-27 signalling promotes adipocyte thermogenesis and energy expenditure. *Nature* **600**, 314–318 (2021).
149. Amrhein, V., Greenland, S. & McShane, B. Scientists rise up against statistical significance. *Nature* **567**, 305–307 (2019).
150. Wasserstein, R. L., Schirm, A. L. & Lazar, N. A. Moving to a world beyond "*P*<0.05". *Am. Stat.* **73**, 1–19 (2019).
151. Ma, J. et al. iProX: an integrated proteome resource. *Nucleic Acids Res.* **47**, D1211–D1217 (2019).
152. Chen, T. et al. iProX in 2021: connecting proteomics data sharing with big data. *Nucleic Acids Res.* **50**, D1522–D1527 (2022).

Acknowledgements We thank S. Morrison for providing the *AMPKA1*$^{F/F}$ mice and *AMPKA2*$^{F/F}$ mice, and R. Huganir for the *PKCZ*$^{F/F}$ mice; M. Zhang for technical assistance with hyperinsulinaemic–euglycemic clamp assays; S.-Q. Wu, Y. He and J. Song for mouse IVF; Y. Liu for nematode experiments; B. Liu and K. Zheng for fly strains and experiments; W. Wu for fly embryo microinjections; Y. Zheng for fly strains; Y. Chen and Y. Sun for technical help with the electrotransfection of MEFs; Q. Guo for the analysis of fibre types of muscle tissues; Q. Huang and X. Chi for optimizing the expression and purification methods of TULP3; Y. Chen for the statistical analysis of cell images; X. Guo for help with importing the fly strains; all the other members of the S.-C.L. Laboratory for technical assistance; staff at the *Caenorhabditis* Genetics Center and National BioResource Project for supplying nematode strains; staff at the BDSC, Vienna *Drosophila* Resource Center, and the Core Facility of *Drosophila* Resource and Technology, Center for Excellence in Molecular Cell Science, Chinese Academy of Sciences for providing fly strains and reagents. The artworks shown in Fig. 3a and Extended Data Fig. 7c were modified from elements created by Servier Medical Art (https://smart.servier.com/) licensed under a Creative Commons Attribution 3.0 unported licence. This work was supported by grants from the National Key R&D Program of China (2022YFA0806501), the National Natural Science Foundation of China (92057204, 82088102, 32070753 and 323B2035), Fundamental Research Funds for the Central Universities (20720200069), Project '111' sponsored by the State Bureau of Foreign Experts and Ministry of Education of China (BP2018017), Joint Funds for the Innovation of Science and Technology, Fujian Province (2021Y9232, 2021Y9227 and 2023Y9448), the Fujian Provincial Health Technology Project (2022ZD01005 and 2022ZQNZD009), Special Research Funds for Local Science and Technology Development Guided by Central Government (2023L3020), a XMU–Fujian Cancer Hospital Cooperation Grant for the Research Center of Metabolism, the XMU Open Innovation Fund and Training Programme of Innovation and Entrepreneurship for Undergraduates (KFJJ-202103 and S202210384682), and the Agilent Applications and Core Technology–University Research Grant (4769).

Author contributions Q.Q., C.-S.Z. and S.-C.L. conceived the study and designed the experiments. Q.Q. verified the requirement of the lysosomal pathway for LCA-mediated AMPK activation with the assistance from M.L. and X.T. Q.Q. identified the acetylated sites of v-ATPase required for AMPK activation with assistance from J.-W.F., and determined the sirtuin requirement of LCA-mediated AMPK activation. Y.C. performed mouse and fly experiments, and Y. Wang conducted nematode experiments. W.W. and S.L. identified TULP3 as a receptor for LCA. S.L. and H.-Y.Y. verified the binding affinity of TULP3 towards LCA, and the interaction between TULP3 and SIRT1 in vitro with assistance from J.C. and B.S. J.C. performed the DSC assays. Y.F., H.F. and H.T. synthesized *Cas9* mRNA and generated the HA-tagged *Sirt3–Sirt5* knock-in MEFs. S.L., H.-Y.Y. and C.Y. determined the activity of SIRT1. J.W. generated the V1E1(3KR)-expressing mice. X.W. determined the OCRs of mouse muscles. Y.-H.L. and S.X. determined the mRNA levels of the mitochondrial OXPHOS complex. J.X. analysed the interaction between TULP3 and SIRT1 inside cells using FRET–FLIM assays. Z.W. and X.D. designed and synthesized the LCA probe, and X.H. generated the V1E1(K99)ac antibody. C.X., Y. Wu and Z.X. determined the acetylation sites of V1E and the SIRT1-interacting protein by protein MS. Y. Wu. performed PRM-based quantitative MS to determine the protein levels of the bile acid receptors. C.Z. analysed metabolites utilizing HPLC–MS, and H.-L.P. used CE–MS. B.Z. and X.D. performed the in silico docking assays. L.L. generated TULP3(4G)-expressing nematodes, and ZK.X. the V1E1(3KR) nematodes, both supervised by Y.Y. X.-S.X. helped interpret the v-ATPase acetylation data. C.-S.Z. and S.-C.L. wrote the manuscript.

Competing interests The authors declare no competing interests.

Additional information

Supplementary information The online version contains supplementary material available at https://doi.org/10.1038/s41586-024-08348-2.

Correspondence and requests for materials should be addressed to Chen-Song Zhang or Sheng-Cai Lin.

Peer review information *Nature* thanks Bruce Kemp, Jonathan S. Oakhill, David Sinclair, and the other, anonymous, reviewer(s) for their contribution to the peer review of this work. Peer reviewer reports are available.

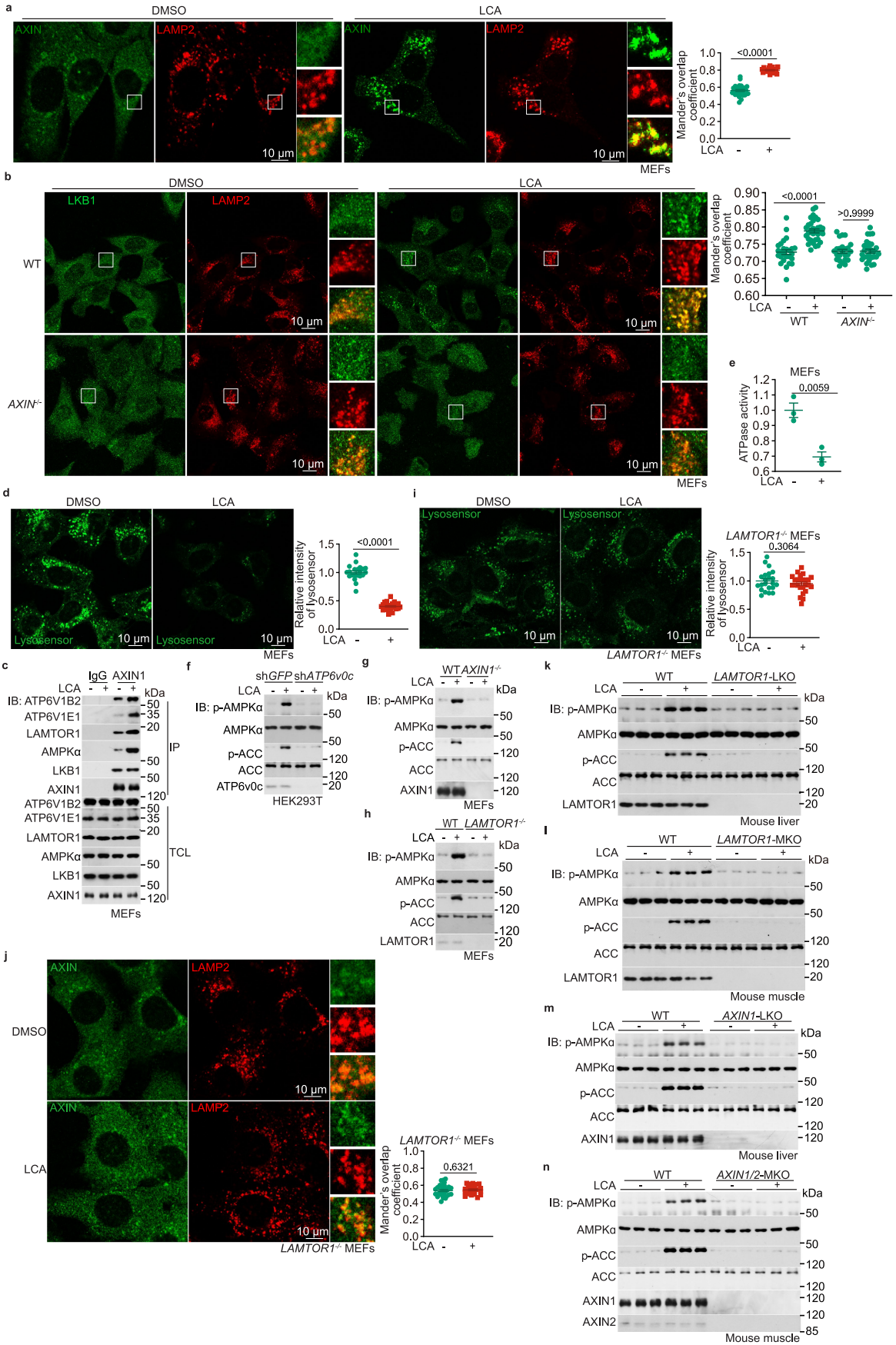

Extended Data Fig. 1 | See next page for caption.

Extended Data Fig. 1 | LCA activates AMPK through the lysosomal AMPK pathway. a, LCA triggers lysosomal translocation of AXIN. MEFs were incubated with 1 μM LCA for 4 h, followed by immunostaining to determine the lysosomal localization of AXIN (accessed by the co-localization, i.e., the Mander's overlap coefficients, with the lysosomal marker LAMP2). Results are shown as mean ± s.e.m.; $n = 29$ (DMSO) or 20 (LCA) cells, and P value by two-sided Student's t-test with Welch's correction. **b**, LCA triggers lysosomal translocation of LKB1. Wildtype and *AXIN* knockout ($AXIN^{-/-}$) MEFs were incubated with 1 μM LCA for 4 h, followed by immunostaining to determine the lysosomal translocation of LKB1. Mander's overlap coefficients are shown as mean ± s.e.m.; $n = 26$ (DMSO, WT) 32 (LCA, WT), 24 (DMSO, $AXIN^{-/-}$) or 28 (LCA, $AXIN^{-/-}$) cells, and P value by two-way ANOVA, followed by Tukey. **c**, LCA induces the formation of the lysosomal AMPK-activating complex. MEFs were treated with 1 μM LCA for 4 h, and the cell lysates were immunoprecipitated (IP) with an antibody against AXIN. Immunoblotting (IB) reveals that AXIN co-immunoprecipitates with v-ATPase, Ragulator, AXIN and LKB1. TCL, total cell lysate. **d**, **e**, LCA inhibits v-ATPase. MEFs were incubated with 1 μM LCA for 4 h, followed by determination of the activity of v-ATPase (**d**, accessed by the decreased intensities of the Lysosensor that monitors acidification of lysosomes; representative images are shown on the left panel, and the statistical analysis data on the right as mean ± s.e.m., normalized to the DMSO group; $n = 21$ (DMSO) or 23 (LCA) cells, and P value by two-sided Mann-Whitney test) and the proton transport rates of v-ATPase in vitro (**e**, data are shown as mean ± s.e.m., normalized to the DMSO group; $n = 3$ replicates, and P value by two-sided Student's t-test). **f**-**n**, The lysosomal AMPK pathway is required for the LCA-induced AMPK activation. HEK293T cells with *ATP6vOc* (*vOc*) knockdown (sh*ATP6vOc*; **f**), MEFs with *AXIN* knockout (**g**), *LAMTOR1* knockout ($LAMTOR1^{-/-}$; **h**-**j**), mice with liver- or muscle-specific *LAMTOR1* knockout (*LAMTOR1*-LKO, in **k**; *LAMTOR1*-MKO, in **l**), or mice with liver- or muscle-specific *AXIN* knockout (*AXIN1*-LKO, in **m**; or *AXIN1/2*-MKO, in **n**), were treated with LCA at 1 μM for 4 h (**f**-**j**; for cells) or at 1 g/l with LCA coated with (2-hydroxypropyl)-β-cyclodextrin in drinking water for 1 month (**k**-**n**; for mice), followed by determination for AMPK activation (**f**-**h**, **k**-**n**; the levels of p-AMPKα and p-ACC) by immunoblotting, the v-ATPase inhibition (**i**, see representative images on the left panel, and the statistical analysis data on the right panel), and the lysosomal translocation of AXIN evidenced by co-localization with LAMP2 (**j**, see representative images on the left panel, and the statistical analysis data on the right panel). Results in **i**, **j** are shown as mean ± s.e.m. (in **i**, data are normalized to the DMSO group); $n = 22$ (DMSO group of **i**), 25 (LCA group of **i**), 29 (DMSO group of **j**) or 23 (LCA group of **j**) cells, and P value by two-sided Student's t-test. Experiments in this figure were performed three times, except **a** and **d** four times.

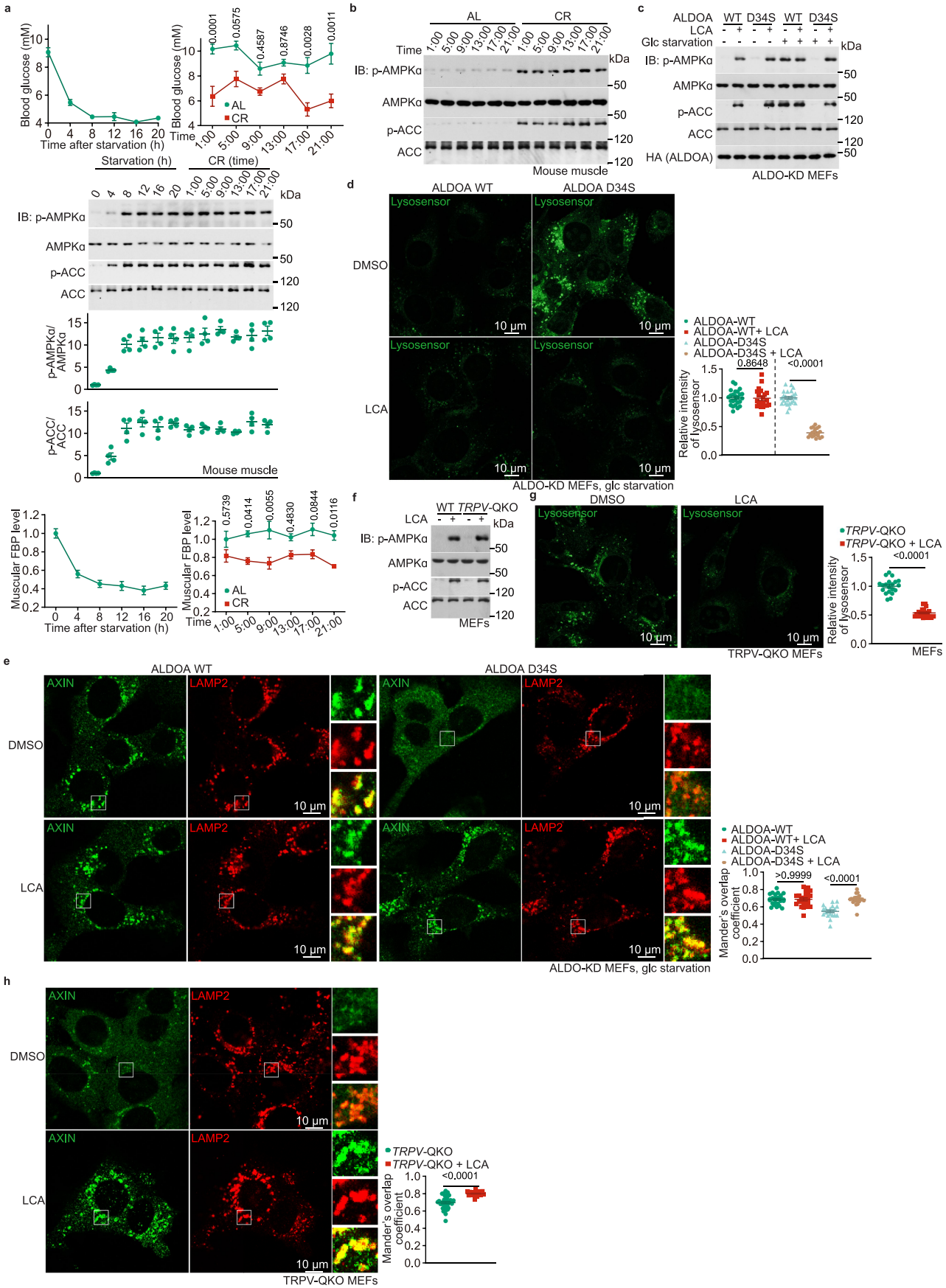

Extended Data Fig. 2 | See next page for caption.

Extended Data Fig. 2 | LCA activates the lysosomal AMPK pathway downstream of the low glucose sensor aldolase-TRPV axis. a, Glucose decline in CR mice does not suffice to cause AMPK activation. Levels of blood glucose (upper panel), muscle FBP (lower panel), and the activity of muscle AMPK (middle panel) were determined in mice subjected to starvation for 4 h, 8 h, 12 h, 16 h, and 20 h, or CR, at indicated times of the day. Results are shown as mean ± s.e.m.; $n = 5$ (blood glucose of CR and starvation groups) or 4 (others) mice for each time point, and P value by two-way ANOVA followed by Tukey's test. **b**, CR leads to a constant activation of AMPK in muscle. Mice were subjected to CR for 4 months, followed by determination of the muscular AMPK activation at different times of the day. **c**-**h**, LCA triggers the lysosomal AMPK pathway downstream of aldolase and TRPVs. MEFs with knockdown of aldolase A-C (ALDO-KD) and re-introduced with ALDOA-D34S that mimics high glucose/FBP condition[10] (**c**-**e**), or MEFs with TRPV1-4 knockout (**f**-**h**; TRPV-QKO, blocking signalling from low glucose to AMPK activation[12]), were incubated in normal (**c**, **f**-**h**) or glucose-free (**c**-**e**) medium (Glc starvation) containing 1 μM LCA for 4 h, followed by determination for AMPK activation (**c**, **f**), v-ATPase inhibition (**d**, **g**), and lysosomal localization of AXIN (**e**, **h**). Statistical analysis data are shown as mean ± s.e.m., where **d** and **g** were normalized to the DMSO group; $n = 25$ (ALDOA-WT + DMSO and ALDOA-D34S + DMSO of **d**), 21 (TRPV-QKO + LCA of **g** and TRPV-QKO + LCA of **h**), 23 (ALDOA-WT + LCA of **e** and TRPV-QKO + DMSO of **h**), 24 (ALDOA-WT + DMSO of **e**), or 20 (others) cells; and P value by two-sided Student's t-test (**d**, ALDOA-WT), two-sided Student's t-test with Welch's correction (**d**, ALDOA-D34S; and **g**), or two-way ANOVA followed by Tukey's test (**e**). Experiments in this figure were performed three times.

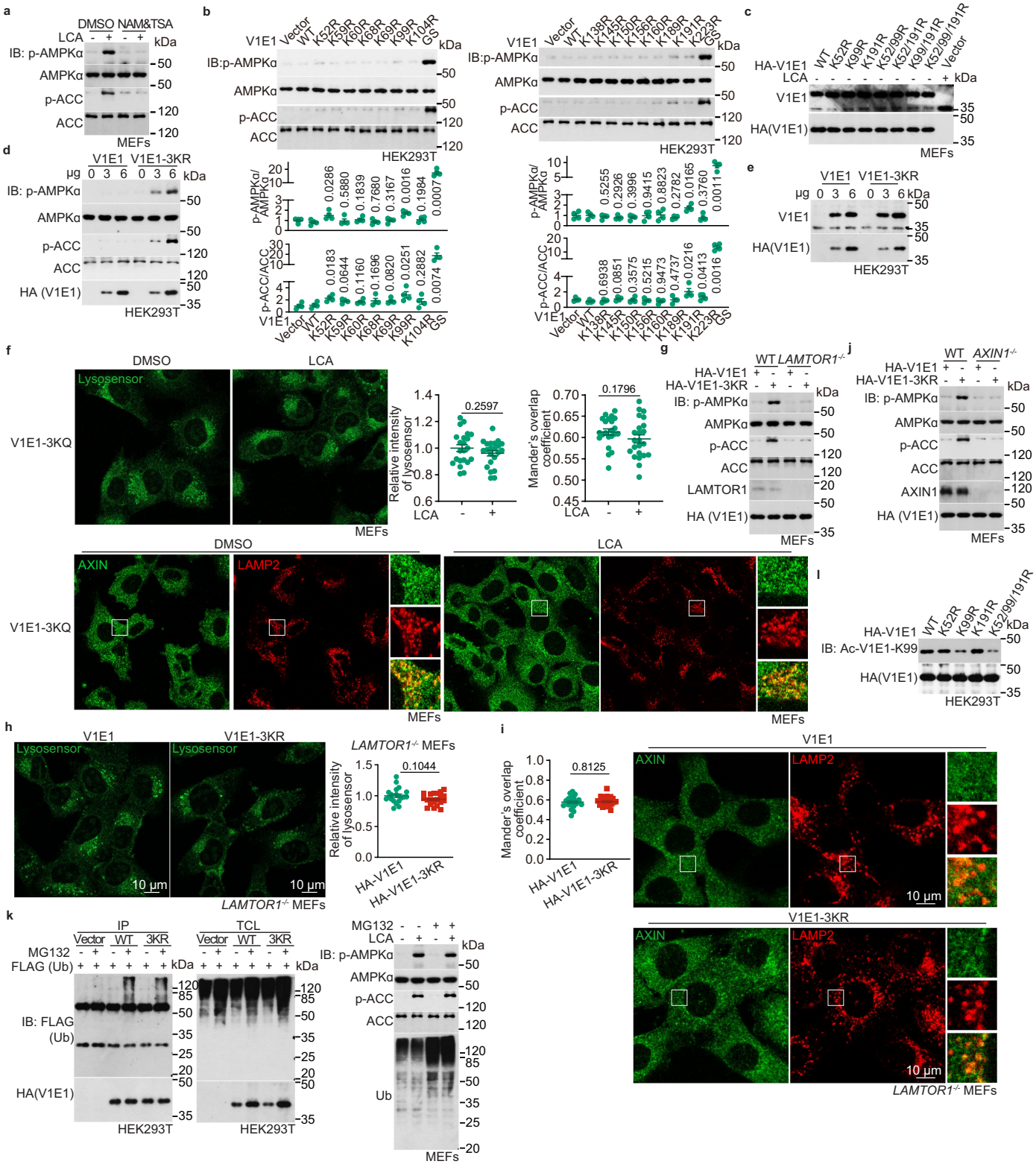

Extended Data Fig. 3 | See next page for caption.

Extended Data Fig. 3 | LCA triggers the lysosomal AMPK pathway through deacetylation of v-ATPase. a, Deacetylation is required for LCA-induced activation of AMPK. MEFs were pre-treated with 2 μM TSA and 8 mM NAM for 12 h, followed by incubating with 1 μM LCA for 4 h. Cells were then lysed, and the AMPK activities were determined by immunoblotting. **b**-**e**, V1E1-3KR renders the lysosomal AMPK pathway constitutively active. HEK293T with ectopic expression of V1E1, V1E1-3KR (**d**; triple mutation of K52, K99 and K191 of V1E1 to arginine; mimicking the deacetylated state of V1E1), or other single K to R mutations (**b**) of V1E1, or MEFs with stable expression of single, double, or triple mutation of K52, K99 and K191 residues (**c**) were lysed, followed by determination of the activity of AMPK (**b**, in which the statistical analysis results are shown as mean ± s.e.m.; $n = 4$ replicates for each treatment, and P value by two-sided Student's t-test; and **d**) or the expression levels of V1E1 (**c**, **e**). **f**, V1E1-3KQ impairs the LCA-induced lysosomal translocation of AXIN and v-ATPase inhibition. MEFs with stable expression of V1E1-3KQ, mimicking the constitutively acetylated states of V1E1, were treated with 1 μM LCA for 4 h, followed by determination of the activity of v-ATPase (upper panel), and the lysosomal localization of AXIN (lower panel). Statistical analysis data are shown as mean ± s.e.m.; $n = 23$ (right panel, LCA group) or 22 (others) cells for each treatment, and P value by two-sided Student's t-test. **g**-**j**, V1E1-3KR activates AMPK through the lysosomal pathway. *LAMTOR1*$^{-/-}$ (**g**-**i**) and *AXIN*$^{-/-}$ (**j**) MEFs, and control MEFs, were infected with lentivirus carrying HA-tagged V1E1-3KR, followed by determination for AMPK activation (**g**, **j**), activity of v-ATPase (**h**), and the lysosomal localization of AXIN (**i**). Statistical analysis data in **h**, **i** are shown as mean ± s.e.m.; $n = 20$ (**h**), 22 (V1E1 of **i**) or 23 (V1E1-3KR of **i**) cells, and P value by two-sided Student's t-test. **k**, Acetylation does not affect ubiquitination of V1E1. HEK293T cells were transfected with HA-tagged V1E1 or V1E1-3KR, along with FLAG-tagged Ub. At 12 h post-transfection, cells were treated with 20 nM MG-132 for another 12 h, and the ubiquitination levels of V1E1 were determined by immunoprecipitation of HA-tag, followed by immunoblotting (left panel). See also the right panel for the AMPK activation in MEFs after treatment of 20 nM MG-132 for 12 h and 1 μM LCA for 4 h. **l**, Validation of the antibody against K99-acetylated V1E1. HEK293T cells were transfected with V1E1-K99R, or V1E1-K52R, V1E1-K191R and the wildtype V1E1 as controls, followed by determination of the reaction specificity of the Ac-K99-V1E1 antibody by immunoblotting. Experiments in this figure were performed three times, except **b** four times.

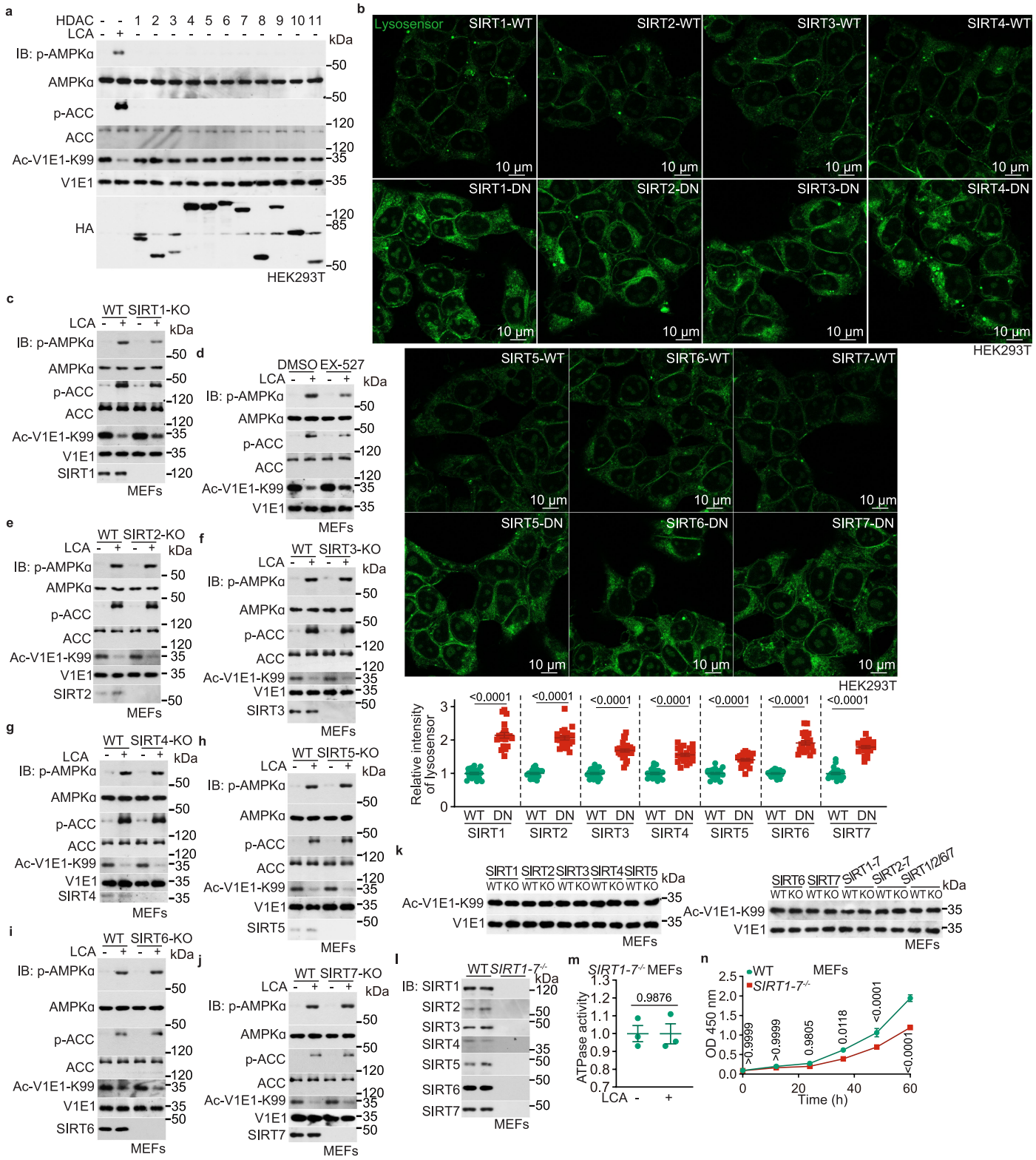

Extended Data Fig. 4 | See next page for caption.

Extended Data Fig. 4 | LCA promotes sirtuins to deacetylase v-ATPase. **a**, Sirtuins, but not HDACs, deacetylate V1E1 and activate AMPK. HEK293T cells were infected with lentiviruses carrying HA-tagged HDAC1 to HDAC11, followed by determination of the acetylation of V1E1 and the activation of AMPK. The effects of sirtuins on AMPK activation are shown in Fig. 2a. **b**, Sirtuins inhibit v-ATPase. HEK293T cells infected with lentiviruses carrying each sirtuin (HA-tagged SIRT1 to SIRT7), or its dominant negative (DN) form, were subjected to determine the activity of v-ATPase by immunostaining. Representative images are shown, and the statistical analysis data are mean ± s.e.m., normalised to the WT group of each sirtuin; $n = 21$ (SIRT2-DN and SIRT4-DN), 26 (SIRT3-DN), 23 (SIRT5-DN), 22 (SIRT6-DN) or 20 (others), and P value by two-sided Student's t-test (SIRT4, SIRT5 and SIRT7) or two-sided Student's t-test with Welch's correction (others). **c**-**j**, Sirtuins redundantly mediate the activation of AMPK by LCA. MEFs with SIRT1 (**c**), SIRT2 (**e**), SIRT3 (**f**), SIRT4 (**g**), SIRT5 (**h**), SIRT6 (**i**), or SIRT7 (**j**) knockout, or pre-treated with 10 μM EX-527 for 12 h to inhibit SIRT1 (**d**), were treated with 1 μM LCA for 4 h, followed by determination of AMPK activation and the V1E1 acetylation by immunoblotting. **k**, SIRTs are not required for regulating the basal acetylation levels of V1E1. MEFs with single knockout of SIRTs 1-7, hepta-knockout of SIRTs 1-7, knockout of SIRTs 2-7, or knockout of SIRT1/2/6/7, were lysed, and the acetylation of V1E1-K99 was determined by immunoblotting. **l**, **m**, Sirtuins are required for LCA-mediated inhibition of v-ATPase. MEFs with hepta-knockout of SIRT1 to SIRT7 (*SIRT1-7*$^{-/-}$; validation data are shown in **l**, see also knockout strategy in Supplementary Table 2) were treated with 1 μM LCA for 4 h, followed by determination of the activity of v-ATPase (**m**, assessed by the proton transport rates). Data are mean ± s.e.m.; $n = 3$ replicates, and P value by two-sided Student's t-test. **n**, The *SIRT1-7*$^{-/-}$ MEFs grow much slower than wildtype MEFs. The *SIRT1-7*$^{-/-}$ MEFs and wildtype MEFs were regularly cultured, followed by determination of the proliferation rates by CCK8 assays. Results are shown as mean ± s.e.m.; $n = 6$ biological replicates, and P value by two-way ANOVA followed by Tukey's test. Experiments in this figure were performed three times, except **a** four times.

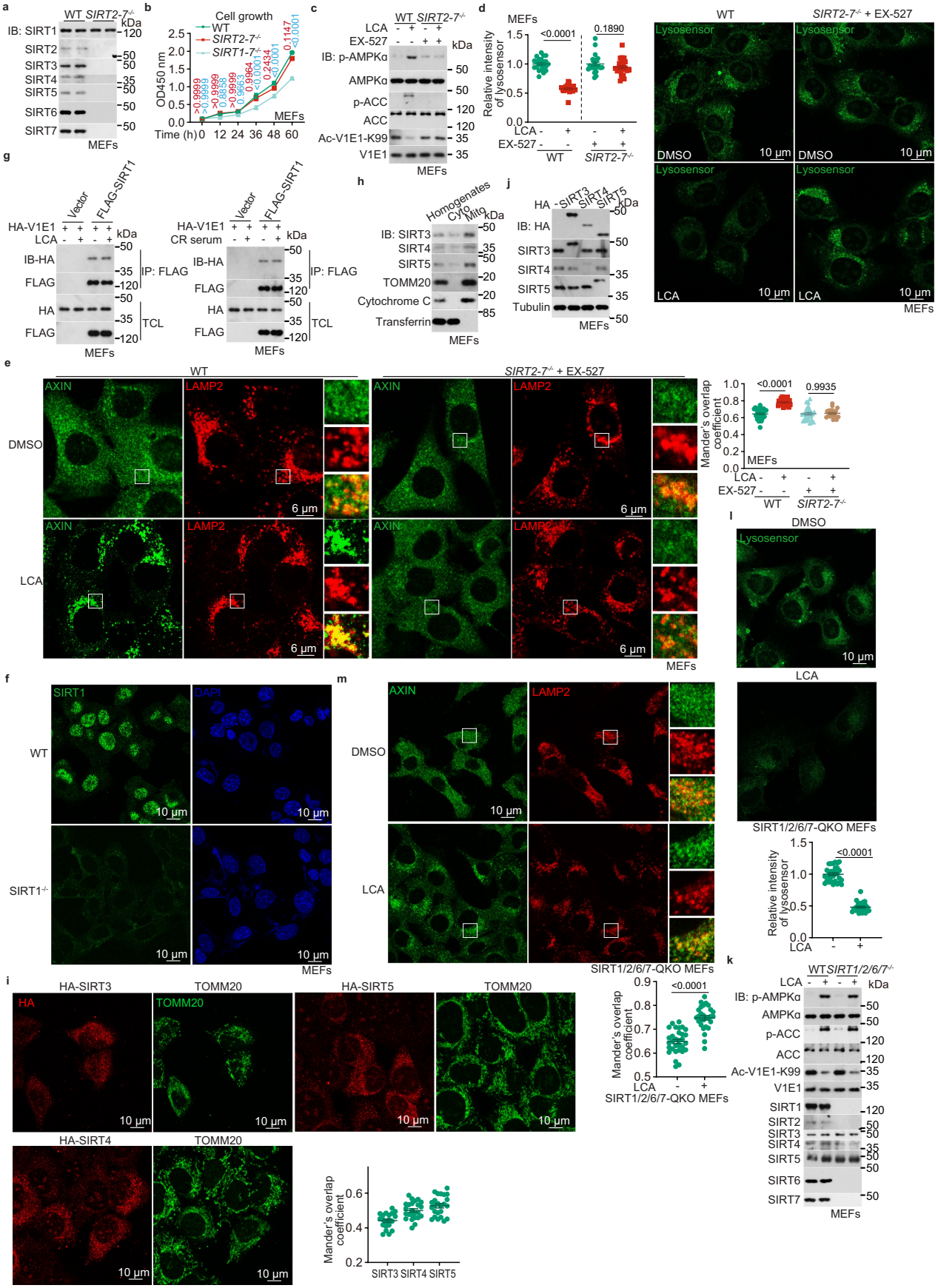

Extended Data Fig. 5 | See next page for caption.

Extended Data Fig. 5 | Sirtuins redundantly mediate the regulation of v-ATPase by LCA. a, **c**-**e**, Inhibition of SIRT1 in *SIRT2-7*$^{-/-}$ MEFs blocks the activation of AMPK by LCA. MEFs with sirtuins depletion by hexa-knockout of SIRT2 to SIRT7 (*SIRT2-7*$^{-/-}$, validated in **a**) are treated with 10 μM EX-527 for 12 h to inhibit SIRT1 (**c**-**e**). Cells were then treated with 1 μM LCA for another 4 h, followed by determination for AMPK activation (**c**), the activity of v-ATPase (**d**, assessed by the intensities of Lysosensor; statistical analysis data are mean ± s.e.m., normalized to the DMSO group of each genotype; n = 22 (WT, DMSO and *SIRT2-7*$^{-/-}$ + EX-527, DMSO), 25 (*SIRT2-7*$^{-/-}$ + EX-527, LCA), or 21 (WT, LCA), and P value by two-sided Student's t-test; see also proton transport rates on the right panel of Fig. 2d), and lysosomal localization of AXIN (**e**; data are mean ± s.e.m.; n = 26 (*SIRT2-7*$^{-/-}$ + EX-527, DMSO), 25 (WT, LCA), 30 (WT, DMSO), or 21 (*SIRT2-7*$^{-/-}$ + EX-527, LCA), and P value by two-way ANOVA followed by Tukey's test). **b**, *SIRT2-7*$^{-/-}$ MEFs grow at a similar rate to wildtype MEFs. Growth curves of *SIRT2-7*$^{-/-}$ MEFs, wildtype MEFs, and *SIRT1-7*$^{-/-}$ MEFs as a control, are shown. Results are mean ± s.e.m.; n = 7 (60 h of *SIRT2-7*$^{-/-}$) or 8 (others) replicates for each time point/cell line, and P value by two-way ANOVA followed by Tukey's test. **f**, Validation of the antibody able to recognise endogenous SIRT1. Wildtype MEFs or *SIRT1*$^{-/-}$ MEFs were immunostained with the antibody against SIRT1. The nuclei were stained with the DAPI dye. **g**, Sirtuins interact with V1E1. MEFs stably expressing HA-tagged V1E1 and FLAG-tagged SIRT1 were treated with 1 μM LCA (left panel), or incubated in DMEM with an equal volume of serum from CR or ad libitum fed mice as a control (right panel) instead of FBS, for 4 h. Cells were then lysed, followed by determination of V1E and SIRT1 interaction by immunoprecipitation of FLAG-tag. **h**, Portions of SIRTs 3, 4 and 5 are localized outside mitochondria. MEFs were subjected to subcellular fractionation, followed by determination of SIRT3, SIRT4 and SIRT5 in mitochondrial and cytosolic fractions by immunoblotting. **i**, **j**, SIRTs 3-5 are partially localized outside the mitochondria. MEFs with 3× HA-tagged SIRT3, SIRT4 or SIRT5 knocked in (located in front of the first exon of SIRTs 3-5; see validation data in **j** for the protein levels of SIRTs 3-5 after the HA-tag knocking in, and the sequence of the knocked-in HA-tag in Supplementary Table 2) were stained with antibodies against HA-tag and the mitochondrial marker TOMM20 (**i**). Representative images are shown, and the Mander's overlap coefficients between SIRTs 3-5 and TOMM20 are shown as mean ± s.e.m.; n = 20 (SIRT3), 24 (others) cells. **k**, LCA can activate AMPK in MEFs expressing SIRTs 3-5. MEFs with quadruple knockout of other SIRTs 1, 2, 6, and 7 (SIRT1/2/6/7-QKO) were treated with 1 μM LCA for 4 h, followed by determination of AMPK activation and V1E1 acetylation by immunoblotting. **l**, **m**, LCA can inhibit the activity of v-ATPase and promote the lysosomal translocation of AXIN in MEFs expressing SIRTs 3-5. The SIRT1/2/6/7-QKO MEFs were treated with 1 μM LCA for 4 h, followed by determination of v-ATPase activity (**l**; statistical analysis data are shown as mean ± s.e.m.; n = 30 (DMSO), 27 (LCA) cells for each treatment, and P value by two-sided Student's t-test), and the lysosomal localization of AXIN (**m**; statistical analysis data are shown as mean ± s.e.m.; n = 31 (DMSO), 28 (LCA) cells for each treatment, and P value by two-sided Student's t-test). Experiments in this figure were performed three times.

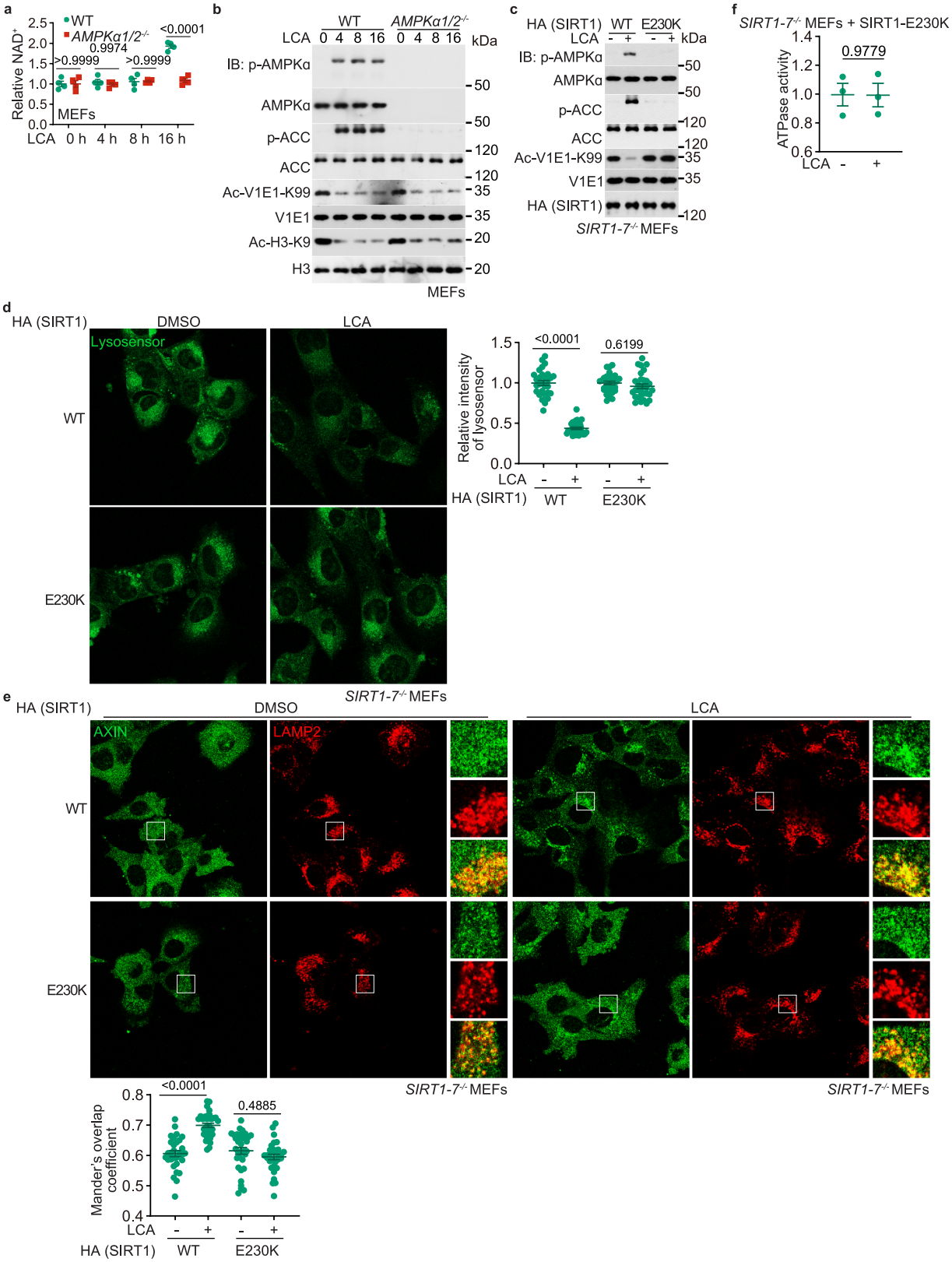

Extended Data Fig. 6 | See next page for caption.

Extended Data Fig. 6 | LCA activates sirtuins before the increase of NAD^+. **a**, **b**, LCA stimulates the activity of sirtuins before the elevation of NAD^+. Wildtype and *AMPKα1/2*$^{-/-}$ MEFs were treated with 1 μM LCA for indicated periods of time, followed by determination of the acetylation of histone H3 (on K9 residue, or Ac-H3-K9; **b**), the acetylation of V1E1 (**b**), activity of AMPK (**b**), and the levels of NAD^+ (**a**; results are shown as mean ± s.e.m.; *n* = 4 samples, and *P* value by two-way ANOVA followed by Tukey's test). **c**, Mutant SIRT1-E230K, unable to be activated by allosteric activators such as resveratrol, blocks LCA-mediated AMPK activation. *SIRT1-7*$^{-/-}$ MEFs were re-introduced with SIRT1-E230K, or wildtype SIRT1 as a control, and were treated with 1 μM LCA for 4 h. Cells were then lysed, followed by determination of AMPK activity and acetylated V1E1 by immunoblotting. **d**-**f**, SIRT1-E230K blocks LCA-mediated v-ATPase inhibition and AXIN translocation. *SIRT1-7*$^{-/-}$ MEFs were re-introduced with SIRT1-E230K or wildtype SIRT1 as a control, followed by treatment with 1 μM LCA for 4 h. The activity of v-ATPase, accessed by the intensities of the Lysosensor (**d**; data are mean ± s.e.m., normalised to the DMSO group; n = 29 (DMSO, WT) or 30 (others) cells) and by the proton transport rates of v-ATPase (**f**; data are mean ± s.e.m., normalised to the DMSO group; n = 3 replicates), and the lysosomal localization of AXIN (**e**; data are mean ± s.e.m.; n = 30 (DMSO, WT), 33 (LCA, WT), 34 (DMSO, E230K), or 32 (LCA, E230K) cells) were then determined. *P* value are determined by two-way ANOVA followed by Tukey's test (**d**, **e**), or by two-sided Student's *t*-test (**f**). Experiments in this figure were performed three times.

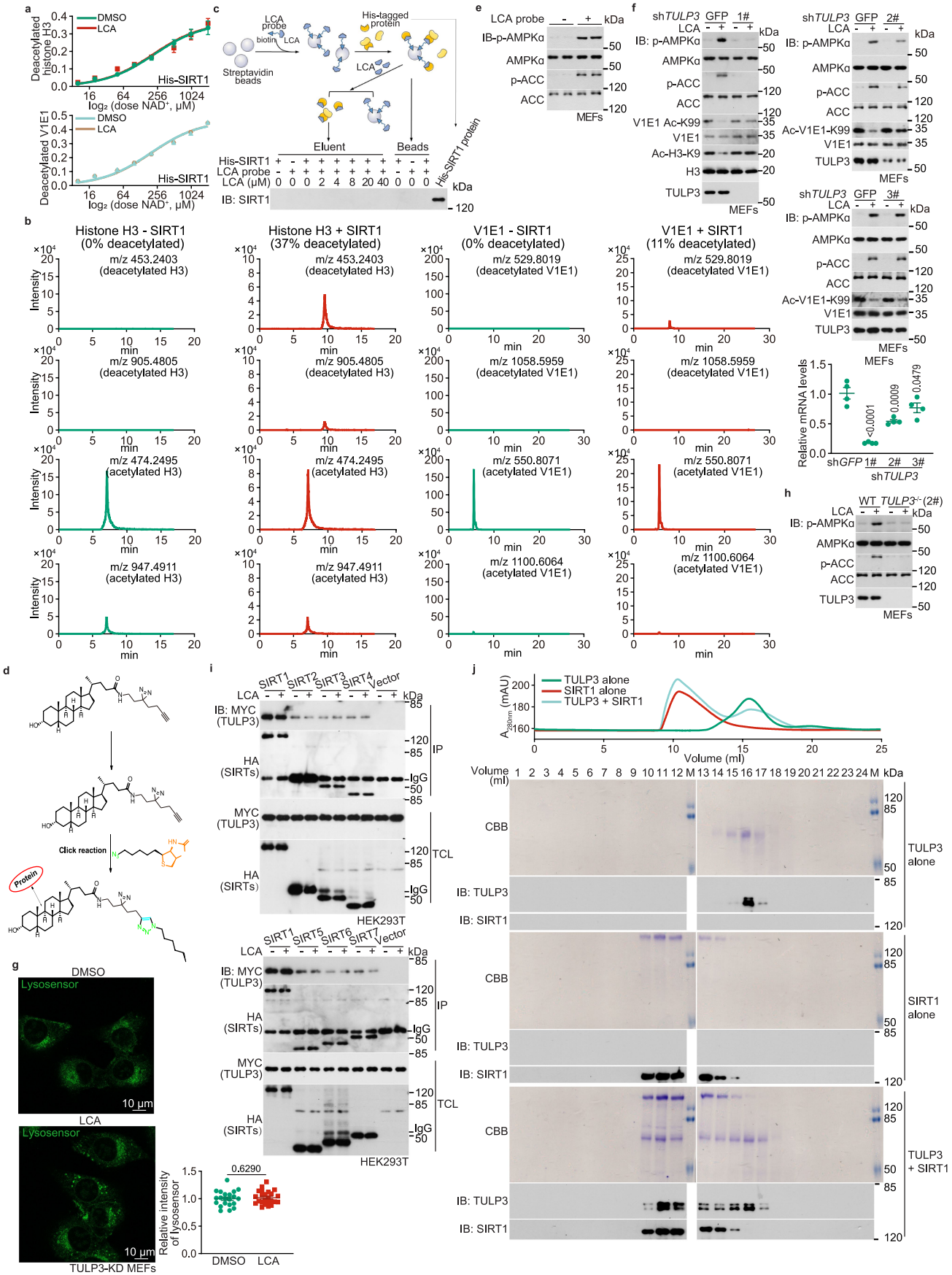

Extended Data Fig. 7 | See next page for caption.

Extended Data Fig. 7 | TULP3 mediates LCA to activate sirtuins. a-**c**, Purified bacterially expressed SIRT1 is unable to bind to or be activated by LCA. His-tagged SIRT1 was incubated with close-to-intracellular concentrations of LCA (5 μM). The deacetylase activities of SIRT1 towards histone H3 and V1E1 (**a**) were determined through a cell-free assay (see Methods section for details; results are shown as mean ± s.e.m., $n = 4$ samples), and the affinity of SIRT1 towards LCA through an affinity pull-down assay using LCA probe as a bait, followed by competitive elution with LCA (**c**; the procedure of this assay was depicted in the upper panel, and the LCA probe was synthesized and purified as described in Supplementary Fig. 3). See also validation for the SIRT1 activity assay in **b**, in which the representative spectrograms of acetylated histone H3 (left panel) and acetylated V1E1 (right panel) peptides before (−SIRT1) and after (+SIRT1) incubating with SIRT1 are shown. The presence of deacetylated histone H3 (m/z 453.2403 and 905.4805) and V1E1 (m/z 529.8019 and 1058.5959) peaks indicate that SIRT1 effectively catalysed the deacetylation reaction. **d**, Schematic diagram depicting the steps and reaction principles for the formation of the complex between the LCA probe and TULP3-SIRT1. The LCA probe was first biotinylated by mixing with Cu(II) salt, which catalyses a [3 + 2] azide-alkyne cycloaddition with a biotin-azide linker, followed by incubating with Streptavidin beads for 2 h, and then the TULP3 and SIRT1 proteins. **e**, LCA probe is able to activate AMPK. MEFs were treated with 10 μM LCA probe for 4 h, followed by determination of AMPK activation by immunoblotting. **f**, TULP3 is required for the LCA-mediated activation of SIRT1 and AMPK. MEFs with *TULP3* knocked down by three distinct siRNAs (#1, #2 or #3, see knockdown efficiency of each siRNA on the lower right panel) were treated with 1 μM LCA for 4 h, followed by determination of the activity of AMPK and the acetylation of V1E1 by immunoblotting. Results are mean ± s.e.m.; $n = 4$ for each condition, and *P* value by two-way ANOVA followed by Tukey's test. **g**, TULP3 is required for LCA-mediated inhibition of v-ATPase. MEFs with *TULP3* knocked down (by siRNA #1, and the same hereafter for all *TULP3* knocked down experiments) were treated with 1 μM LCA for 4 h, followed by determination of the activity of v-ATPase. Statistical analysis data are shown as mean ± s.e.m., normalized to the DMSO group; $n = 21$ (DMSO) or 24 (LCA) cells, and *P* value by two-sided Student's *t*-test. **h**, Knockout of TULP3 abrogates LCA-induced activation of SIRT1 and AMPK. The clone #2 of *TULP3*$^{-/-}$ MEFs were treated with 1 μM LCA for 4 h, followed by determination of the activity of AMPK by immunoblotting. See also the data for clone #1 of *TULP3*$^{-/-}$ MEFs in Fig. 3b. **i**, TULP3 interacts with all 7 members of the sirtuin family independently of LCA. HEK293T cells were transfected with Myc-tagged TULP3 and each HA-tagged sirtuin (SIRT1 to SIRT7). Cells were then lysed, and a concentration of 5 μM LCA was added to the lysate. After incubation for 1 h, each SIRT was immunoprecipitated, and the co-immunoprecipitated TULP3, followed by immunoblotting. **j**, TULP3 is constitutively associated with SIRT1, independently of LCA. Bacterially expressed and purified TULP3 and SIRT1 were co-incubated, followed by size exclusion chromatography. The elution chromatograms of SIRT1 alone (red), TULP3 alone (green), or SIRT1 together with TULP3 (cyan) were shown (upper panel). The presence of SIRT1-TULP3 complex was confirmed by the shift of the peak retention volume of TULP3 from 16 ml to 11 ml after incubating with SIRT1 (upper panel), and the presence of both SIRT1 and TULP3 in the fractions with a shifted peak (lower panel; analysed by SDS-PAGE and immunoblotting). CBB, Coomassie brilliant blue staining. Experiments in this figure were performed three times. The schematic in **c** was created using elements from Servier Medical Art under a Creative Commons Attribution 3.0 unported licence.

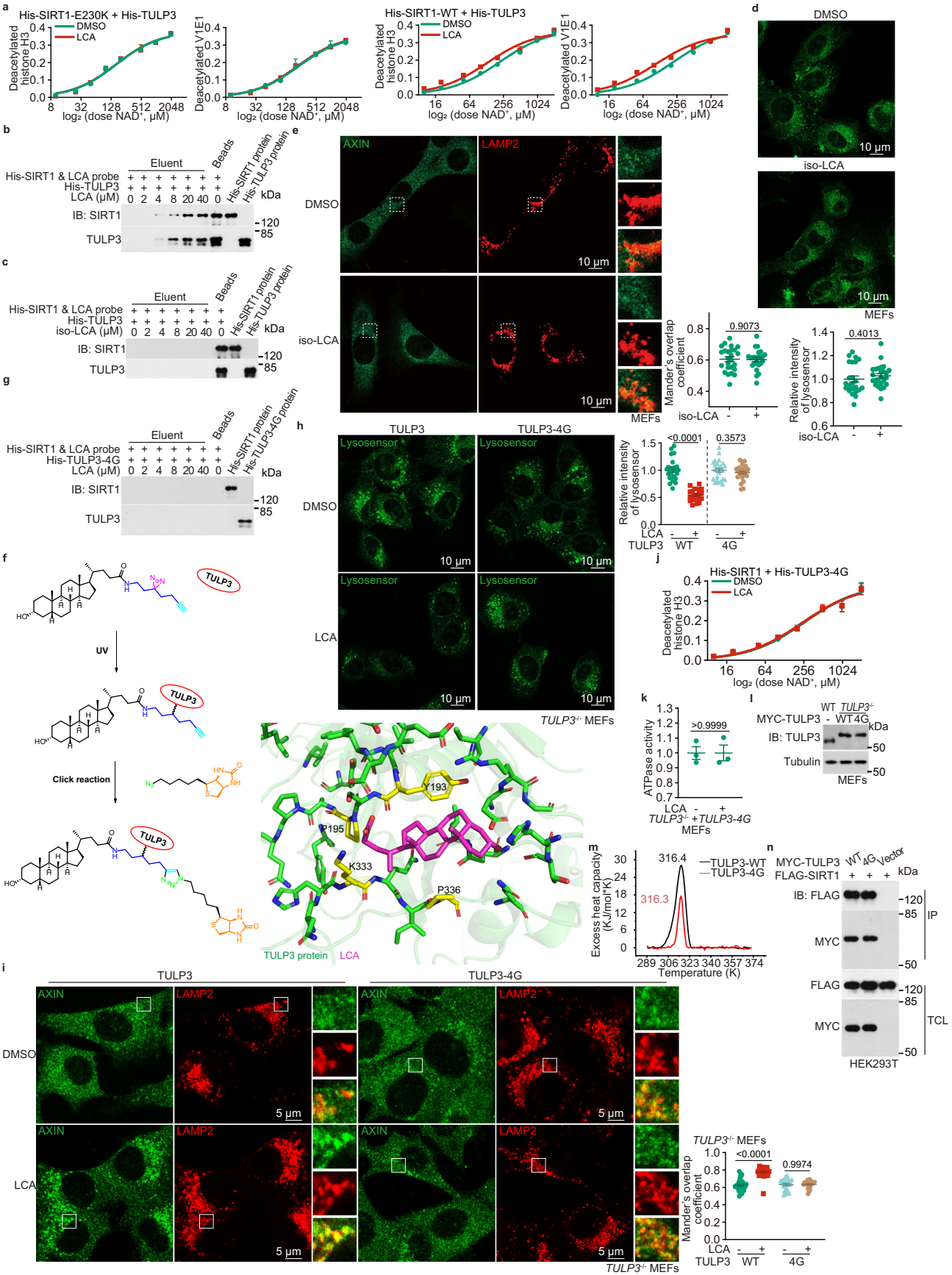

Extended Data Fig. 8 | See next page for caption.

Extended Data Fig. 8 | TULP3 binds LCA for activation of sirtuins. a, **b**, TULP3 binds LCA and mediates activation of SIRT1. His-tagged SIRT1 (**b**) or SIRT1-E230K (**a**) mutant was co-eluted with bacterially expressed His-tagged TULP3 on a Superdex column, followed by incubation with LCA at 5 μM (**a**) or indicated concentrations (**b**). The deacetylase activities of TULP3-SIRT1 complex towards histone H3 and V1E1 were determined through a cell-free assay (**a**, results are shown as mean ± s.e.m., $n = 4$ samples), and the affinity of TULP3-SIRT1 complex towards LCA through an affinity pull-down assay using LCA probe as a bait, followed by competitive elution with LCA (**b**). **c**, TULP3 does not bind to iso-LCA. Experiments were performed as in **b**, except that iso-LCA was used to elute the TULP3-SIRT1 complex pre-bound to LCA-probe-conjugated beads. **d**, **e**, Iso-LCA does not inhibit v-ATPase or trigger the lysosomal translocation of AXIN. MEFs were treated with 1 μM iso-LCA for 4 h, followed by determination of the activity of v-ATPase (**d**; data are shown as mean ± s.e.m., normalized to the DMSO group; $n = 23$ (DMSO) or 25 (iso-LCA) cells) and the lysosomal localisation of AXIN (**e**; data are shown as mean ± s.e.m.; $n = 25$ (DMSO) or 24 (iso-LCA) cells). *P* value in this panel was determined by two-sided Student's *t*-test. **f**, In silico modelling of LCA bound to TULP3. The His-tagged TULP3 protein was incubated with the LCA probe, followed by exposure to UV light. The LCA probe-protein conjugates were then mixed with Cu(II) salt and the biotin-azide linker, thus biotinylating probe-target complexes, allowing for the pull-down of such complexes for MS analysis with Streptavidin beads (left panel; see details in "Determination of the binding affinity of LCA to TULP3" of Methods section). Modelling was then performed according to the results of MS on purified TULP3 conjugated to the LCA-probe, and the AlphaFold-predicted TULP3 structure. The Y193, P195, K333 and P336 residues (coloured in yellow) that comprise a hydrophobic pocket for LCA (coloured in red) binding as indicated were mutated to glycine (TULP3-4G) to create a TULP3 mutant that is defective in binding to LCA. **g**-**j**, TULP3-4G unable to bind LCA blocks LCA-induced activation of SIRT1 and AMPK. The LCA-binding affinity (**g**) was determined as in **b**, except that the His-tagged TULP3-4G was used. The LCA-mediated AMPK activation was determined as in **h** and **i**, in which the *TULP3*$^{-/-}$ MEFs were infected with lentivirus carrying TULP3-4G mutant or its wildtype control, followed by treatment with 1 μM LCA for 4 h. The activity of v-ATPase (**h**) and the lysosomal localisation of AXIN (**i**) were then determined. The effects of LCA on SIRT1 activity were determined in **j** (as in Fig. 3e, except that the TULP3-4G was co-eluted with SIRT1 before the experiment). The results are shown as mean ± s.e.m. $n = 4$ (**j**), 21 (WT, LCA of **h**), 26 (WT, LCA of **i**), 28 (WT, DMSO of **i**), 23 (4G, DMSO of **i**), 30 (4 G, LCA of **i**) or 25 (others) samples; and *P* value by two-sided Student's *t*-test (**h**, 4G), two-sided Student's *t*-test with Welch's correction (**h**, WT), or two-way ANOVA followed by Tukey's test (**i**). **k**, TULP3-4G blocked LCA-mediated inhibition of the proton transport rate of v-ATPase. *TULP3*$^{-/-}$ MEFs were infected with lentivirus carrying TULP3-4G, followed by treatment with 1 μM LCA for 4 h. The proton transport rate of v-ATPase was then determined. The results are shown as mean ± s.e.m. $n = 3$ replicates for each treatment; and *P* value by two-sided Student's *t*-test. **l**, Validation for the close-to-endogenous protein levels of wildtype TULP3 and TULP3-4G when re-introduced into the *TULP3*$^{-/-}$ MEFs. **m**, TULP3-4G has a thermal transition midpoint (Tm) similar to that of the wildtype TULP3. Some 10 μM His-tagged TULP3 or TULP3-4G was incubated in the His-elution Buffer (see contents in Methods section), followed by determination of the Tm on a differential scanning calorimetre. Enthalpy changes of TULP3 at indicated temperatures are shown. **n**, TULP3-4G exhibits a comparable affinity for SIRT1 to wildtype TULP3. HEK293T cells were transfected with different combinations of Myc-tagged TULP3, TULP3-4G, and FLAG-tagged SIRT1 for 24 h. The interaction between TULP3 and SIRT1 was determined by immunoprecipitating Myc-tag, followed by immunoblotting. Experiments in this figure were performed three times.

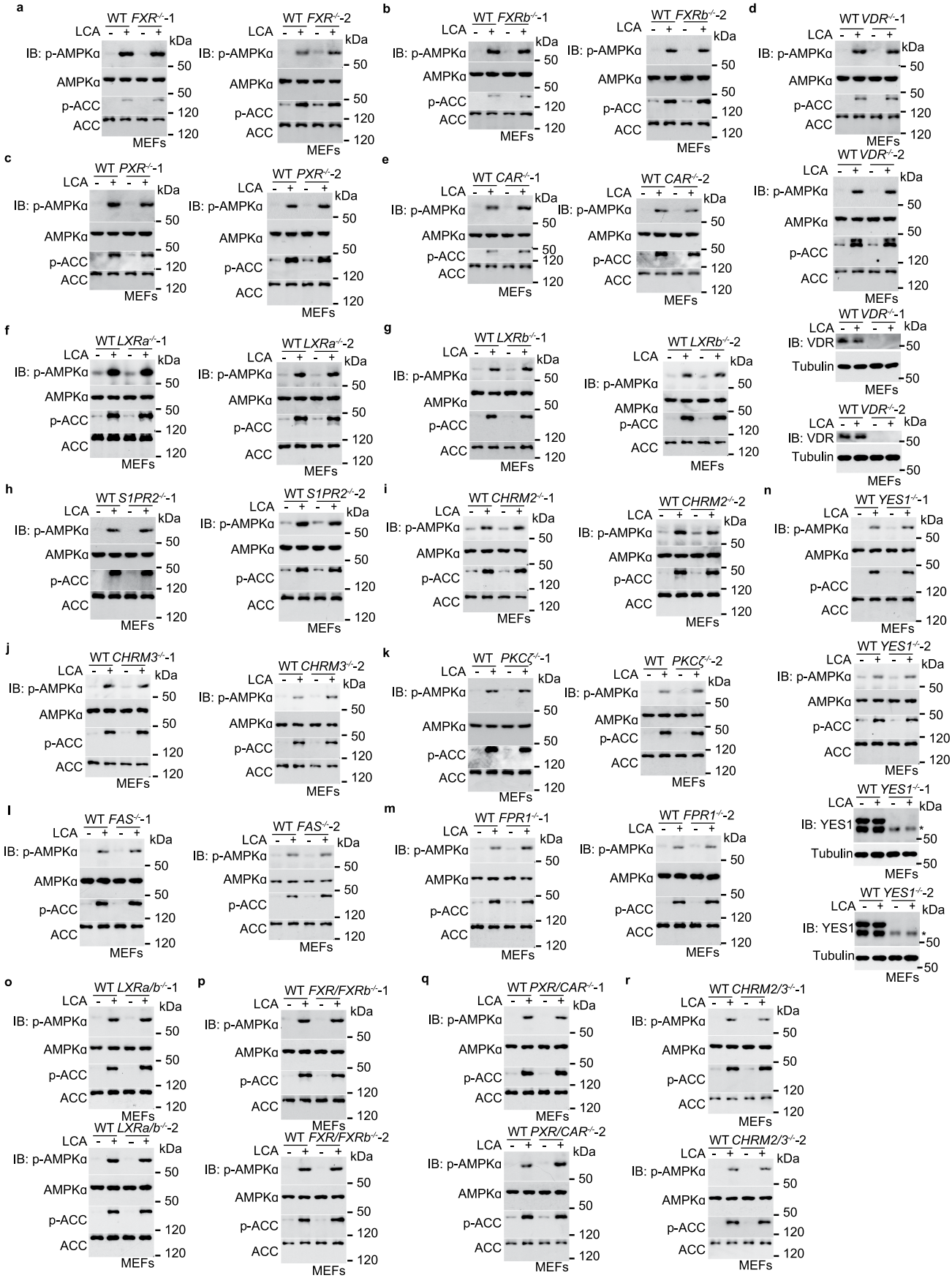

Extended Data Fig. 9 | See next page for caption.

Extended Data Fig. 9 | Other known binding partners of LCA are not required for the activation of AMPK. a-**r**, MEFs with knockout of known binding partner/targets of LCA or derivatives, including *FXR*[34–36] (**a**, clone #1 on the left panel, and clone #2 right, and the same hereafter in this figure), *FXRb*[37] (**b**), *PXR*[38,39] (**c**), *VDR*[40] (**d**), *CAR*[41,42] (**e**), *LXRa*[43] (**f**), *LXRb*[43] (**g**), *S1PR2* (ref. 44; **h**), *CHRM2* (ref. 45; **i**), *CHRM3* (ref. 46; **j**), *PKCζ*[47] (**k**), *FAS*[48] (**l**), *FPR1* (ref. 49; **m**), or *YES1* (ref. 50; **n**), or with double knockout of *LXRa* and *LXRb* (**o**), *FXR* and *FXRb* (**p**), *PXR* and *CAR* (**q**), or *CHRM2* and *CHRM3* (**r**), were treated with 1 μM LCA for 4 h, followed by determination of the activity of AMPK. See validation data for each knockout cell line by immunoblotting (**d**, **n**) or parallel reaction monitoring (PRM)-based, quantitative mass spectrometry (others; in which the MS/MS spectrum of the quantotypic peptides selected for each protein, and the peak area of the quantotypic peptide detected in each cell line, are shown in Supplementary Table 4). See also data for TGR5 (ref. 51) in extended data figure 1q of ref. 1. Experiments in this figure were performed three times.

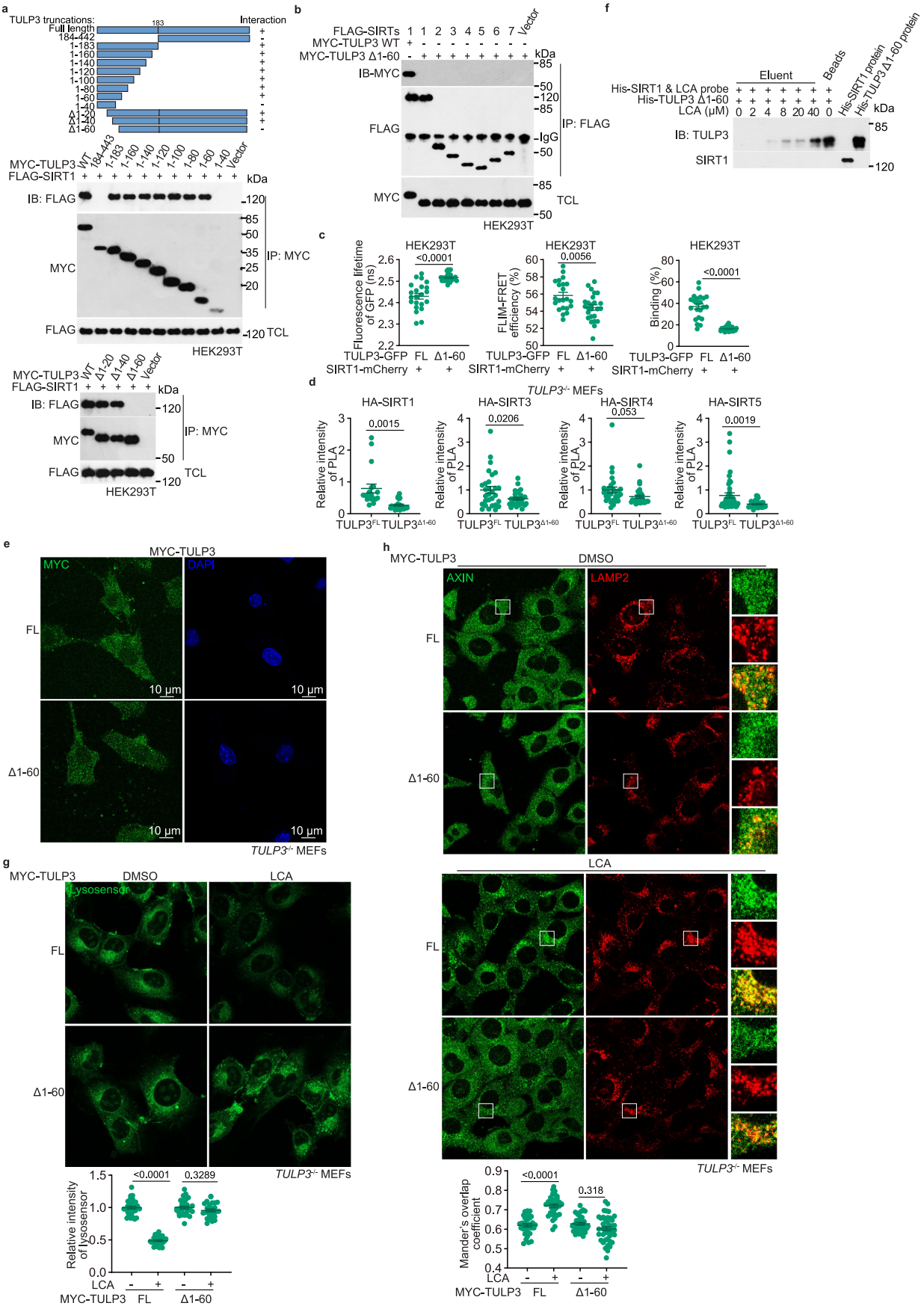

Extended Data Fig. 10 | See next page for caption.

Extended Data Fig. 10 | Interaction between TULP3 and sirtuin is required for AMPK activation by LCA. a, **b**, The segment of aa 1-60 of TULP3 is required for interaction with SIRT1. HEK293T cells were co-transfected with Myc-tagged full-length TULP3, or its deletion mutants, and FLAG-tagged SIRT1 (**a**) or other sirtuins (**b**). After 12 h of transfection, cells were lysed, followed by immunoprecipitation of Myc- (**a**) or FLAG-tag (**b**). The co-immunoprecipitated SIRT1 (**a**) or TULP3 (**b**) was determined by immunoblotting. **c**, **d**, TULP3$^{\Delta 1\text{-}60}$ does not interact with sirtuins. *TULP3*$^{-/-}$ MEFs with HA-tagged SIRT1, SIRT3, SIRT4 or SIRT5 knocked in (**d**), or wildtype HEK293T cells (**c**), were infected with lentivirus carrying the GFP-tagged (**c**) or Myc-tagged (**d**) TULP3$^{\Delta 1\text{-}60}$, and the mCherry-tagged SIRT1 (**c**). The interaction between TULP3 and SIRTs was determined through the FRET-FLIM (**c**, the fluorescence lifetime of GFP-TULP3 donor, the FRET-FLIM efficiency, and the percentage of SIRTs-associated TULP3 calculated accordingly, are shown as mean ± s.e.m.; n = 22 (full-length TULP3) or 25 (TULP3$^{\Delta 1\text{-}60}$) cells for each treatment, and P value by two-sided Student's t-test) and the Duolink (**d**, the relative intensities of PLA signals – after normalizing to DAPI - are shown as mean ± s.e.m.; n = 19 (TULP3-SIRT1), 23 (TULP3$^{\Delta 1\text{-}60}$-SIRT1), 29 (TULP3-SIRT3), 27 (TULP3$^{\Delta 1\text{-}60}$-SIRT3), 28 (SIRT4), 44 (TULP3-SIRT5), 31 (TULP3$^{\Delta 1\text{-}60}$-SIRT5) cells for each treatment, and P value by two-sided Student's t-test (middle panel of **c**) or two-sided Student's t-test with Welch's correction (others)) assays. **e**, TULP3 and TULP3$^{\Delta 1\text{-}60}$ show similar subcellular localization. *TULP3*$^{-/-}$ MEFs with stable expression of Myc-tagged TULP3 or TULP3$^{\Delta 1\text{-}60}$ were stained with antibody against Myc-tag. Representative images are shown. **f**, TULP3$^{\Delta 1\text{-}60}$ retains the ability to bind LCA. Experiments were performed as in Extended Data Fig. 8b, except that His-tagged TULP3$^{\Delta 1\text{-}60}$ was used. **g**, **h**, TULP3$^{\Delta 1\text{-}60}$ blocks LCA-induced activation of AMPK. *TULP3*$^{-/-}$ MEFs were infected with lentivirus carrying the Myc-tagged TULP3$^{\Delta 1\text{-}60}$, or full-length TULP3 as a control, followed by treatment with 1 μM LCA for 4 h. The activity of v-ATPase (**g**, data are mean ± s.e.m.; n = 30 (TULP3 and TULP3$^{\Delta 1\text{-}60}$), 28 (TULP3 + LCA), or 27 (TULP3$^{\Delta 1\text{-}60}$ + LCA)), and the lysosomal localization of AXIN (**h**, data are mean ± s.e.m.; n = 31 (TULP3), 34 (TULP3 + LCA), 38 (TULP3$^{\Delta 1\text{-}60}$) or 42 (TULP3$^{\Delta 1\text{-}60}$ + LCA)) were then determined. P value were determined by two-way ANOVA followed by Tukey's test. Experiments in this figure were performed three times.

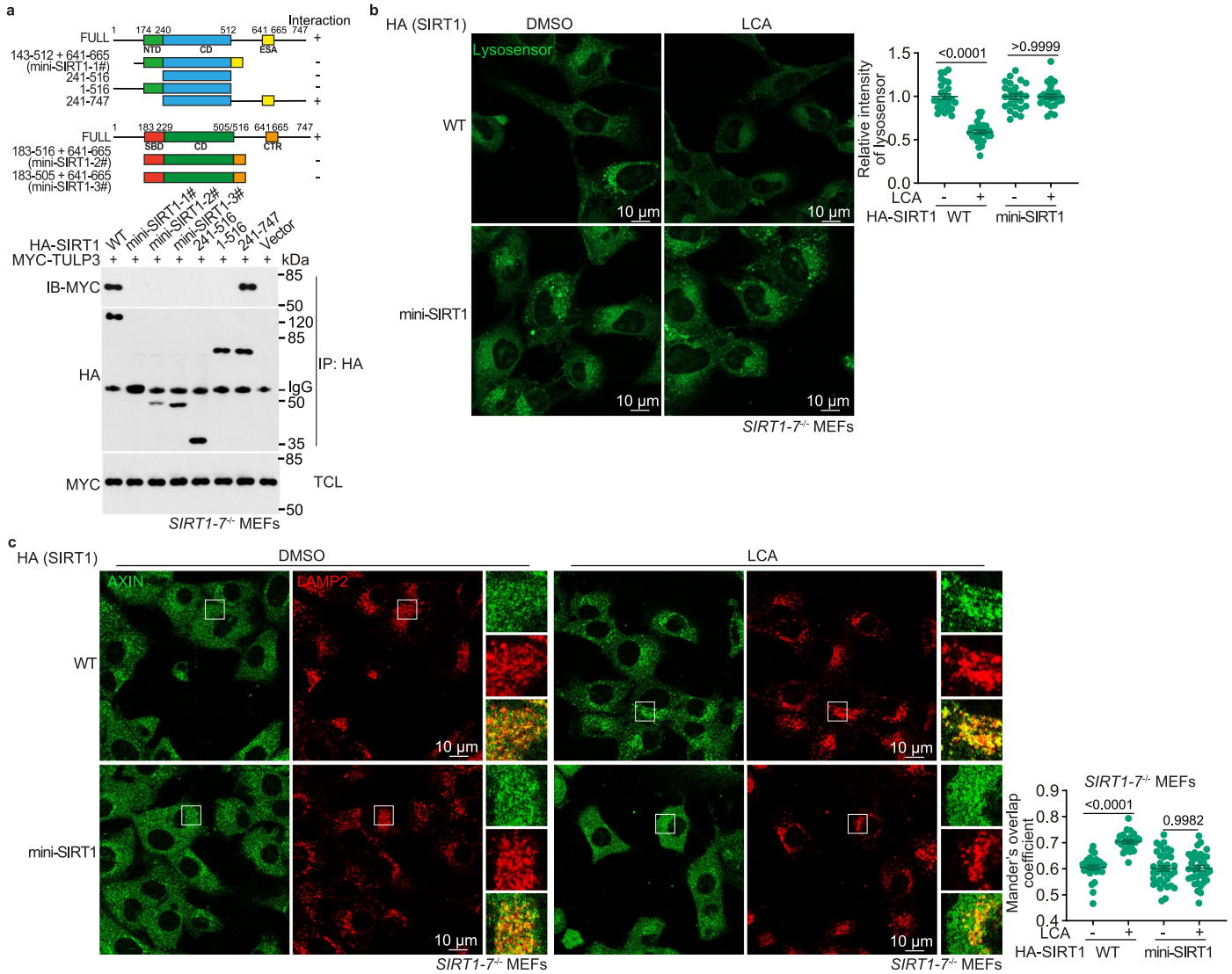

Extended Data Fig. 11 | The mini-SIRT1 mutant unable to interact with TULP3 blocks LCA-induced activation of AMPK. a, The mini-SIRT1 mutant is unable to interact with TULP3. HEK293T cells were transfected with various combinations of Myc-tagged TULP3 with HA-tagged SIRT1 deletion mutants: three different versions of mini-SIRT1 (according to different references: version #1 described in ref. 55, and #2 and #3 according to ref. 56; unless stated otherwise, only mini-SIRT1-#1 is used afterwards in this study) and other SIRT1 deletion mutants. At 12 h after transfection, the cells were lysed, followed by the immunoprecipitation of the HA-tag. Co-immunoprecipitated TULP3 was determined by immunoblotting. NTD: N-terminal domain; CD: catalytic domain; and ESA: essential for SIRT1 activity sequence; defined as in ref. 55. SBD: sirtuins-activating compound-binding domain; and CTR: C-terminal regulatory segment; defined as in ref. 56. **b**, **c**, The mini-SIRT1 mutant blocks LCA-induced activation of AMPK. *SIRT1-7*$^{-/-}$ MEFs were infected with lentivirus carrying the HA-tagged mini-SIRT1, or the full-length SIRT1 as a control, followed by treatment with 1 μM LCA for 4 h. The lysosomal localization of AXIN (**c**, statistical analysis data are shown as mean ± s.e.m.; $n = 27$ (SIRT1), 24 (SIRT1 + LCA), 36 (mini-SIRT1), or 35 (mini-SIRT1 + LCA)) and the activity of v-ATPase (**b**, statistical analysis data are shown as mean ± s.e.m.; $n = 26$ (SIRT1), 27 (LCA) or 25 (mini-SIRT1)) were then determined. *P* value were determined by two-way ANOVA followed by Tukey's test. Experiments in this figure were performed three times.

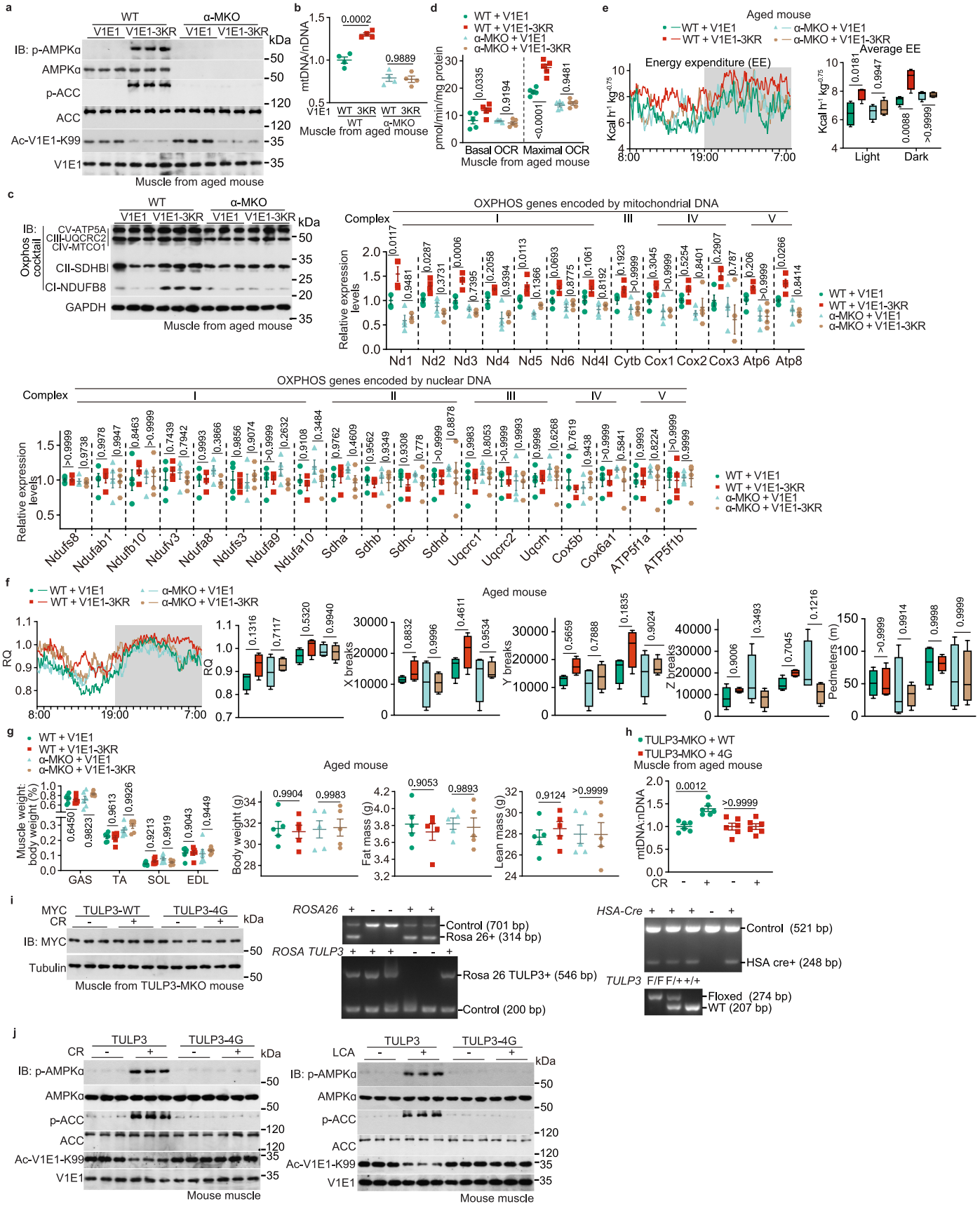

Extended Data Fig. 12 | See next page for caption.

Extended Data Fig. 12 | The LCA-TULP3-sirtuins-v-ATPase axis enhances muscle functions in aged mice. a-**d**, V1E1-3KR improves muscle function in aged mice. WT or muscle-specific *AMPKα* knockout (α-MKO) mice with muscle-specific expression (induced by tamoxifen at 16 months old; see "mouse strains" section of the Methods section for the procedures for constructing this strain) of V1E1-3KR or wildtype V1E1 were subjected to analysis for AMPK activation (**a**), the ratios of mtDNA:nDNA (**b**), the mRNA and protein levels of the OXPHOS complex (**c**), and the OCR (**d**) in the gastrocnemius muscle. Results are shown as mean ± s.e.m.; $n = 4$ (**b**, c) or 5 (**d**) mice for each genotype/treatment, and P value by two-way ANOVA followed by Tukey's test. **e**-**g**, V1E1-3KR elevates energy expenditure (EE) and respiratory quotient (RQ) in aged mice. Mice were treated as in **a**, followed by determination of EE (**e**). Data are shown as mean (left panel; at 5-min intervals during a 24-h course after normalization to the body weight ($kg^{0.75}$)), or as box-and-whisker plots (right panel, in which the lower and upper bounds of the box represent the first and the third quartile scores, the centre line represents the median, and the lower and upper limits denote minimum and maximum scores, respectively; and the same hereafter for all box-and-whisker plots; $n = 4$ mice for each genotype/treatment, and P value by two-way ANOVA followed by Tukey's test). See also respiratory quotient (RQ) and the ambulatory activity data generated in this experiment in **f** (data are shown as mean (at 5-min intervals during a 24-h course; $n = 4$ mice for each genotype), or box-and-whisker plots ($n = 4$ mice for each genotype, and P value by two-way ANOVA followed by Tukey's test)), and the body composition data in **g** (mean ± s.e.m., $n = 5$ mice for each genotype, and P value by two-way ANOVA followed by Tukey's test). **h**, **i**, **j**, TULP3-4G blocks CR-elevated mitochondrial content in muscle. The muscle-specific *TULP3* knockout (TULP3-MKO) mice with re-introduced muscular expression of TULP3-4G or wildtype TULP3 (induced by tamoxifen at 16 months old; see validation data in **i**, and the procedures for constructing this strain in "mouse strains" section of the Methods section) were subjected to CR for 3.5 months, followed by determination of mtDNA:nDNA ratios (**h**). Results in **h** are shown as mean ± s.e.m., $n = 6$ mice for each genotype/treatment, and P value by two-way ANOVA followed by Tukey's test. See also AMPK activation in the muscle of TULP3-4G-re-introduction mice after 3.5 months of CR (left panel), or 1 month of (2-hydroxypropyl)-β-cyclodextrin-coated LCA treatment (1 g/l in the drinking water; right panel) in **j**. Experiments in this figure were performed three times.

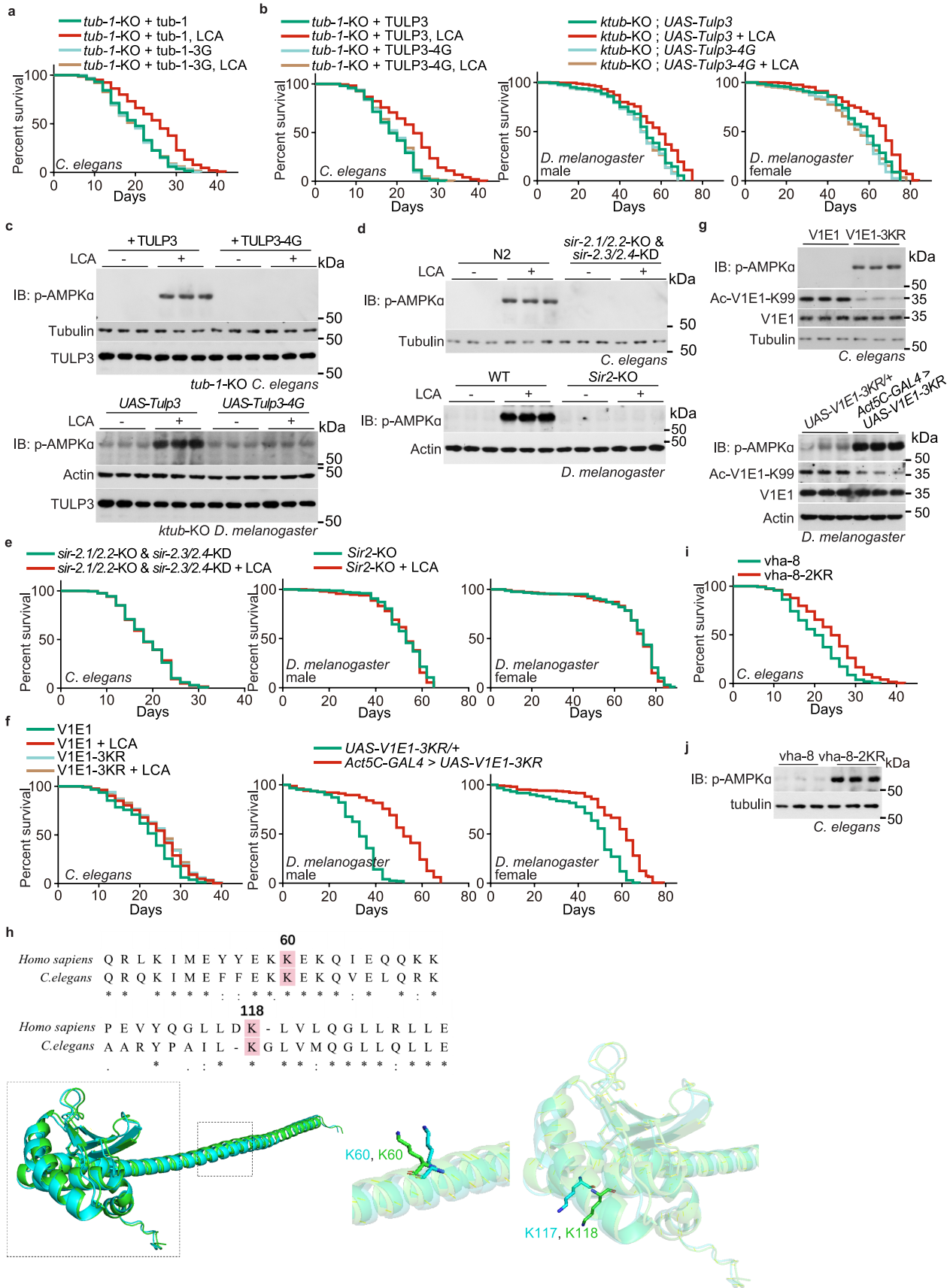

Extended Data Fig. 13 | See next page for caption.

Extended Data Fig. 13 | The LCA-TULP3-sirtuins-v-ATPase axis extends lifespan in nematodes and flies. a, Tub-1-3G blocks LCA-induced extension of lifespan in nematodes. Nematodes with Tub-1-3G re-introduced in the *tub-1*-knockout background were treated with 100 μM LCA, followed by determination of lifespan (shown as Kaplan-Meier curves). **b**, **e**, **f**, **i**, TULP3, sirtuins and v-ATPase are required for lifespan extension by LCA. The *tub-1*-knockout nematodes re-introduced with TULP3-4G (**b**, left panel), sirtuins-depleted nematodes (**e**, left panel; *sir-2.1*/*sir-2.2*-double knockout nematodes with *sir-2.3* and *sir-2.4* knockdown (KD)), nematodes expressing V1E1-3KR (**f**, left panel) or vha-8-2KR (**i**), along with control nematodes, were cultured in the medium containing LCA at 100 μM. Lifespan data are shown as Kaplan-Meier curves. Shown are also data obtained from experiments using flies with *TULP3* knockout (*ktub*-KO) re-introduced with TULP3-4G (*UAS-TULP3-4G*) (**b**, middle and right panels), flies with sirtuin knockout (*sir2*-KO) (**e**, middle and right panels), and flies expressing V1E1-3KR (*Act5C-GAL4 > UAS-V1E1-3KR*) (**f**, middle and right panels). The flies were cultured in the medium containing 100 μM LCA. **c**, **g**, TULP3 and V1E1 regulate LCA-mediated activation of AMPK in nematodes and flies. The *tub-1*-KO nematodes (upper panel of **c**) or *ktub*-KO flies (lower panel of **c**), both with TULP3-4G reintroduction (**c**), or wildtype nematodes and flies with V1E1-3KR expression (**g**), were cultured in the medium containing LCA at 100 μM, followed by determination of the activation of AMPK. **d**, Sirtuins in nematodes and flies are required for LCA-induced AMPK activation. Nematodes (upper panel) or flies (lower panel) with sirtuin depletion were cultured in the medium containing LCA at 100 μM, followed by determination of AMPK activation. **h**, **j**, Mutant of vha-8 subunit (equivalent to mouse V1E2), vha-8-2KR, is a deacetylated state-mimetic and activates AMPK in nematodes. Nematodes with expression of vha-8 or vha-8-K60R/K117R (vha-8-2KR) mutant (see structural alignment results in **h**, in which the AlphaFold-predicted vha-8 structure is coloured in green, and V1E2 in blue) were cultured in the regular NGM plate, followed by determination of the activation of AMPK (**j**). Experiments in this figure were performed three times.

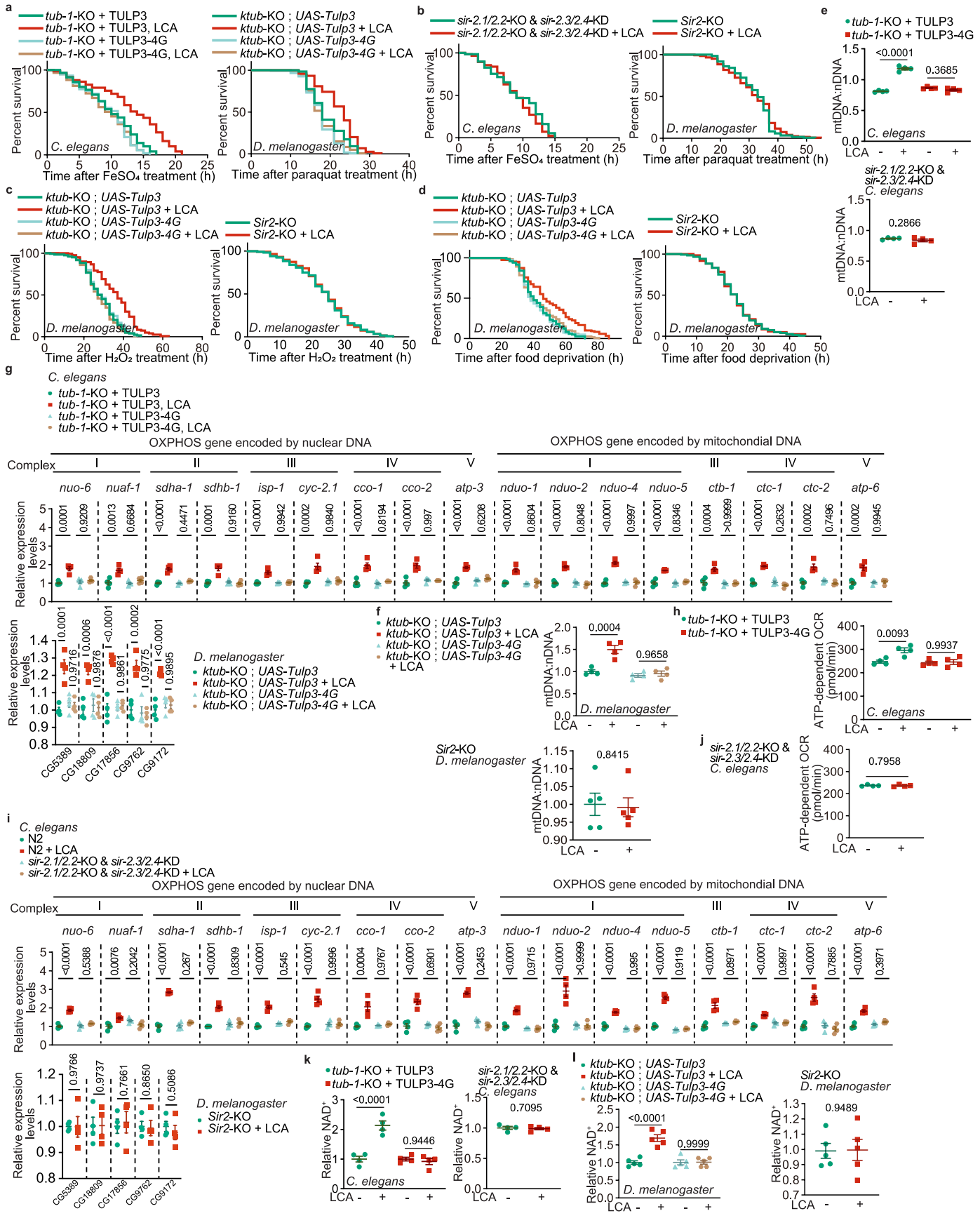

Extended Data Fig. 14 | See next page for caption.

Extended Data Fig. 14 | The LCA-TULP3-sirtuins-v-ATPase axis extends healthspan in nematodes and flies. a-**d**, TULP3 and sirtuins are required for LCA-enhanced resistance to oxidative stress and starvation. Nematodes and flies with TULP3-4G re-introduction in the *tub-1*- or *ktub*-knockout background (**a**, **c**, **d**), or with sirtuins depletion (**b**-**d**) were treated with 100 μM LCA for 2 days (left panels of **a**, **b**) or 30 days (right panels of **a**, **b**, and **c**, **d**), followed by transferring to media containing 15 mM $FeSO_4$ (left panels of **a**, **b**), 20 mM paraquat (right panels of **a**, **b**) or 5% H_2O_2 (**c**) that elicited oxidative stress, or deprived of food (**d**). Lifespan data are shown as Kaplan-Meier curves. **e**, **f**, TULP3 and sirtuins are required for elevation of mtDNA:nDNA ratios in nematodes and flies. The *tub-1*-KO nematodes (upper panel of **e**) or *ktub*-KO flies (upper panel of **f**), both with TULP3-4G reintroduction, or sirtuins-depleted nematodes (lower panel of **e**) and flies (lower panel of **f**) were treated with 100 μM LCA, either for 2 days (**e**, for nematodes) or for 30 days (**f**, for flies), followed by determination of the ratios of mtDNA:nDNA. Results are mean ± s.e.m.; $n = 5$ (lower panels of **f**) or 4 (others) samples for each genotype/condition, and *P* value by two-way ANOVA followed by Tukey's test (upper panels) or two-sided Student's *t*-test (lower panels). **g**-**j**, TULP3 and sirtuins are required for elevation of mitochondrial contents and respiratory functions in nematodes and flies. The *tub-1*-KO nematodes (upper panel of **g**, and **h**) or *ktub*-KO flies (lower panel of **g**), both re-introduced with TULP3-4G, or sirtuins-depleted nematodes (upper panel of **i**, and **j**) and flies (lower panel of **i**) were treated with LCA, either for 2 days (for nematodes) or 30 days (for flies), followed by determination of the mRNA levels of OXPHOS complex (**g**, **i**; results are mean ± s.e.m.; $n = 4$ samples for each genotype/treatment, and *P* value by two-way ANOVA followed by Tukey's test, except those of flies in **i** two-sided Student's *t*-test), and OCR (**h**, **j**; results are mean ± s.e.m.; $n = 4$ samples for each genotype/treatment, and *P* value by two-way ANOVA followed by Tukey's test, except **j** two-sided Student's *t*-test). **k**, **l**, TULP3 and sirtuins are required for the elevation of NAD^+ levels in nematodes and flies. Nematodes and flies with TULP3-4G re-introduction in the *tub-1*- or *ktub*-knockout background (left panels), or with sirtuins depletion (right panels), were treated with 100 μM LCA for 2 days (**k**) or 30 days (**l**), followed by determination of the levels of NAD^+. Results are mean ± s.e.m.; $n = 5$ (**l**) or 4 (**k**) samples for each genotype/condition, and *P* value by two-way ANOVA followed by Tukey's test (left panels) or two-sided Student's *t*-test (right panels). Experiments in this figure were performed three times.

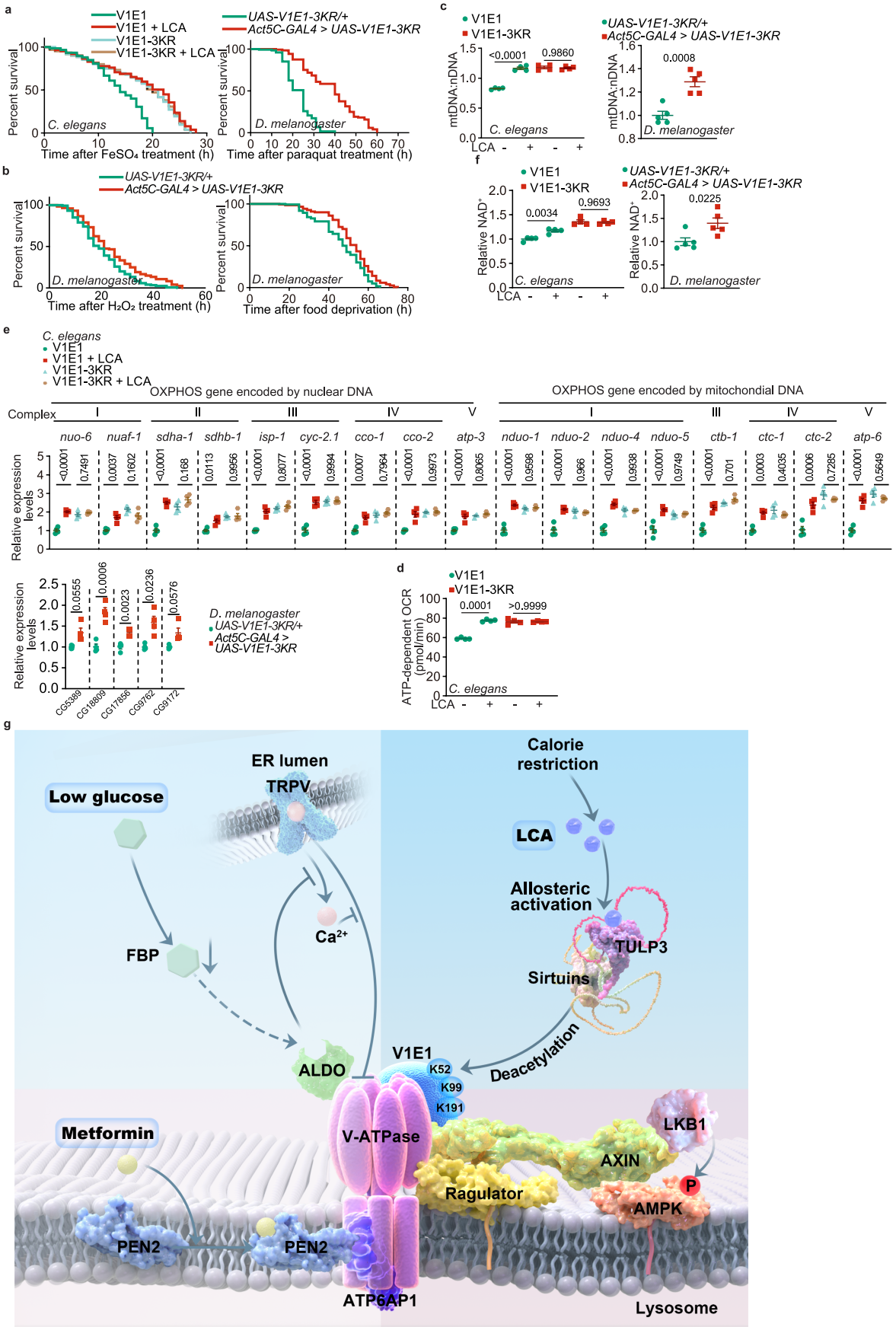

Extended Data Fig. 15 | See next page for caption.

Extended Data Fig. 15 | V1E1-3KR dominantly exerts anti-ageing effects in nematodes and flies. a, **b**, V1E1-3KR improves oxidative stress and starvation resistance. Nematodes and flies with V1E1-3KR expressing were treated with 100 μM LCA for 2 days (left panel of **a**) or 30 days (others), followed by transferring to media containing 15 mM $FeSO_4$ (left panels of **a**), 20 mM paraquat (right panels of **a**) or 5% H_2O_2 (left panels of **b**) that elicited oxidative stress, or deprived of food (right panels of **b**). Lifespan data are shown as Kaplan-Meier curves. **c**, V1E1-3KR elevates the ratios of mtDNA:nDNA. Nematodes and flies with V1E1-3KR expressing were treated with 100 μM LCA for 2 days (left panel) or 30 days (right panel), followed by determination of the ratios of mtDNA:nDNA. Results are mean ± s.e.m.; $n = 5$ (right panel) or 4 (left panel) samples for each genotype/condition, and P value by two-way ANOVA followed by Tukey's test (left panel) or two-sided Student's t-test (right panel). **d**, **e**, V1E1-3KR elevates mitochondrial contents and respiratory functions in nematodes and flies. Nematodes and flies with V1E1-3KR expression were treated with LCA, followed by determination of the mRNA levels of OXPHOS complex (**e**; results are mean ± s.e.m.; $n = 4$ samples for each genotype/treatment, and P value by two-way ANOVA followed by Tukey's test, except those of flies in **e** two-sided Student's t-test), and OCR (**d**; results are mean ± s.e.m.; $n = 4$ samples for each genotype/treatment, and P value by two-way ANOVA followed by Tukey's test). **f**, V1E1-3KR elevates NAD^+ levels in nematodes and flies. Nematodes and flies with expression of V1E1-3KR were treated with 100 μM LCA for 2 days (left panel) or 30 days (right panel), followed by determination of the levels of NAD^+. Results are mean ± s.e.m.; $n = 5$ (right panel) or 4 (left panel) samples for each genotype/condition, and P value by two-way ANOVA followed by Tukey's test (left panel) or two-sided Student's t-test (right panel). **g**, Schematic diagram showing that the v-ATPase serves as a common entry into the lysosomal AMPK pathway: i) LCA, elevated by CR, binds to TULP3 and activates sirtuins, which in turn deacetylate the V1E1 subunit of v-ATPase (on K52, K99 and K191 residues) and inhibits v-ATPase, which along with conformationally changed Ragulator allows for AXIN/LKB1 to translocate to the surface of the lysosome, where LKB1 phosphorylates and activates AMPK; ii) in response to low glucose, the FBP-unoccupied aldolase interacts and inhibits the cation channel TRPV, which in turn interacts and reconfigures v-ATPase, allowing for AXIN/LKB1 to translocate to the lysosome to activate AMPK; and iii) metformin binds to its target PEN2, and the metformin-bound PEN2 is recruited to v-ATPase via interacting with ATP6AP1, thereby inhibiting v-ATPase. The v-ATPase complex hence acts as a common node for the signalling of low glucose, metformin and LCA to intersect, all leading to AMPK activation and manifestation of anti-ageing effects. Experiments in this figure were performed three times.

nature portfolio

Corresponding author(s): Chen-Song Zhang and Sheng-Cai Lin

Last updated by author(s): 2024/9/17

Reporting Summary

Nature Portfolio wishes to improve the reproducibility of the work that we publish. This form provides structure for consistency and transparency in reporting. For further information on Nature Portfolio policies, see our Editorial Policies and the Editorial Policy Checklist.

Statistics

For all statistical analyses, confirm that the following items are present in the figure legend, table legend, main text, or Methods section.

n/a	Confirmed	
☐	☒	The exact sample size (*n*) for each experimental group/condition, given as a discrete number and unit of measurement
☐	☒	A statement on whether measurements were taken from distinct samples or whether the same sample was measured repeatedly
☐	☒	The statistical test(s) used AND whether they are one- or two-sided *Only common tests should be described solely by name; describe more complex techniques in the Methods section.*
☐	☒	A description of all covariates tested
☐	☒	A description of any assumptions or corrections, such as tests of normality and adjustment for multiple comparisons
☐	☒	A full description of the statistical parameters including central tendency (e.g. means) or other basic estimates (e.g. regression coefficient) AND variation (e.g. standard deviation) or associated estimates of uncertainty (e.g. confidence intervals)
☐	☒	For null hypothesis testing, the test statistic (e.g. *F*, *t*, *r*) with confidence intervals, effect sizes, degrees of freedom and *P* value noted *Give P values as exact values whenever suitable.*
☒	☐	For Bayesian analysis, information on the choice of priors and Markov chain Monte Carlo settings
☒	☐	For hierarchical and complex designs, identification of the appropriate level for tests and full reporting of outcomes
☒	☐	Estimates of effect sizes (e.g. Cohen's *d*, Pearson's *r*), indicating how they were calculated

Our web collection on statistics for biologists contains articles on many of the points above.

Software and code

Policy information about availability of computer code

Data collection	Epson Scan software (v.3.9.3.4) was used to scan blots from X-ray films. Zen 3.4 (Zeiss) and LAS X (version 3.0.2.16120, Leica) were used to collect microscopic images, as described in related method sections. OCR results were collected by Wave 2.6.1 (for nematodes) or Wave 2.6.3 (for muscle). Analyst software (v.1.7.1, SCIEX) was used to collect data from preparative HPLC-MS. Data from CE/MS were collected using MassHunter LC/MS acquisition 10.1.48 (Agilent). MS data were collected by Peaks Studio Xpro software (PEAKS Studio 10.6 build 20201221, Bioinformatics Solutions) or Proteome Discoverer (v.2.2, Thermo). Data acquisition and instrument control for determining mouse energy expenditure were performed using MetaScreen software (v.2.3.15.12, Sable Systems). The in silico docking assay was then performed with the AutoDock vina 1.1.2 software, during which the structure of LCA and the AlphaFold-predicted TULP3, ktub, tub-1, V1E2, and vha-8 structure (https://alphafold.ebi.ac.uk/entry/O75386, https://alphafold.ebi.ac.uk/entry/Q86PC9;https://alphafold.ebi.ac.uk/entry/Q09306; https://alphafold.ebi.ac.uk/entry/ Q96A05; https://alphafold.ebi.ac.uk/entry/Q95X44) were used. Data were then illustrated using the PyMOL (ver. 2.5, Schrodinger) software. DSC data were collected using MicroCal VP-Capillary DSC software.
Data analysis	Plots were generated by Prism 9, measured by ImageJ (v.1.8.0, National Institutes of Health Freeware) software and were formatted by Illustrator 2022. Statistical analysis was performed by Prism 9 (GraphPad Software) and SPSS 27.0 (IBM). Microscopic images were analysed and processed by Zen 3.4 and LAS X (version 3.0.2.16120, Leica), as described in related Methods section, and were formatted on Photoshop 2023 software (Adobe). Results of metabolites measured on HPLC-MS were analysed using MultiQuant software (v.3.0.3, SCIEX). Results of metabolites measured on CE-MS were processed using Qualitative Analysis B.06.00 (Agilent). The PRM data were analysed using Skyline-daily software (21.2.1.424) RT-PCR results were analysed using LightCycler software (v.96 1.1, Roche) and CFX Manager software (v.3.1, Bio-Rad, for determining the

levels of sir-2.3 and sir-2.4 mRNAs in nematodes).
Data of mouse energy expenditure were processed using Macro Interpreter (v.2.32, Sable Systems)
DSC data were analysed using origin 2016.

For manuscripts utilizing custom algorithms or software that are central to the research but not yet described in published literature, software must be made available to editors and reviewers. We strongly encourage code deposition in a community repository (e.g. GitHub). See the Nature Portfolio guidelines for submitting code & software for further information.

Data

Policy information about availability of data

All manuscripts must include a data availability statement. This statement should provide the following information, where applicable:

- Accession codes, unique identifiers, or web links for publicly available datasets
- A description of any restrictions on data availability
- For clinical datasets or third party data, please ensure that the statement adheres to our policy

All plasmids and experimental data that support the findings of this study are available from the corresponding author upon request. Full immunoblots are provided as Supplementary Information. Source data are provided with this paper.
The analysis was performed using standard protocols with previously described analysis tools. No custom code was used in this study.

Field-specific reporting

Please select the one below that is the best fit for your research. If you are not sure, read the appropriate sections before making your selection.

☒ Life sciences ☐ Behavioural & social sciences ☐ Ecological, evolutionary & environmental sciences

For a reference copy of the document with all sections, see nature.com/documents/nr-reporting-summary-flat.pdf

Life sciences study design

All studies must disclose on these points even when the disclosure is negative.

Sample size	The chosen sample sizes were similar to those used in this field: n = 4-5 samples were used to evaluate the levels of metabolites in serum (ref. 76,77), cells (ref. 10,78), tissues (ref. 10,16,78,79), nematodes (ref. 80-82) and flies (ref. 83-85); n = 4-5 samples to determine OCR in tissues (ref. 78,86) and nematodes (ref. 87-89); n = 3-4 samples to determine the mRNA levels of a specific gene (ref. 11); n = 2-6 samples to determine the expression levels and phosphorylation levels of a specific protein (ref. 11); n = 20-33 cells to determine AXIN translocation and lysosomal pH (ref. 10,12); n = 4 replicates to determine SIRT1 activity (ref. 30,90); n = 200 worms to determine lifespan (ref. 91-93); n = 60 worms to determine healthspan (ref. 94-96); n = 200 flies, male or female, to determine lifespan (ref. 97-99); n = 60 flies, male or female, to determine healthspan (ref. 100-102); n = 4-8 mice for EE and RQ (ref. 78); n = 5 mice for body composition (ref. 78); n = 6 mice for muscle fibre type (ref. 74,103,104); n = 10-11 mice for running duration (ref. 12,78); and n = 35-38 mice for grasp strength (ref. 78). No statistical methods were used to predetermine sample size.
Data exclusions	No data was excluded.
Replication	All experimental findings were repeated at least three times as stated in figure legends.
Randomization	Randomisation was applied wherever possible. For example, during MS analyses (for metabolites and proteins), samples were processed and subjected to the MS in random orders. For animal experiments, sex-matched (for mice and flies), age-matched litter-mate animals in each genotype were randomly assigned to LCA or vehicle treatments. In cell experiments, cells of each genotype were parallel seeded and randomly assigned to different treatments. Otherwise, randomisation was not performed. For example, when performing immunoblotting, samples needed to be loaded in a specific order to generate the final figures.
Blinding	Blinding was applied wherever possible. For example, samples, cages or agar plates/vials during sample collection and processing were labelled as code names that were later revealed by the individual who picked and treated animals or cells, but did not participate in sample collection and processing, until assessing outcome. Similarly, during microscopy data collection and statistical analyses, the fields of view were chosen on a random basis, and are often performed by different operators, preventing potentially biased selection for desired phenotypes. Otherwise, blinding was not performed, such as the measurement of OCR and SIRT1 activity in vitro, as different reagents were added for particular reactions.

Reporting for specific materials, systems and methods

We require information from authors about some types of materials, experimental systems and methods used in many studies. Here, indicate whether each material, system or method listed is relevant to your study. If you are not sure if a list item applies to your research, read the appropriate section before selecting a response.

Materials & experimental systems

n/a	Involved in the study
☐	☒ Antibodies
☐	☒ Eukaryotic cell lines
☒	☐ Palaeontology and archaeology
☐	☒ Animals and other organisms
☒	☐ Human research participants
☒	☐ Clinical data
☒	☐ Dual use research of concern

Methods

n/a	Involved in the study
☒	☐ ChIP-seq
☒	☐ Flow cytometry
☒	☐ MRI-based neuroimaging

Antibodies

Antibodies used

Rabbit polyclonal antibody against acetylated V1E1-K99 (Ac-V1E1-K99; 1:1,000 dilution for immunoblotting (IB)) was raised using the peptide CARDDLITDLLNEA(AcK) of human V1E1 conjugated to the KLH immunogen (linked to the cysteine residue), and was purified as described in the Methods section.

Rabbit anti-phospho-AMPKα-Thr172 (cat. #2535, RRID: AB_331250; 1:1,000 for immunoblotting (IB)), anti-AMPKα (cat. #2532, RRID: AB_330331; 1:1,000 for IB), anti-phospho-ACC-Ser79 (cat. #3661, RRID: AB_330337; 1:1,000 for IB), anti-ACC (cat. #3662, RRID: AB_2219400; 1:1,000 for IB), anti-LKB1 (cat. #3047, RRID: AB_2198327; 1:1,000 for IB), anti-His-tag (cat. #12698, RRID: AB_2744546; 1:1,000 for IB), anti-Myc-tag (cat. #2278, RRID: AB_490778; 1:120 for immunofluorescence (IF)), anti-AXIN1 (cat. #2074, RRID: AB_2062419; 1:1,000 for IB), anti-SIRT1 (cat. #9475, RRID: AB_2617130; 1:1,000 for IB and 1:100 for IF), anti-SIRT2 (cat. #12650, RRID: AB_2716762; 1:1,000 for IB), anti-SIRT3 (cat. #5490, RRID: AB_10828246; 1:1,000 for IB), anti-SIRT5 (cat. #8782, RRID: AB_2716763; 1:1,000 for IB), anti-SIRT6 (cat. #12486, RRID: AB_2636969; 1:1,000 for IB), anti-SIRT7 (cat. #5360, RRID: AB_2716764; 1:1,000 for IB), anti-histone H3 (cat. #4499, RRID: AB_10544537; 1:1,000 for IB), anti-acetyl-histone H3-Lys9 (cat. #9649, RRID: AB_823528; 1:1,000 for IB), anti-LAMTOR1 (cat. #8975, RRID: AB_10860252; 1:1,000 for IB), anti-GAPDH (cat. #5174; RRID: AB_10622025; 1:1,000 for IB), mouse anti-Myc-tag (cat. #2276, RRID: AB_331783; 1:120 for IF), antibodies were purchased from Cell Signaling Technology. Mouse anti-HA-tag (cat. sc-7392, RRID: AB_2894930; 1:500 for IP or 1:120 for IF), anti-LKB1 (cat. sc-32245, RRID: AB_627890, 1:100 for IF), goat anti-AXIN (cat. sc-8567, RRID: AB_22277891; 1:100 for IP (immunoprecipitation) and 1:120 for IF), rabbit anti-VDR (cat. sc-13133, RRID: AB_628040, 1:1,000 for IB), and mouse anti-goat IgG-HRP (cat. sc-2354, RRID: AB_628490; 1:2,000 for IB) antibodies were purchased from Santa Cruz Biotechnology. Mouse anti-total OXPHOS (cat. ab110413, RRID: AB_2629281; 1:5,000 for IB), rat anti-LAMP2 (cat. ab13524, RRID: AB_2134736; 1:120 for IF), rabbit anti-laminin (cat. ab11575, RRID: AB_298179; 1:200 for IF), anti-phospho-AMPKα2-Ser345 (cat. ab129081, 1:1,000 for IB), anti-transferrin (cat. ab1223, RRID: AB_298951; 1:500 for IB), anti-ATP6V1B2 (cat. ab73404, RRID: AB_1924799; 1:1,000 for IB), anti-PEN2 (cat. ab154830, 1:1,000 for IB), and goat anti-SIRT4 (cat. ab10140, RRID: AB_2188769; 1:1,000 for IB) antibodies were purchased from Abcam. Mouse anti-eMHC (cat. BF-G6, RRID: AB_10571455; 1:100 for IHC), anti-Pax7 (cat. Pax-7, RRID: AB_2299243; 1:100 for IHC), anti-MHCIIa (cat. SC71, RRID: AB_2147165; 1:100 for IHC), anti-MHCIIb (cat. BF-F3, RRID: AB_2266724; 1:100 for IHC), and anti-MHCI (cat. C6B12, RRID: AB_528351; 1:100 for IHC) antibodies were purchased from Developmental Studies Hybridoma Bank. Rabbit anti-tubulin (cat. 10068-1-AP, RRID: AB_2303998; 1:1,000 for IB nematode tubulin), anti-ATP6V1E1 (cat. 15280-1-AP, RRID: AB_2062545; 1:1,000 for IB), anti-TULP3 (cat. #13637-1-AP, RRID: AB_2211547, 1:20,000 for IB), anti-TOMM20 (cat. #11802-1-AP, RRID: AB_2207530; 1:1,000 for IB), anti-YES (cat. #20243-1-AP, RRID: AB_10697656; 1:1,000 for IB), and mouse anti-tubulin (cat. 66031-1-Ig, RRID: AB_11042766; 1:20,000 for IB mammalian tubulin), and anti-HA-tag (cat. 66006-2-Ig, RRID: AB_2881490; 1:20,000 for IB) antibodies were purchased from Proteintech. Rabbit anti-ATP6v0c (cat. NBP1-59654, RRID: AB_11004830; 1:1,000 for IB) antibody was purchased from Novus Biologicals. Mouse anti β-ACTIN (cat. A5316, RRID: AB_476743; 1:1,000 for IB) and anti-FLAG M2 affinity gel (cat. A2220, 1:500 for IP) were purchased from Sigma. Donkey anti-Goat IgG (H+L) Highly Cross-Adsorbed Secondary Antibody, Alexa Fluor Plus 488 (cat. A-32814, RRID: AB_2762838; 1:100 for IF), Donkey anti-Rat IgG (H+L) Highly Cross-Adsorbed Secondary Antibody, Alexa Fluor 594 (cat. A-21209, RRID: AB_2535795; 1:100 for IF), Goat anti-Mouse IgM (Heavy chain) Cross-Adsorbed Secondary Antibody, Alexa Fluor 488 (cat. A-21042, RRID: AB_2535711; 1:200 for IHC), Goat anti-Mouse IgG2b Cross-Adsorbed Secondary Antibody, Alexa Fluor 594 (cat. A-21145, RRID: AB_2535781; 1:200 for IHC), Goat anti-Mouse IgG1 Cross-Adsorbed Secondary Antibody, Alexa Fluor 647 (cat. A-21240, RRID: AB_2535809; 1:200 for IHC), Goat anti-Mouse IgG1 Cross-Adsorbed Secondary Antibody, Alexa Fluor 488 (cat. A-21121, RRID: AB_2535764; 1:200 for IHC), Goat anti-Rabbit IgG (H+L) Highly Cross-Adsorbed Secondary Antibody, Alexa Fluor 488 (cat. A11034, RRID: AB_2576217; 1: 200 for IF), and Goat anti-Rabbit IgG (H+L) Cross-Adsorbed Secondary Antibody, Alexa Fluor 594 (cat. A-11012, RRID: AB_2534079; 1:200 for IHC) were purchased from Thermo. The horseradish peroxidase (HRP)-conjugated goat anti-mouse IgG (cat. 115-035-003, RRID: AB_10015289; 1:5,000 dilution for IB) and goat anti-rabbit IgG (cat. 111-035-003, RRID: AB_2313567; 1:5,000 dilution for IB) antibodies were purchased from Jackson ImmunoResearch.

Validation

Rabbit polyclonal antibody against acetylated V1E1-K99 was validated in Extended Data Fig. 3c of this study. The anti-PEN2 (cat. ab154830, 1:1,000 for IB) antibody was validated in our previous study (PMID 35197629).

The following commercially available antibodies were validated by the company, as well as other researchers (as the information collected by the RRID database):
Rabbit anti-phospho-AMPKα-Thr172 (cat. #2535, RRID: AB_331250; 1:1,000 for immunoblotting (IB)), anti-AMPKα (cat. #2532, RRID: AB_330331; 1:1,000 for IB), anti-phospho-ACC-Ser79 (cat. #3661, RRID: AB_330337; 1:1,000 for IB), anti-ACC (cat. #3662, RRID: AB_2219400; 1:1,000 for IB), anti-LKB1 (cat. #3047, RRID: AB_2198327; 1:1,000 for IB), anti-His-tag (cat. #12698, RRID: AB_2744546; 1:1,000 for IB), anti-Myc-tag (cat. #2278, RRID: AB_490778; 1:120 for immunofluorescence (IF)), anti-AXIN1 (cat. #2074, RRID: AB_2062419; 1:1,000 for IB), anti-SIRT1 (cat. #9475, RRID: AB_2617130; 1:1,000 for IB and 1:100 for IF), anti-SIRT2 (cat. #12650, RRID: AB_2716762; 1:1,000 for IB), anti-SIRT3 (cat. #5490, RRID: AB_10828246; 1:1,000 for IB), anti-SIRT5 (cat. #8782, RRID: AB_2716763; 1:1,000 for IB), anti-SIRT6 (cat. #12486, RRID: AB_2636969; 1:1,000 for IB), anti-SIRT7 (cat. #5360, RRID: AB_2716764; 1:1,000 for IB), anti-histone H3 (cat. #4499, RRID: AB_10544537; 1:1,000 for IB), anti-acetyl-histone H3-Lys9 (cat. #9649, RRID: AB_823528; 1:1,000 for IB), anti-LAMTOR1 (cat. #8975, RRID: AB_10860252; 1:1,000 for IB), anti-GAPDH (cat. #5174; RRID:

AB_10622025; 1:1,000 for IB), mouse anti-Myc-tag (cat. #2276, RRID: AB_331783; 1:120 for IF), anti-Ubiquitin (cat. #3936, RRID: AB_331292; 1:1,000 for IB) and HRP-conjugated mouse anti-rabbit IgG (conformation-specific, cat. #5127, RRID: AB_10892860; 1:2,000 for IB) and HRP-conjugated mouse anti-rabbit IgG (conformation-specific, cat. #5127, RRID: AB_10892860; 1:2,000 for IB) antibodies were purchased from Cell Signaling Technology. Mouse anti-HA-tag (cat. sc-7392, RRID: AB_2894930; 1:500 for IP or 1:120 for IF), anti-LKB1 (cat. sc-32245, RRID: AB_627890, 1:100 for IF), goat anti-AXIN (cat. sc-8567, RRID: AB_22277891; 1:100 for IP (immunoprecipitation) and 1:120 for IF), rabbit anti-VDR (cat. sc-13133, RRID: AB_628040, 1:1,000 for IB), and mouse anti-goat IgG-HRP (cat. sc-2354, RRID: AB_628490; 1:2,000 for IB) antibodies were purchased from Santa Cruz Biotechnology. Mouse anti-total OXPHOS (cat. ab110413, RRID: AB_2629281; 1:5,000 for IB), rat anti-LAMP2 (cat. ab13524, RRID: AB_2134736; 1:120 for IF), rabbit anti-laminin (cat. ab11575, RRID: AB_298179; 1:200 for IF), anti-phospho-AMPKα2-Ser345 (cat. ab129081, 1:1,000 for IB), anti-transferrin (cat. ab1223, RRID: AB_298951; 1:500 for IB), anti-ATP6V1B2 (cat. ab73404, RRID: AB_1924799; 1:1,000 for IB), anti-PEN2 (cat. ab154830, 1:1,000 for IB), and goat anti-SIRT4 (cat. ab10140, RRID: AB_2188769; 1:1,000 for IB) antibodies were purchased from Abcam. Mouse anti-eMHC (cat. BF-G6, RRID: AB_10571455; 1:100 for IHC), anti-Pax7 (cat. Pax-7, RRID: AB_2299243; 1:100 for IHC), anti-MHCIIa (cat. SC71, RRID: AB_2147165; 1:100 for IHC), anti-MHCIIb (cat. BF-F3, RRID: AB_2266724; 1:100 for IHC), and anti-MHCI (cat. C6B12, RRID: AB_528351; 1:100 for IHC) antibodies were purchased from Developmental Studies Hybridoma Bank. Rabbit anti-tubulin (cat. 10068-1-AP, RRID: AB_2303998; 1:1,000 for IB nematode tubulin), anti-ATP6V1E1 (cat. 15280-1-AP, RRID: AB_2062545; 1:1,000 for IB), anti-TULP3 (cat. #13637-1-AP, RRID: AB_2211547, 1:20,000 for IB), anti-TOMM20 (cat. #11802-1-AP, RRID: AB_2207530; 1:1,000 for IB), anti-YES (cat. #20243-1-AP, RRID: AB_10697656; 1:1,000 for IB), and mouse anti-tubulin (cat. 66031-1-Ig, RRID: AB_11042766; 1:20,000 for IB mammalian tubulin), and anti-HA-tag (cat. 66006-2-Ig, RRID: AB_2881490; 1:20,000 for IB) antibodies were purchased from Proteintech. Rabbit anti-ATP6v0c (cat. NBP1-59654, RRID: AB_11004830; 1:1,000 for IB) antibody was purchased from Novus Biologicals. Mouse anti β-ACTIN (cat. A5316, RRID: AB_476743; 1:1,000 for IB) and anti-FLAG M2 affinity gel (cat. A2220, 1:500 for IP) were purchased from Sigma. Donkey anti-Goat IgG (H+L) Highly Cross-Adsorbed Secondary Antibody, Alexa Fluor Plus 488 (cat. A-32814, RRID: AB_2762838; 1:100 for IF), Donkey anti-Rat IgG (H+L) Highly Cross-Adsorbed Secondary Antibody, Alexa Fluor 594 (cat. A-21209, RRID: AB_2535795; 1:100 for IF), Goat anti-Mouse IgM (Heavy chain) Cross-Adsorbed Secondary Antibody, Alexa Fluor 488 (cat. A-21042, RRID: AB_2535711; 1:200 for IHC), Goat anti-Mouse IgG2b Cross-Adsorbed Secondary Antibody, Alexa Fluor 594 (cat. A-21145, RRID: AB_2535781; 1:200 for IHC), Goat anti-Mouse IgG1 Cross-Adsorbed Secondary Antibody, Alexa Fluor 647 (cat. A-21240, RRID: AB_2535809; 1:200 for IHC), Goat anti-Mouse IgG1 Cross-Adsorbed Secondary Antibody, Alexa Fluor 488 (cat. A-21121, RRID: AB_2535764; 1:200 for IHC), Goat anti-Rabbit IgG (H+L) Highly Cross-Adsorbed Secondary Antibody, Alexa Fluor 488 (cat. A11034, RRID: AB_2576217; 1: 200 for IF), and Goat anti-Rabbit IgG (H+L) Cross-Adsorbed Secondary Antibody, Alexa Fluor 594 (cat. A-11012, RRID: AB_2534079; 1:200 for IHC) were purchased from Thermo. The horseradish peroxidase (HRP)-conjugated goat anti-mouse IgG (cat. 115-035-003, RRID: AB_10015289; 1:5,000 dilution for IB) and goat anti-rabbit IgG (cat. 111-035-003, RRID: AB_2313567; 1:5,000 dilution for IB) antibodies were purchased from Jackson ImmunoResearch.

Eukaryotic cell lines

Policy information about cell lines

Cell line source(s)	HEK293T cells were purchased from ATCC. MEFs were obtained from the indicated mouse strains.
Authentication	HEK293T cells and MEFs were authenticated by STR sequencing performed by Immocell Biotechnology Corporation (Xiamen, China).
Mycoplasma contamination	The cell lines were routinely tested negative for mycoplasma contamination in our lab.
Commonly misidentified lines (See ICLAC register)	No commonly misidentified lines were used.

Animals and other organisms

Policy information about studies involving animals; ARRIVE guidelines recommended for reporting animal research

Laboratory animals	Animal maintenance: Unless stated otherwise, mice were housed with free access to water and standard diet (65% carbohydrate, 11% fat, 24% protein) under specific pathogen-free conditions. The light was on from 8:00 to 20:00, with the temperature kept at 21-24 °C and humidity at 40-70%. Only male mice were used in the study, and male littermate controls were used throughout the study. Mice were individually caged for 1 week before each treatment. For starvation, the diet was withdrawn from the cage at 5 p.m., and mice were sacrificed at desired time points by cervical dislocation. For CR, each mouse was fed with 2.5 g of standard diet (70% of ad libitum food intake for a mouse at 4 months old and above) at 5 p.m. at each day. The following ages of mice were used: a) for immunoblotting and the measurement of adenylates: wildtype mice aged 5 weeks (treated with LCA for 1 week starting from 4 weeks old), or the AXIN-LKO, AXIN-MKO, LAMTOR1-LKO and LAMTOR1-MKO mice aged 7 weeks (treated with LCA for 1 week starting from 6 weeks old); b) for immunohistochemistry: the V1E1-3KR- or wildtype V1E1-expressing mice aged 18 months (into which tamoxifen was injected at 16 months old, and treated with LCA for 1 month starting from 17 months old), and TULP3-4G-, or wildtype TULP3 expressing mice aged 20.5 months (into which tamoxifen was injected at 16 months old, and subjected to CR for 3.5 months starting from 17 months old); c) for determination of mouse healthspan: the V1E1-3KR- or wildtype V1E1-expressing mice aged 18 months (into which tamoxifen was injected at 16 months old, and treated with LCA for 1 month starting from 17 months old), and TULP3-4G-, or wildtype TULP3 expressing mice aged 20.5 months (into which tamoxifen was injected at 16 months old, and subjected to CR for 3.5 months starting from 17 months old); and d) for all the other experiments, mice aged 4 weeks. Unless stated otherwise, all flies were cultured at 25 °C and 60% humidity with a 12-hour light and dark cycle. The light was on from 8:00 to 20:00. Adult flies were cultured in Bloomington Drosophila Stock Center (BDSC) Standard Cornmeal Medium (for regular culture), 2% (for CR), or 3% (the control, ad libitum fed group for CR) CSY agar diet. Larvae and the crossed fly strains were reared on Semi-Defined, Rich Medium, which is prepared as described previously, with minor modifications. Briefly, 10 g of agar, 80 g of dry yeast, 20 g of yeast extract, 20 g of peptone, 30 g of sucrose, 60 g of glucose, 0.5 g of MgSO4·6H2O and 0.5g of CaCl2·6H2O were dissolved in 1,000 ml of di-distilled water, and then boiled, followed by cooling to 60 °C. Some 6 ml of propionic acid was then added

to the medium, and the medium was dispensed into culture vials, 6 ml each. The media vials were covered with gauze and blown with the breeze as in BDSC and CSY diets, and were kept at 20 °C (for no more than 3 days) before experiment.
In this study, the following ages of flies were used: a) for analysing AMPK activation and the pharmacokinetics of LCA, third instar larvae or newly eclosed adults were used; b) for determining lifespan, adults at day 2 after eclosion were used (for LCA or CR treatment); c) for determining healthspan, mtDNA:nDNA, NAD+ levels and mitochondrial genes expression, adults at day 30 after eclosion (treated with LCA for 28 days starting from 2 days after eclosion) were used.
Unless stated otherwise, nematodes (hermaphrodites) were maintained on nematode growth medium (NGM) plates (1.7% (w/v) agar, 0.3% (w/v) NaCl, 0.25% (w/v) bacteriological peptone, 1 mM CaCl2, 1 mM MgSO4, 25 mM KH2PO4-K2HPO4, pH 6.0, 0.02% (w/v) streptomycin and 5 μg/ml cholesterol) spread with Escherichia coli OP50 as standard food. All worms were cultured at 20 °C. The administration of LCA or DMSO was initiated at the L4 stage.

Animal source:
Wildtype C57BL/6J mice (#000664) were obtained from The Jackson Laboratory. AXINF/F (AXIN1F/F) and LAMTOR1F/F mice were generated and validated as described previously18. AMPKα1F/F (#014141) and AMPKα2F/F mice (#014142) were obtained from Jackson Laboratory, provided by Dr. Sean Morrison, and PKCζF/F mice (#024417) by Dr. Richard Huganir. AXIN2F/F mice (Cat. T008456) were purchased from Shanghai Model Organisms Center, Inc. LAMTOR1-MKO and LAMTOR1-LKO mice were generated by crossing LAMTOR1F/F mice with Mck-Cre and Alb-Cre mice as described and validated previously18, AXIN-LKO mice by crossing AXINF/F mice with Alb-Cre mice (validated in ref. 21), and AXIN1/2-MKO mice by crossing AXIN1/2F/F mice with HSA-CreERT2 mice (#025750; Jackson Laboratory). Muscular AXIN1 and AXIN2 from the AXIN1/2F/F, HSA-CreERT2 mice were removed by intraperitoneally injecting mice with tamoxifen (dissolved in corn oil) at 200 mg/kg, 4 times a week for a week. TULP3F/F mice (cat. S-CKO-17725) were purchased from Cyagen. Wildtype V1E1 or V1E1-3KR was introduced to the muscle of AMPKα1/2F/F mice through the Rosa26-LSL(LoxP-Stop-LoxP) system (ref. 128), followed by crossing with the HSA-CreERT2 mice and then intraperitoneally injecting with tamoxifen. To generate mice with muscular knockout of TULP3 and with re-introduction of TULP3 or TULP3-4G, Myc-tagged TULP3 or TULP3-4G was introduced to the TULP3F/F mice under the Rosa26-LSL system as described above, followed by crossing with HSA-CreERT2 mice and intraperitoneally injecting mice with tamoxifen.
The wildtype fly strain (w1118; #3605), Sir24.5 strain (Sirt14.5 cn1/SM6b, P{ry+t7.2=eve-lacZ8.0}SB1; #32568), Sir25.26 strain (Sirt15.26 cn1; #32657), Cas9-expressing strain (y1 sc* v1 sev21; P{y+t7.7 v+t1.8=nanos-Cas9.R}attP2; #78782), Bloomington DB strain (w1118; wgSp-1/CyO; MKRS/TM6B, Tb1; #76357) and the GAL4-expressing strain (y1 w*; P{Act5C-GAL4-w}E1/CyO; #25374) were obtained from the BDSC. The GAL4-induced, ktub RNAi-carrying strain (w1118; P{GD14210}v29111; #29111) was obtained from the Vienna Drosophila Resource Center (VDRC). The ywR13S strain (yw; Sp/CyO; MKRS/TM2), CAS DB strain (w1118; BL1/CyO; TM2/TM6B), attp3# (68A4) strain (y1 M{vas-int.Dm}ZH-2A w*; P{CaryP}attP2) and the attp2# (25C6) strain (y1 M{vas-int.Dm}ZH-2A w*; P{CaryP}attP40) were obtained from Core Facility of Drosophila Resource and Technology, Chinese Academy of Sciences. Files with Sir2 knockout were obtained by crossing the Sir24.5 and the Sir25.26 strains, followed by picking the F1 offspring with red eyes and straight wings (Sir24.5/Sir25.26). Flies with GAL4 expressed on the w1118 background (w1118; P{Act5C-GAL4-w}E1/CyO) was first generated as described in our preceding paper by crossing the y1 w*; P{Act5C-GAL4-w}E1/CyO males with w1118; Sp/CyO females, followed by crossing the F1 males with straight wings (w1118; P{Act5C-GAL4-w}E1/Sp) with w1118; Sp/CyO females.
To generate TULP3 (ktub, CG9398) knockout flies, the synchronised (see "Evaluation of lifespan and healthspan of flies" for details), Cas9-expressing flies were housed in a collection cage (cat. 59-101; Genesee Scientific) containing a grape juice plate for 2 days. Human TULP3-4G was re-introduced to the ktub-/- flies by expressing TULP3-4G in the attp3# flies (with TULP3 inserted into the chromosome III). The modified flies were then sequentially crossed with ywR13S and DB flies to backcross to a w1118 background, followed by crossing with the ktub-/- flies. The human V1E1-3KR was introduced to the wildtype flies as in TULP3, except that the attp2# strain (with V1E1 inserted into the chromosome II) was used as the acceptor.
Wildtype (N2 Bristol) and sir-2.1 (VC199) strains were obtained from Caenorhabditis Genetics Center, and sir-2.2 (tm2673) from National BioResource Project. All mutant strains were outcrossed 6 times to N2 before the experiments. The sir-2.1/sir-2.2-double knockout strain was generated by crossing sir-2.1-knockout with sir-2.2-knockout strains.The sir-2.3 and sir-2.4 genes were then knocked down in the sir-2.1/sir-2.2-double knockout strain following the previously described procedures23.The tub-1 knockout nematode strains expressing human TULP3 or TULP3-4G were established through a 3-step strategy as described previously23, with minor modifications: a) TULP3 or TULP3-4G was first introduced to the N2 strain; b) such generated strains were then subjected to knockout of the tub-1 gene; and c) the tub-1-knockout worms were then picked up for the further outcrossing with N2 strain.Nematode strain (N2) with human V1E1 or V1E1-3KR expression was constructed as described above, except that cDNAs of human V1E1 or V1E1-3KR were used, and that the sur-5 promoter on the pJM1 vector was replaced by the promoter of V1E1 (vha-8) itself.

Wild animals	The study did not involve wild animals
Field-collected samples	The study did not involve samples collected from the field.
Ethics oversight	Protocols for all rodent experiments were approved by the Institutional Animal Care and the Animal Committee of Xiamen University (XMULAC20180028 and XMULAC20220050).

Note that full information on the approval of the study protocol must also be provided in the manuscript.